

Studies of Ultrasound Distribution and Ultrasound Generation Efficiency of Transducers

by

Chang Ge

A thesis submitted in partial fulfillment of the requirements for the degree of

Master of Science
In
Integrated Circuit and Systems

Department of Electrical and Computer Engineering
University of Alberta

©Chang Ge, 2014

Abstract

Renewable energy production is an important application of ultrasound waves.

Ultrasound waves can increase the ethanol and biodiesel generated by biomass during metabolic behaviour. Ultrasound distribution and ultrasound generation efficiency of transducers are important for these applications.

The ultrasound distribution and ultrasound generation efficiency of transducers were studied in this project. Theories of ultrasound distribution and ultrasound transducer were studied during literature survey. A method of transducer modeling was proposed based on research works before for studies of ultrasound distribution of a cylindrical transducer, which will be used in biodiesel production system in the future. Validation of the model was carried out. The model of a cylindrical transducer was built. The ultrasound distribution described by the model was validated by both simulation in MATLAB and measurement by a hydrophone. Studies of ultrasound generation efficiency were carried out from a mechanics point of view. Governing equations for displacement distribution over the transducer active surface were studied. A physical quantity was proposed for comparison of generation efficiency between different transducer structures. Transducer arrays with rectangular plate transducers being the element were validated by MATLAB simulation to be more efficient in ultrasound generation than a cylindrical transducer. A triangular prism transducer array was proposed to replace a cylindrical transducer in applications.

Acknowledgement

I would like to thank Dr Jie Chen and Dr Qingxia Liu for giving me the opportunity to pursue the Master of Science degree in University of Alberta and giving me the opportunity to finish this research project. I learned more about how to systematically carry out research works and how to become a qualified researcher. I would like to extend my appreciation to my committee members: Dr Di Niu and Dr Qing Zhao for their guidance and advice. I am also very grateful to the help of Xiaojian Yu and Jida Xing, the PhD students in Dr Jie Chen's research group, during the experiment.

Contents

Chapter 1 Introduction.....	1
1.1 Motivation	1
1.2 Thesis Scope.....	2
1.3 Outlines	2
Chapter 2: Literature Review	3
2.1 Basic Ultrasound Physics.....	3
2.2 Mainstream Ultrasound Wave Generation Method: Piezoelectric Transducers	9
2.3 Measurement of Ultrasound Waves	14
2.4 Application of Ultrasound Waves in Biology	17
2.5 Selection of Simulation Tools	24
2.6 Summary	26
Chapter 3: Studies of Ultrasound Distribution for Transducers	27
3.1 Theoretical Analysis.....	27
3.2 Model Building	34
3.3 Simulation of The Equivalent Model.....	37
3.4 Experiment Materials and Methods	53
3.5 Data Processing	59
3.6 Discussion	60
3.7 Conclusion.....	70
Chapter 4: Optimization of the Efficiency of Transducer Structures	71
4.1 Mechanics Theories for Transducer Efficiencies.....	71
4.2 Theoretical Efficiency Comparison	79
4.3 Optimization of Efficient Structure.....	80

4.4 Conclusion.....	86
Chapter 5 Conclusion and Scope on Future Work	87
5.1 Conclusion.....	87
5.2 Scope on Future Work.....	87
References	88
Appendix	91

List of Figures

- 2.1 The illustration of transmission and reflection of ultrasound
- 2.2 General structure of a piezoelectric transducer
- 2.3 The mechanism explaining how the matching layer works
- 2.4 Error Rate Comparison of K-space and Leapfrog PS
- 3.1 Description of ultrasound changes in the near field and the far field
- 3.2 The Pressure distribution of ultrasound waves produced by a circular disk transducer
- 3.3 Calculation results for rectangular transducer using Eq(3.3)
- 3.4 Ultrasound field distribution along a vertical line in the side wall
- 3.5 Simulation results of vibration amplitudes distribution in tangent planes of wave fronts for the line sources proposed in this project
- 3.6 Definition of 'adjacent grids' in 'K-wave'
- 3.7 Examples of geometric structures in 'K-wave'
- 3.8 Source array and sensors arrays built for simulations in this project
- 3.9 Simulation results of vibration amplitudes distribution in tangent planes of wave fronts for the line sources proposed in this project
- 3.10 Simulation results of vibration amplitudes distribution in tangent planes of wave fronts for the line sources proposed in this project
- 3.11 Simulation results for the cylinder
- 3.12 The mount with 3 degrees of freedom used in experiments in this project.
- 3.13 Transducers used in experiments.

3.14 Apparatuses and devices after connection

3.15. The spatial relationship between each degree of freedom and the projection of active surfaces of the transducer on them

3.16 Relationship between sensitivity coefficients and ultrasound frequencies of the hydrophone used

3.17 Curves of vibration amplitudes distribution measured along diameter lines of the circular disk transducer

3.18 Curves of vibration amplitudes distribution measured along height lines of the circular disk transducer with distance to the active surface being 1mm

3.19 Curves of vibration amplitudes distribution measured along height lines of the circular disk transducer with distance to the active surface being 10mm

4.1 Rectangular plate transducer for deflection description

4.2 Cylindrical shell for deflection description

4.3 Calculation results of equations describing deflection of different transducer structures

4.4 The Ratio of voltage required for a rectangular plate transducer and a cylindrical shell with cut out angle being π

4.5 Implementations of different transducer structures in 'K-wave'

4.6 Simulation results of different transducer structure

List of Tables

2.1 Propagation Speed in Common Media

2.2 Acoustic Impedance of Common Media

2.3 Acoustic Attenuation Coefficient of Common Media

2.4 $\frac{B}{A}$ Constants of Common Media

2.5 Properties for Some Common Piezoelectric Materials

2.6 Comparison of Ultrasound Measurement Methods for Different Parameters

2.7 Common Value of Poplar Bio-medical Ultrasound Application's Parameter

2.8 Classification of Ultrasound Imaging System Based on Ultrasound Wave Type

3.1 Global Environment Settings for Simulation

3.2 Information about Degrees of Freedom for the Mount Used

3.3 Dimension Information of Transducers

3.4 Devices and Apparatuses Used in Experiments

4.1 Calculation Result for Frequency Involved

Chapter 1 Introduction

1.1 Motivation

Renewable energy production has been a popular research focus for years. Compared with traditional fossil fuels or nuclear power, renewable energy like ethanol generated from biomass has the merits of being reproducible and less hazardous to both human and the environment. However, currently, a large proportion of renewable energy is produced by the fermentation procedure of agricultural raw materials. Controversially, some of the materials are also food sources. With the rapid increase of global energy demand and continuous increase of global population, the conflict of farmland between renewable energy source and food become more and more fierce.

Biologists have found that many alcohols are the intermediate products during the metabolic pathways of yeasts using carbon dioxide as raw materials. What is more exciting is that several species of algae can also produce bio-diesels. Taking advantage of the character of these microorganisms, it is promising that renewable energy can alleviate the world energy shortage.

Ultrasound waves, especially low intensity ultrasound waves, have been found to be able to accelerate the metabolism producing bio-fuels, as a typical example of ultrasound-induced biological related effects. Led by Dr Jie Chen, our research group has focused on the application of ultrasound waves to increase the yield of bio-fuels.

The ultrasound waves used play the key role in an ultrasound-based renewable energy production system. With different structures of transducers, the output ultrasound distribution varies, and the requirements on electrical driving circuit and containers together with the stirring equipment need to be adjusted as well. A renewable energy production system should also be highly efficient to pursuit ideal energy gain. These facts all require some studies on the transducer used in the system and the distribution of output ultrasound.

This project contributes to the research on renewable energy production by studying the transducers and the distribution of output ultrasound used. Studies are mainly carried out

for cylindrical transducers. The major reason for selection of cylindrical transducers is that cylindrical transducers can project ultrasound waves omnidirectionally. Stir equipments are not required for renewable energy production systems using cylindrical transducer. Therefore, the system can be more economical from the power consumption point of view.

1.2 Thesis Scope

The scope of this thesis is to investigate the output ultrasound distribution. The outputs of ultrasound were recorded by hydrophones. Simulations based on MATLAB were carried out and a model matching ultrasound distribution measurement was proposed. In addition, studies for an optimal and more efficient transducer structure were carried out.

1.3 Outlines

Chapter 2 presents literature survey, which provides a brief introduction of physical principles of ultrasound waves. General information of piezoelectric ultrasound transducer is introduced, followed by the methods of measurement of ultrasound including parameters and corresponding popular calibrating methods. Mainstream biomedical related ultrasound applications are also presented in Chapter 2. The MATLAB simulation toolbox used in this project is described as well.

Chapter 3 addresses how the studies about ultrasound distribution were carried out. The distribution of ultrasound beams from different transducers and calculations are described. Experiment preparation is included, and an ideal model for cylindrical transducer is built as well.

Chapter 4 provides the theoretical analysis about optimizing transducer structure. The idea of using elements arrays to substitute an entire transducer structure for higher efficiency is validated in this chapter. Mechanisms about the vibration leading to ultrasound waves are discussed. In addition, the calculations for a efficiency-optimized structure and selection of different structures based on simulation are also presented.

The thesis is concluded in Chapter 5 by a summary of the project and a brief discussion of future work.

Chapter 2: Literature Review

In this chapter, background knowledge from literature survey is introduced. It covers basic ultrasound physics, implementation of ultrasound generator, measurement of ultrasound, applications of ultrasound and the selection of the simulation tools.

2.1 Basic Ultrasound Physics

2.1.1 Types of Ultrasound Waves

Ultrasound waves are mechanical waves over 20 KHz, which is beyond the frequency range of human audibility. Theoretically, the maximum frequency can reach 10^{13} Hz[1]. Like other mechanical waves, ultrasound waves are generated by the displacement of material particles[1]. Based on the spatial relationship between the displacement direction and wave propagation direction, ultrasound waves are mainly divided into two types: transverse waves and longitudinal waves[1,2], which are also known as shear waves and compressional waves, respectively. For transverse waves, the medium's displacement direction is perpendicular to the propagation direction. For longitudinal waves, the medium displacement direction is along the propagation direction.

Transverse waves and longitudinal waves also differ in the capability to propagate in different media. Transverse waves can only propagate in solid media, but longitudinal waves can travel freely in any media. This is due to the weak bond between molecules in liquid and gas, which limits the displacement of transverse waves to transfer to adjacent points along the propagation direction.

In addition to these two major types, surface waves (Rayleigh waves) are waves that can propagate in the liquid-solid boundary. Plate waves(Lamb waves) are waves that appear when the dimension of the medium is comparable to the wavelength.

2.1.2 Expression of Waves in Media

Ultrasound waves are mechanical waves. The mathematical expression of ultrasound waves can be deduced using the methods for mechanical waves based on the same principle: in ideal cases, waves' displacement, displacement speed and corresponding stress form sine function related to the position on the propagation waves, frequency,

propagation speed and duration time. Take the displacement for one-dimension case as an example, its ideal-case expression is [1]:

$$\xi = A_1 \sin(\omega t + k_1 x) + A_2 \sin(\omega t - k_2 x) \quad . \quad (2.1)$$

ξ is the displacement. A_1 and A_2 are the amplitudes in unit of MPa for ultrasound waves. k_1 and k_2 are the position-related constants, which in general are equal, and x is the position along the propagation direction. The difference in symbol before k_1 and k_2 means the wave propagates bidirectionally.

In different media, ultrasound waves have different propagation speed c , decided by the stiffness k and density of the media ρ as[2]:

$$c = \sqrt{\frac{k}{\rho}} \quad . \quad (2.2)$$

In general, the propagation speeds in solid media are the highest, followed by the liquid and gas media. Typical propagation speeds in common medias are provided in Table 2.1[1][2].

Table 2.1 Propagation Speed in Common Media[1,2]

Materials	Propagation Speed(m/s)
Liver	1578
Kidney	1560
Amniotic Fluid	1534
Fat	1430
Average Tissue	1540
Water	1480
Bone	3190-3406
Air	340

For ultrasound waves, the displacement frequency of the media particles in linear media is decided by the frequency of excitation sources, which can be expressed as the propagation speed divided by the frequency. However, non-linearity media is more common, which will be introduced in section 2.1.5.

2.1.3 Ultrasound Wave Characters during Propagation

Like electronic resistance of materials, media have acoustic impedance for ultrasound. This impedance can be described in an equation similar to the expression of Ohm's Law as[2]:

$$Z = \frac{P}{v} \quad . \quad (2.3)$$

P is the local stress that causes the particle displacement. V is the velocity of the displacement. Attention should be paid to avoid mixing the displacement velocity with propagation speed. Just like electric resistance, the acoustic impedance is an intrinsic property of materials. Eq(2.3) can only be used to calculate the acoustic impedance, however, another equation can be used to determine the acoustic impedance[2]:

$$Z = \sqrt{\rho * k} \quad . \quad (2.4)$$

ρ is the material density and k is the material stiffness. Substitution of k based on Eq (2.2), a more commonly used acoustic impedance calculation equation is shown as[2]:

$$Z = \rho * c \quad . \quad (2.5)$$

ρ is the material density and c is the acoustic propagation speed in a medium. Acoustic impedance has a unit as $\text{kg} \cdot \text{m}^{-2} \cdot \text{s}^{-1}$. Term Rayl is used to express this unit[2]. Table 2.2 provides the acoustic impedance of common media[2].

Table 2.2 Acoustic Impedance of Common Media[1,2]

Materials	Acoustic Impedance($\text{kg} \cdot \text{m}^{-2} \cdot \text{s}^{-1}$)
Liver	$1.66 \cdot 10^6$
Kidney	$1.64 \cdot 10^6$
Amniotic Fluid	$1.67 \cdot 10^6$
Fat	$1.33 \cdot 10^6$
Water	$1.48 \cdot 10^6$
Bone	$6.47 \cdot 10^6$
Air	430

Similar to electro-magnetic waves, existence of acoustic impedance leads to transmission and reflection of ultrasound when the propagation encounters a boundary of two different media.

Figure 2.1[2] is used to better illustrate the characters.

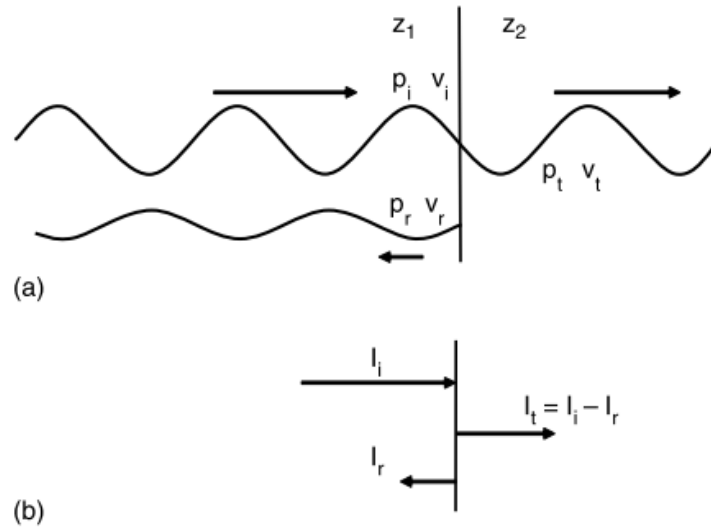


Figure 2.1 The illustration of transmission and reflection of ultrasound[2]. (a) the illustration in pressure and velocity view. (b) the illustration in intensity view. In both (a) and (b), index i refers to incident wave. Incident t refers to transmitted wave. Incident r refers to reflected wave. p is the pressure. v is the velocity of displacement. I is the acoustic energy intensity. These two equation are always effective: $p_i = p_r + p_t$ $I_i = I_t + I_r$

Similar to electromagnetic waves, for p_i and p_r , their relationship always follows the equation below[2]:

$$\frac{p_r}{p_i} = \frac{Z_2 - Z_1}{Z_2 + Z_1} = R_A \quad (2.6)$$

R_A is defined as amplitude reflection coefficient[2]. The relationship between acoustic intensity of transmitted wave and that of incident wave is[2]:

$$\frac{I_t}{I_i} = R_A^2 \quad (2.7)$$

The reflection depends primarily on the media conditions. For a flat boundary with a dimension much larger than the wavelength, the reflection follows a reflection law

described as Eq(2.6). The reflected intensity can be obtained by Eq(2.7). For a boundary with a dimension comparable to the wavelength, scattering happens, and the power scattered is proportional to the product of f^4 and d^6 [2]. f is the frequency, and d is the dimension of the boundary. For a more rough boundary with large dimension, a combination of the above two phenomena occurs, which is known as the diffuse reflection[2].

The refraction is also an important character of ultrasound wave when encountering a boundary of different media[2]. Refraction of ultrasound is similar to the one of electromagnetic wave: the ratio of the sine value of incident angle and transmitted angle is equal to the ratio of propagation speed[2], which can be described by:

$$\frac{\sin \theta_i}{\sin \theta_r} = \frac{c_1}{c_2} . \quad (2.8)$$

θ_i is the incident angle. θ_r is the refraction angle. c_1 is the propagation speed of medium that the waves are transmitted from. c_2 is the propagation speed of medium that the waves are transmitted into.

Beam forming is another character of ultrasound waves during the propagation stage. Beam forming derives from the ultrasound interference and ultrasound diffraction, which are very similar to the interference and diffraction of light waves. Beam forming plays an important role in the explanation of the topic of the project. The detail is discussed in section 3.1.

2.1.4 Attenuation

Ultrasound waves, like other mechanical waves, attenuate during propagation. The ultrasound attenuation is defined as a phenomenon in which the energy of the wave gradually decreases during propagation[2]. The major mechanism behind the ultrasound attenuation is the absorption, in which the mechanical energy of medium particles is transferred to heat[2]. At typical ultrasound frequencies, particles can't immediately follow the position changes of the adjacent ones in the medium, resulting in the energy transfer to heat through absorption. In general, the ultrasound attenuation coefficient of a medium can be described as:

$$\alpha = \alpha_0 * \omega^\eta . \tag{2.9}$$

α is the attenuation coefficient of a certain medium. Its unit is $\text{dB} * \text{MHz}^{-1} * \text{cm}^{-1}$. α_0 is the attenuation constant. ω is angular frequency of the ultrasound wave. η is the exponent, which varies based on medium type, ranging from 0 to 3. η is 2 for water(distilled) [2]. Table 2.3[2] provides the attenuation coefficient for common media.

Table 2.3 Acoustic Attenuation Coefficient of Common Media[2].

Materials	Acoustic Attenuation Coefficient($\text{dB} * \text{MHz}^{-1} * \text{cm}^{-1}$)
Liver	0.399
Brain	0.435
Muscle	0.570
Blood	0.150
Water(distilled)	0.022
Bone	22

2.1.5 Nonlinearity of Ultrasound Waves

Linearity of ultrasound waves is defined as the linear relationship between source amplitude and amplitude elsewhere in the medium. In a linear case, it is assumed that the propagation speed of ultrasound is constant. This approximation works well when the amplitude of point vibration in the medium is low[2]. However, when the amplitude is high, typically over 1MPa, it has been demonstrated that the propagation speed depends on the displacement velocity and medium properties[2]. Taking longitudinal ultrasound waves with high amplitudes as an example, the compressive effect increases the stiffness of the medium at high pressure area in the medium. Therefore the propagation speed is increased according to Eq (2.2). The rarefaction leads to a decrease in stiffness at low pressure area. Therefore the propagation speed is decreased[2]. For different media, the nonlinearity shows up at different degrees. The parameter: $\frac{B}{A}$ is used to express the nonlinearity in applications. The value of A and B are the coefficients of first and second orders, respectively, in Taylor series expansion of the equation describing the relationship between pressure and density[4]. Table 2.4[4] provides $\frac{B}{A}$ for some common media[2].

Table 2.4 $\frac{B}{A}$ Constants of Common Media[2].

Material	$\frac{B}{A}$
Blood	6.1
Brain	6.6
Fat	10
Liver	6.8
Muscle	7.4
Water	5.2

2.2 Mainstream Ultrasound Wave Generation Method: Piezoelectric Transducers

2.2.1 Piezoelectric Effect and Piezoelectric Materials

Currently, the mainstream method to generate ultrasound wave is using piezoelectric transducers [2]. Compared with other methods like mechanical, capacitive, electrodynamic, magnetostrictive methods[1], there is a specific advantage for piezoelectric method that it can reach a frequency over 1M Hz or even higher, while other methods are limited to the frequency around 100k Hz.

The word 'piezoelectricity' comes from the Greek meaning 'Electricity' and 'Pressure'[5]. The piezoelectric effect was found in 1880 by Pierre and Jacques Curie brothers[5]. Piezoelectric effects can be divided into: the direct piezoelectric effects and the reverse piezoelectric effects.

The direct piezoelectric effect describes the appearance of charges at the surface of a piece of piezoelectric material under the pressure. The explanation for this phenomenon involves splitting up of the positive and negative charge centers when the material molecules are under an external pressure. The splitting up finally leads to the internal polarization [5]. The polarization results in an electric field accumulating charges at the surface. Electric current can be generated if the piezoelectric material is connected using conductive wires, thus the mechanical energy is changed into electrical energy[5].

Reverse piezoelectric effect is the reversed version of direct piezoelectric effect[5]. When the piezoelectric material is exposed to voltage bias[5], the electric field causes the internal polarization, which generates a pressure. If the electric field is alternating and

strong enough, the displacement of piezoelectric material occurs, which transfers the electrical energy into mechanical energy[5]. Sensors measuring ultrasound waves and ultrasound transducers generating ultrasound waves can be manufactured based on the principles of direct and reverse piezoelectric effects.

The earliest piezoelectric material used is quartz, followed by titanate(PZT) and polyvinylidene difluoride(pVF₂/PVDF) [1]. Properties of some commonly used piezoelectric materials are shown in table 2.5[1]. In table 2.5[1], constant d is the piezoelectric charge constant. Constant g is the piezoelectric voltage constant. k is the stiffness of the material. ϵ is the dielectric constant. ρ is the density. C is the ultrasound propagation speed in the material. Z is the acoustic impedance of the material. T_c is the curie point of the material.

Table 2.5 Properties for Some Common Piezoelectric Materials[1].

	Quartz	PZT4	PZT5A	Pvdf
d(m/V)	$2.31 \cdot 10^{-12}$	$284 \cdot 10^{-12}$	$374 \cdot 10^{-12}$	$20 \cdot 10^{-12}$
g(Vm/N)	$5.78 \cdot 10^{-2}$	$2.61 \cdot 10^{-2}$	$2.48 \cdot 10^{-2}$	$17.4 \cdot 10^{-2}$
k	0.095	0.70	0.705	0.10
ϵ (F/m)	$4.0 \cdot 10^{-11}$	$1150 \cdot 10^{-11}$	$1500 \cdot 10^{-11}$	$0.98 \cdot 10^{-11}$
ρ (kg/m ³)	2650	7500	7750	1780
C(m/s)	5740	4000	3780	3000
Z(kg/m ² /s)	$15.21 \cdot 10^6$	$30 \cdot 10^6$	$29.29 \cdot 10^6$	$5.34 \cdot 10^6$
T _c (°C)	573	328	365	80

Among all piezoelectric materials, the most popular material is PZT which has lots of advantages compared with others, including high efficiency for energy transferring and relatively easy to be matched.

2.2.2 Electrical Models and Driving Circuit for Piezoelectric Transducer

Generation of ultrasound waves using reverse piezoelectric effect involves transformation of electrical energy into mechanical energy. Electrical models should be studied to get the maximum efficiency of transferring.

The electrical equivalent parameters can be measured using an impedance meter to get the maximum power output of a circuit. The load impedance, defined as the equivalent impedance of the transducer, should be equal to the internal impedance of the alternating

power supply[2,5]. This fact leads to the requirement of impedance matching network in the driving circuit. It has been concluded that pulses with amplitude ranging from tens to hundreds volts can satisfy ultrasound generation requirement in most cases[5], indicating that the pulse generator is a part of the driving circuit. As the frequency required is mostly within the range from 1MHz to 10MHz, pairs of MOSFET are mainly used to generate pulses[5].

Even though direct measurement of equivalent impedance brings great convenience to the matching network design, it is still difficult to determine exactly the values of resistance, capacitance and inductance in the equivalent impedance. Therefore, some approximations of the electric model are used in applications. In some research work, equivalent impedance model is simplified into a parallel network made by capacitance and resistance only[6].

2.2.3 General Structure of Piezoelectric Transducer

The high acoustic impedance of piezoelectric material is a significant disadvantage that disables the direct contact of piezoelectric materials with any external medium[5]. The acoustic impedances of piezoelectric materials are 20 times higher than those of water and soft tissues. In direct contact cases, nearly 80% of the incident ultrasound waves are reflected back at the boundary of piezoelectric material and external medium, resulting in extremely severe internal reverberation[2]. To solve this problem, additional structures are required in piezoelectric transducers. Generally, there are piezoelectric thin disks, back layers and matching layers in piezoelectric ultrasound transducers. Figure 2.2 shows the general piezoelectric transducer structure[1].

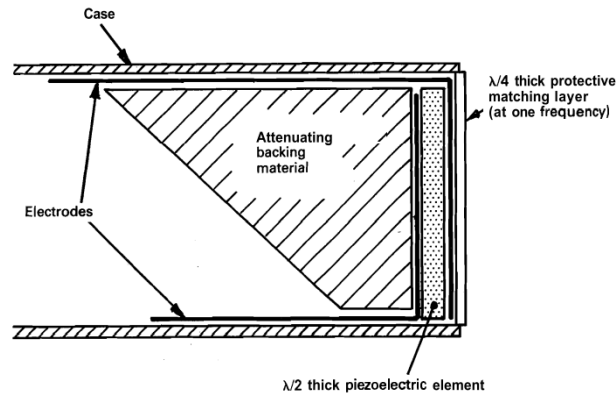


Figure 2.2 General structure of a piezoelectric transducer[1].

Both sides of the piezoelectric disk are coated with conductive painting for wire connections[2]. To ensure maximum output, the thickness of piezoelectric disk is half of the ultrasound wavelength related to the central frequency due to a phenomenon called 'half-wave resonance', which leads to the maximum displacement of the disk.

The reverberation due to the high impedance can cause the piezoelectric material to form 'rings' even long after the electric excitation stops [2], making the transducer uncontrollable. To reduce this negative impact, backing layers are used to damp the reflected waves[2]. Generally, the impedance of a backing layer is 20 times higher than the piezoelectric disk. Therefore, most of the reflected waves are transmitted into the backing layer and transferred to heat. For ultrasound sensors designed based on the principle of direct piezoelectric effect, the heat does harm to their sensitivities, therefore, special attention is needed for the selection in this situation of sensing material. In actual practise, backing layers with acoustic impedance a little bit lower than that of the piezoelectric disks are used to alleviate the heat problem for sensors[2]. However, it aggravates the problem caused by internal reverberation, because backing layers with lower impedance can't efficiently absorb the reflected waves, which are the main reasons of reverberation. As a result, matching layers in front of the piezoelectric disks are required.

Matching layers are designed to increase the transmission at the front surface of transducers, and thus, the thickness of matching layers should be a quarter of the wavelength. Within the matching layer, reverberations go back and forth, creating a

bunch of overlapping waves with same phase. The overlapping waves increase the overall output[2]. Meanwhile, another bunch of waves are sent back to the piezoelectric material-matching layer boundary, which finally go into the piezoelectric material. This bunch of waves cancel out the reflected waves in piezoelectric material at the boundary, alleviating the problem of heat[2]. Matching layers are required to have impedances with value decided by:

$$Z_m = \sqrt{Z_{piezo} * Z_{external\ media}} \quad (2.10)$$

Z_m is the impedance for a matching layer, Z_{piezo} and $Z_{external\ media}$ are the impedance of piezoelectric disk and external medium respectively.

Figure 2.3 illustrates the mechanisms of how the matching layer works in an ultrasound transducer[2]. The mechanism alleviating 'ringing' problems inside PZT layer can be described in this way: The reflected waves at the matching layer-tissue boundary have a phase difference in π between reflected waves at PZT-matching layer boundary, and the reflected waves at the matching layer-tissue boundary cancel out the reflected waves at PZT-matching layer boundary. The mechanism enhancing output waves can be described in this way: after transmitting into the matching layer and being reflected for five times, waves inside matching layer have a phase difference of 2π compared with the waves transmitting through matching layer-tissue boundary. The reflected waves enhance the transmitting waves by overlapping with waves transmitting through matching later-tissue boundary.

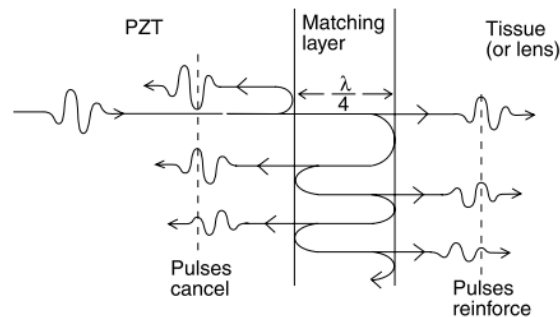


Figure 2.3 The mechanism explaining how the matching layer works[2]

In practice, due to limitations in manufacture technology, the thickness of matching layers is not always exactly equal to a quarter of the wavelength, but the difference does not significantly affect the performance of matching layers. In addition, ultrasound band filters can be fabricated using this strategy.

In addition to these three structures, sometimes, acoustic lens are used because lens can improve sensitivity, and augment vibration amplitudes[2]. Imaging and detection application can benefit from using lens[2].

2.3 Measurement of Ultrasound Waves

2.3.1 Key Parameters for Ultrasound Characterization

It is important to have accurate characterization of ultrasound waves. However, a full characterization requires related data at every point along the propagation path[1]. This is infeasible in practice. Generally, the characterization relies on the measurement of peak values, spatial values, and temporal values of the related parameters[1]. The most commonly used parameters in the characterization of ultrasound wave include: acoustic pressure, acoustic displacement, radiation forces, and temperature rise[1]. Acoustic intensity is also very important, but it can be calculated from acoustic pressure using Eq(2.11)[3]. Unit for acoustic intensity is W/m^2 or mW/cm^2

$$I = \frac{P^2}{\rho * c} \quad . \quad (2.11)$$

I is the acoustic intensity. P is the pressure in MPa. ρ is the density of the medium and c is the propagation speed in the medium.

2.3.2 Acoustic Pressure Measurement

Transducer and sensors designed based on the principle of pulse-echo mechanisms can be used for simple qualitative characterization of acoustic pressure[1]. This method can only get an average profile of the distribution of the acoustic pressure. It is not suitable for the characterization of acoustic pressure for continuous and lithotripter waves[1].

The most commonly used method is using piezoelectric hydrophones[1]. In hydrophones, sensing elements are thin films or plates made by piezoelectric materials[1]. Incident

ultrasound signals are converted into electronic signals. The brilliant temporal and spatial resolutions of hydrophones make the devices capable of measuring all type of ultrasound waves. In addition, the small size and high adaptability also allow hydrophones to be easily integrated into compact systems[1].

In order to carry out accurate characterization, the hydrophones have to fulfill several requirements: the devices should be sensitive enough to produce a reasonable signal level[1]. A linear relationship for the ultrasound-voltage conversion is expected. To ensure the sensitivity, the size of the sensing part should be smaller or comparable to the wavelength of ultrasound wave, generally ranging from 0.1 to 1.5mm[1]. The devices should be able to respond to a wide range of ultrasound, generally with the frequency from 1 to 15M Hz[1]. In addition to these functional requirements, the hydrophones should also be overall robust and stable in various working environment.

Another commonly used measurement method for acoustic pressure relies on optical diffraction techniques. The ultrasound waves can cause compression and rarefaction in the medium. The compression and rarefaction can change the optical properties of media. The higher the amplitude of ultrasound waves, the more significant the compression and rarefaction can be observed. This principle can be applied to design apparatuses for pressure measurement. The biggest merit of these apparatuses is the non-invasive character[1].

2.3.3 Acoustic Displacement Measurement

Acoustic displacement is an important parameter for ultrasound characterization because acoustic displacement can be used in calculations for other acoustic parameters like intensity and velocity. The major method used is to measure displacement using optical interferometries. This method is important because it can be used to calibrate hydrophones[1]. The principle of this method is that an acoustically transparent thin film can move in unison with the surrounding environment, following the displacement of points along propagation direction of ultrasound waves during propagation[1]. In addition to optical methods, capacitor probes can also be used to measure the displacement by monitoring changes between charges and discharges.

2.3.4 Radiation Forces

The propagation of ultrasound in certain medium involves a simultaneous transferring of momentum[1]. This momentum can generate radiation forces when the ultrasound wave is intercepted by an absorbing or reflecting obstacle[1]. This radiation force provides basis for acoustic intensity measurement. Based on the size of the obstacle, the radiation measurement systems are subdivided into types: large target type and small target type. In the large target type, the entire ultrasound wave beam is intercepted by the obstacle. In the small target type, the size of the obstacle is smaller than the extent of the ultrasound field, which generates local power intensity[1]. A typical kind of equipment for small target radiation force measurement is called the suspended sphere radiometer[1]. The amplitude of the radiation force is calculated by the displacement of the small sphere. Radiation forces can also be measured using surface levitation techniques, which take advantage of distortions generated by ultrasound at water-air boundary[1].

2.3.5 Temperature Rise

As mentioned previously, heat is generated from the attenuation of ultrasound waves during propagation, leading to rise of temperature. Temperature control plays a crucial role in many ultrasound applications. In addition, the temperature rising can also be used for ultrasound characterization.

Calorimetries or thermal probes can be used for the measurement of this temperature rising. For calorimetries, the change of liquid agent temperature is monitored, which can be used for determination of power output. In the working stage of a calorimeter, liquid agent continuously passes through the heating chamber, and the temperature is monitored at input and output port. This kind of calorimeter is generally calibrated using electrical heater.

Thermoelectric probes embedded in proper absorbing media can be used to measure local ultrasound intensity[1]. This kind of devices have high spatial resolution due to their small size, but they have a very long response time[1].

2.3.6 Summary of Ultrasound Measurements

Methods used for the ultrasound measurement are decided by the parameters to be measured and the easiness to use the methods in the specific case. Table 2.6 provides a comparison among different methods for different ultrasound measurement[1]. Both economic and technical issues should be considered for the selection of measurement methods. All methods are evaluated using scores from 1 to 4. Higher score means better representation of the consideration.

Table 2.6 Comparison of Ultrasound Measurement Methods for Different Parameters[1]

Consideration		Piezoelectric		Radiation force		Temperature rise	
		Hydrophone	Ultrasound beam Calibrator	Large target	Small target	Thermal probe	Calorimeter
Cost	Capital cost	3	1	3	4	3	3
	Investment cost	2	4	3	3	2	4
Technical	Applicability	4	4	2	1	2	1
	Fidelity	3	3	2	1	1	2
	Ease of use	2	4	3	2	2	2

2.4 Application of Ultrasound Waves in Biology

2.4.1 Ultrasound Induced Bio-effects

Ultrasound has been widely used for different purposes after its discovery. Detection using ultrasound was first developed for military purposes like submarine detection, which is still one of the major applications of ultrasound. The basic principles of ultrasound detection include the reflection and the good directivity of ultrasound beams. Ultrasound waves are also applied for biological purposes. Compared with non-biological

applications, biological applications are complicated due to the complexity of biological tissues as the propagation media and the ultrasound induced bio-effects[7] .

Mechanisms of these bio-effects can be either thermal or nonthermal[7]. Conduction, perfusion and absorption are thermal mechanisms. Cavitation, streaming, radiation forces and torque are nonthermal mechanisms[7]. Ultrasound-induced bio-effects include diffusion, fragmentation, cavitation and ablation[7].

In general, ultrasound induced bio-effects can be classified as reversible ones and irreversible ones. Most of the ultrasound induced bio-effects are reversible[7], This fact contributes to the brilliant safety of biomedical ultrasound applications. Even for those irreversible ones, they can be intentionally applied for specific treatment purposes.

Most of the ultrasound induced bio-effects can be characterized by three ultrasound parameters: time average acoustic power of source(W), spatial peak temporal average intensity(I_{SPTA}), spatial average temporal average intensity(I_{SATA})[7]. Table 2.7 provides the common values of the parameters in some popular bio-medical ultrasound applications[7]. Besides the parameters mentioned above, f_c is the central frequency of the transducer wave. P_r is the ultrasound amplitude in unit of MPa. ΔT is the time interval between waves.

Table 2.7 Common Value of Poplar Bio-medical Ultrasound Application's Parameter[7]

Modality	F_c(MHZ)	Power(W)	P_r(MPa)	I_{SPTA}(W/cm²)	I_{SATA}(W/cm²)	ΔT
B-mode	1-15	0.0003-0.285	0.45-5.54	0.0003-0.991	N/A	<2
PW Doppler	1-10	0.01-0.44	0.67-5.3	0.173-9.08	N/A	<2
Physio-therapy	0.75-3.4	1-15	0.3	3	<3	N/A
Hyperthermia	0.5-5.0	N/A	0.6-6.0	1-10	2-10	4-9
HIFU	1-10	N/A	N/A	1000-10000	N/A	>19
Lithotripsy	0.5-10	N/A	5-15	Very low	N/A	N/A

2.4.2 Therapeutic Ultrasound

Both high-energy ultrasound waves and low-energy ultrasound waves have been used in therapeutic ultrasound applications. Therapeutic ultrasound applications are active ultrasound applications which are expected to alter tissues or functions of the tissues. The changes can be either permanently or temporarily [7]. In some cases, the parameters of the applications of therapeutic ultrasound are beyond the limitations provided in table 2.7. Nevertheless, these extreme applications can still be justified because the alternative treatments are much worse or impossible to carry out[7].

One of the most popular therapeutic ultrasound applications is ultrasound physiotherapy[7], which has been researched and practised over 50 years. The applications of ultrasound physiotherapy include reduction of muscle spasms, treatment of contractures, relief and healing of sports-related injuries, relief of pain, increased extensibility and treatment of contractures for collagen tissues(scar removing), heating of joint structures, treatment to improve limited joint motion and decrease in joint stiffness, arthritis, peri-arthritis, bursitis, wound healing, and healing of varicose ulcers[7]. Both continuous and pulsed waves are used in the physiotherapy. Generally, the duration of ultrasound treatment is no more than 10 minutes[7]. It has been demonstrated that heat absorbed by the tissue is the key factor for ultrasound physiotherapy[8]. The absorption of heat is proportional to the protein content of the tissues, increasing through blood, skin, tendon, cartilage, to bone at the top of the heating scale[7]. It has been suggested that the streaming, cavitation, and increased permeability of the tissues exposed to ultrasound contribute to the healing effects of ultrasound physiotherapy[7]. However, many of the applications mentioned above have only been tested on small animals and in vitro[7]. Further studies are still needed for their implementations and applications.

Sonothrombolysis is another important use of therapeutic ultrasound. Ultrasound waves are used to break up or dissolve blood clots that can cause strokes, disabilities and even sudden death[7]. It has been demonstrated that the transcranial pulsed Doppler ultrasound waves in combination with a thromolytic drug (t-Pa) can accelerate the dissolving of a blood clot and re-establishment of normal blood flow compared to the applications of the drug alone. It can be explained by the usage of repeated acoustic radiation forces at the

rhythm of the doppler pulse repetition rate and streaming effect induced by the ultrasound waves[7]. Adding contrast agents can enhance the dissolving of the clots by stimulation of cavitation, pulsation and collapse, shear forces and temperature elevation[7].

Ultrasound waves can also be used for cosmetic purposes[7]. Main applications of cosmetic ultrasound include body-sculpting, liposuction, tightening the sagging skins[7]. The main contribution of ultrasound waves to liposuction is the relief of unpleasant side effects by ultrasound fragmentation[7]. In a typical example, fluid agent containing micro bubbles is first injected in to the fatty region, and then a small grooved titanium transducer emitting high pressure ultrasound at 35K Hz with a power of 20-25W is placed into the incision. The induced effect, like inertial cavitation, can break apart the adipose tissues, making them easier to be sucked out. In this procedure, nearby vessels, nerves and collagen fibers remain unaffected[9] .

An alternative method is using the high intensity focused ultrasound (HIFU) at MHz extracorporeally to the subcutaneous fat layers. This is a non-invasive approach causing coagulative necrosis in the focal region. Over a 12-week period, the body reabsorbs the necrotized adipose tissue via an inflammatory response, resulting in a net volume reduction without changes in the lipid profile[7]. As for the application of tightening skin, it also involves HIFU integrated in a system named SMAS[7].

Lithotripsy is another non-invasive therapeutic application. Here ultrasound waves are used to smash the calculus in organs such as nephrolith[7].

In recent studies[10], it has been demonstrated that the micro bubbles generated in fluid medium by ultrasound waves can transfer genes and drugs. Also, the cavitation induced by ultrasound can open pores on cell membranes for genes and drugs to pass through.

Ultrasound waves have also been proved to be able to affect both central nervous systems and the peripheral nervous systems[7]. Ultrasound waves provide the possibility of stimulating receptors and unmyelinated nerve fibers either on the surface or deep inside the skin. This shows a potential of ultrasound waves in dealing with damaged skin, skin diseases, burns and hypersensitive nerve disorders.

Up to now, most of the applications are using high energy ultrasound. Recently, an ultrasound device called Exogen has been developed, which is able to generate low intensity pulsed ultrasound waves (LIPUS) at 1.5 MHz with a duty cycle of 20% and a spatial average temporal average intensity of only 30 mW/cm²[7]. The device can accelerate the wound healing time typically by 38%. It has been demonstrated that the LIPUS induces the expression of certain type of genes by the combination of several bio-effects related to the ultrasound waves. The induced gene expressions contribute to not only the proliferation of new cells for healing, but also the absorption of tissues[7]. Another device developed by the BINARY research group in University of Alberta is also capable of generating LIPUS at 1.5 MHz[6]. Different from Exogen, the device is able to produce LIPUS at several different output intensities. The device has been used to accelerate the metabolic behaviour of several species of algae and fungi that can produce biofuel and algal oil[11][12].

HIFU is more commonly used as a non-invasive surgical method to remove tumours, especially the deep-seated ones, such as the tumours in the brain, which are usually risky and difficult to remove by traditional surgical methods[7]. In general, the lesion caused by HIFU is only an ellipsoidal globule with a size of roughly 2mm*2mm*2mm[7]. Two mechanisms are behind the HIFU surgery: histotripsy and hemostasis. Both of them are based on the thermal and mechanical effects induced by the high energy ultrasound waves. Histotripsy is responsible for the ablations of tissues and the removal of the tumour. Hemostasis is used to stop bleeding.

2.4.3 Ultrasound Imaging System

Ultrasound imaging system is one of the oldest ultrasound applications still being used today, which can be subdivided into types shown in Table 2.8[7]. No matter what the type is, all the industrialized ultrasound imaging systems are designed based on a very simple mechanism: pulse and echo. The transducers first act as an ultrasound emitter of ultrasound, and then act as the receiver to listen to the echo. Based on the difference in echo, information is processed and displayed to users[7]. Regardless of the detail of an imaging device, it always contains following parts[7]: a front end with transducer and

scanner for image format, a back end with signal processors, processing modules, displaying modules, and a user interface for interaction.

Table 2.8 Classification of Ultrasound Imaging System Based on Ultrasound Wave Type[7].

Mode Name	Brief Description
Angio	The same as the power Doppler mode
B-mode	Also known as B-scan or 2D mode due to its scanning character, response time is decided by the arrival time of echo
Color flow imaging	A spatial map overlaid on B-mode gray-scale image that can provide information in colors.
Color M-mode	This mode displays the time history of a single color flow line at the same spatial position over time
Continuous wave Doppler	This mode is sensitive to the Doppler shift of blood flow
M-mode	A brightness modulated mode displays the time history of a single line at the same spatial position over time
Doppler mode	A presentation of the Doppler spectrum
Color Doppler mode	A 2D Doppler image of blood flow that is coded by colors to show direction of the flow.
Power Doppler mode	A color coded image of blood flow based on intensity rather than direction with a paler color for higher intensity
Pulsed wave Doppler	A mode using pulses to measure flow in a region
Duplex	Presentation of two modes simultaneously: usually 2D

	and pulsed
Triplex	Presentation of three modes simultaneously: usually 2D, color flow and pulsed Doppler
2D	Imaging in a plane with brightness modulated
3D	An image of a volume or 3D object
4D	A 3D image moving in time
Zoom	A magnification of a region of interest in the video image, where acoustic parameters are modified to enhance the image.

Besides the ultrasound modes, imaging systems can also be classified based on the sizes and functions provided by the system, such as the pocket, the portable, the low-end, the mid-range, and high-end[7]. From the pocket to the high-end systems, the functions are enhanced. Cost and size of devices also increase. Nowadays, there is a trend that the new high-end features tend to migrate downward to the mid-range systems and eventually to the low-end systems over time due to the rapid development of electronic technology[7].

In addition, portable ultrasound imaging systems are becoming more and more popular due to their great convenience. The first portable ultrasound imaging system is the Minivisor, followed by Sonosite, a system weighing 6 lbs and using ASIC chips. OptiGo is another device using ASIC chips and specific for cardiac applications. Both Sonosite and OptiGo are capable of color imaging and automated assistance to help the users. The Terason 2000 system implements the small size by leveraging laptop technology. The system is characterized by its low power consumption as a 128-channel system[7].

Compared with portable devices, the pocket size devices are more attractive because they can provide similar functions. The price of the pocket size devices is also much lower, typically less than 10000 US dollars[7]. Lower power consumption of pocket size devices in comparison with portable devices contributes to the growing popularity of pocket size devices as well. Now, at least four types of pocket size devices are available in the market. Siemens P-10 has a weight of 0.7 kg with an 2-4 MHz 64-element transducer[7].

It has a image ability with scan depths 4-24 cm. The GE V-Scan has a weight of 0.37 kg. It is capable of imaging in B-mode and color flow with frequency ranging from 1.7 to 3.8 MHz and a penetration depth up to 25 cm[7]. The Sonic Window is a pocket-sized, C-scan ultrasound imaging device weighing only 0.17 kg. The MobiUs SP1 is an ultrasound imaging system integrated into a smart phone. The smart phone based device provides wireless and cellular connectivity and display of ultrasound images with four transducers from 3.5 MHz, 5.0 MHz, 7.5 MHz and 12MHz[7].

2.5 Selection of Simulation Tools

One of topics of the project is to investigate the distribution of ultrasound generated by transducers. An important step for the research is to build a model matching with the measurement. This requires the usage of simulation tools. Currently, several different types of ultrasound simulation tools are available. These tools have difference focus in functions[13].

In this project, K-wave, a MATLAB toolbox is used for ultrasound characterization[14]. It is able to characterize most of the characters like attenuation, reflection, diffraction, refraction for ultrasound waves in both homogenous and heterogeneous media.

K-wave is an open source, third party, MATLAB toolbox designed for the time-domain simulation of propagating acoustic waves in 1D, 2D and 3D[14]. With a wide range of functions, K-wave is user friendly and flexible. The key factor that makes it outstanding compared with other simulation tools is the advanced numerical model that can be used for both linear and nonlinear wave propagation[14]. An optimised computational engine is also used for speed and accuracy.

The numerical model used here is based on k-space pseudo spectral method[14]. Generally, for calculation of ultrasound waves, it heavily depends on how the continuous waves are divided into discrete steps and the accuracy of calculation. For classic finite difference and finite element approaches, at least 10 grid points per acoustic wavelength are required to achieve a acceptable accuracy[14]. This leads to the oversize of computational grids which makes it impossible to be calculated on a personal computer. For example, for a diagnostic ultrasound image formed using a 3 MHz curvilinear

transducer with a depth penetration of 15 cm, the 3D computational domain requires 1011 grids in all and to accomplish the calculation in this size, more than 400GB computer memory is required[14], which is unfeasible for a common PC. For k-wave pseudo spectral method, it reduces the requirement of memory and number of time steps for accurate simulations by combining spectral calculation of spatial derivatives with a temporal propagator expressed in the spatial frequency domain or so called k-space, where the Fourier collocation spectral method is used. This contributes to improving efficiency in the spatial domain[14]. As for the time domain, taking the spatial Fourier transform and then discretizing the time derivative using a second-order accurate central difference is used as the solution. This retains the same level of accuracy without significantly increase the simulation time when the size of simulation increases[14].

Accuracy and stability are common considerations for simulation methods. For accuracy, a key factor is that whether the discrete equations are consistent or compatible with the continuous equations. For k-wave, the discrete equations are derived rigorously from the governing equations to ensure the perfect consistence. For stability, it is decided by the size of the time step dt . It is not a significant problem when the simulation spatial distance is small. However, when the spatial distance is of tens or hundreds wavelength, the stability issue becomes significant. The reference speed c_{ref} is used to ensure that for every simulation, dt never exceeds the acceptable range which leads to collapse or errors. In detail, Eq 2.12[14] is used for the judgment of dt .

$$|\sin(c_{ref} * k * dt/2)| \leq \frac{c_{ref}}{c_0} . \quad (2.12)$$

A comparison of phase error rate between k-space and another simulation method called Leapfrog PS is provided in figure 2.4[14]. Figure 2.4 illustrates the ultrasound wave propagation in distilled water for a distance of 50 wavelength[14] . The speed of propagation is set to 1500 m/s. Clearly, the stability control using c_{ref} greatly reduce the phase error rate[14]. When the speed is exactly equal to the reference speed, the error rate is 0.

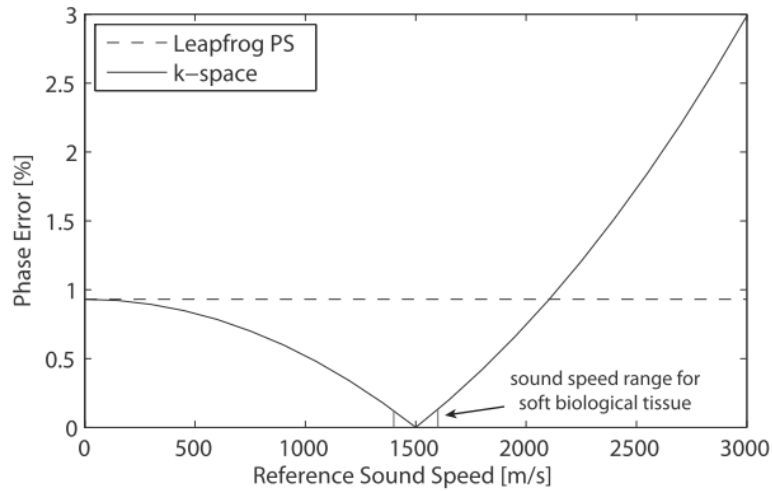


Figure 2.4 Error rate comparison between K-space and Leapfrog PS[14]

2.6 Summary

In this chapter, a detail literature survey is provided. In Section 2.1 the basic physics of ultrasound is introduced, which provides vital parameters for a simulation and analysis of ultrasound distribution by cylindrical transducer. In Section 2.2, the knowledge about the piezoelectric transducers provides information about generation of ultrasound waves and general structure of transducers. This is important for the design of experiments in this project and the research for the improvement of the transducers. The design of the driving circuit can be guided based on the studies in this project. In Section 2.3, various ultrasound methods are introduced. In section 2.4, it shows how the transducers can be widely used. For a successful application, the ultrasound involved should be clearly characterized to reduce risk. This is particularly important for bio medical related applications. Any minor error from a wrong characterization can lead to tissue damage or killing precious microorganism used in renewable energy production. In Section 2.5, a powerful simulation tool is introduced, because this project also involves simulation and model building.

Chapter 3: Studies of Ultrasound Distribution for Transducers

This chapter presents the results of the studies about ultrasound distribution of a circular disk transducer and a cylindrical transducer for renewable energy production. The work carried out includes analyzing, model building, validating, and measuring.

3.1 Theoretical Analysis

Ultrasound beam forming is important because it directly affects the ultrasound distribution, which is one topic of the project. Beam forming has been briefly described in Chapter 2. There are two key factors of ultrasound beam forming: interference and diffraction. In addition, differences in transducer structures can lead to differences in beam formed. In this section, first of all, interference and diffraction are introduced, together with their influences on ultrasound beam forming. Concepts related to ultrasound beam forming are introduced. These concepts are used in descriptions for ultrasound distribution of circular disk transducers and rectangular plate transducers, which are provided after the introduction of concepts.

3.1.1 Governing Principles

The interference of ultrasound waves is not different from other mechanical waves or optical waves. When all waves with the same frequency arrive at a point in the medium, their phase differences decide their interferences with each other, which determine the vibration amplitude of the point. The phase difference between two waves can be expressed as $k\pi$. When k is an even number, the two waves enhance each other, increasing the vibration amplitude. When k is an odd number, the two waves diminish each other, reducing the vibration amplitude.

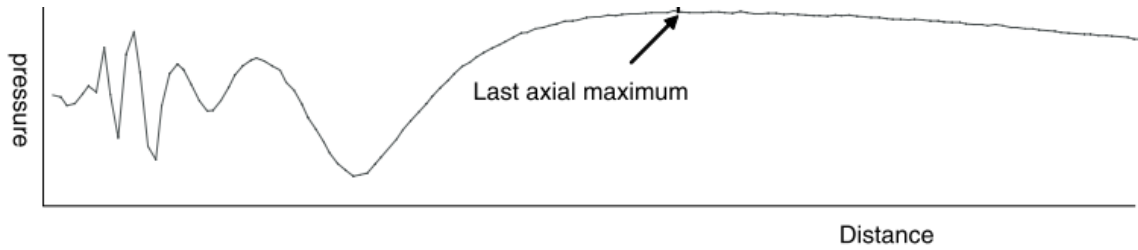
The diffraction of ultrasound waves is more related to the size of the source apertures and wavelength of ultrasound waves[2]. When the aperture is smaller than the wavelength, the ultrasound waves spreading out will form spheres with the source being the center, which are called spherical waves. Sources of spherical waves are called point sources. When the aperture is larger than the wavelength, the waves have relatively flat fronts paralleling to the surface of the source, which are called plane waves[2]. Sources of plane

waves are called plane sources. Generally, transducers are considered as plane sources. Ultrasound waves generated by transducer are plane waves.

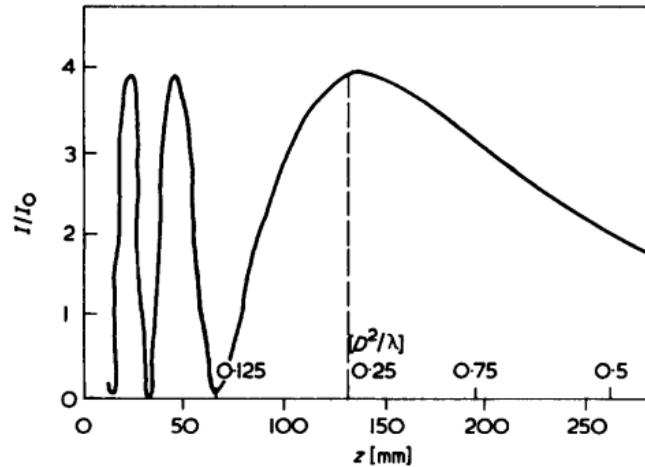
In the description of beam forming for ultrasound waves generated by a transducer, the active surface of the transducer is considered as a huge array of point sources. Each of the point sources generates spherical waves. For the parallel parts of wave fronts from all point sources, they align and propagate ahead with same phase. For the non-parallel parts, they destructively interfere with each other[2]. As a result, plane waves form.

The existence of near field and far field is a typical character of ultrasound beams. There are significant differences in vibration amplitudes distributions between points within the near field and points within the far field. Near field and far field can be distinguished by the differences. In general, ultrasound distribution refers to vibration amplitudes distributions. Therefore, the objects of studies for ultrasound distribution in this project were the vibration amplitudes distributions in the near field and far field of transducers in different structures.

Vibration amplitudes distributions for different transducer structures are not same, but they follow some common patterns. Two important spatial parameters that determine the vibration amplitudes of points within a wave front are the distance to the active surface and the distance to the center point of the wave front. In both near field and far field, vibration amplitudes distributions are functions of these two parameters. Within the near field of a ultrasound beam, periodical changes between peaks and troughs of vibration amplitudes can be observed in wave fronts and along the propagation direction. Within the far field of the beam, no periodical changes can be observed. The amplitudes gradually decrease within wave fronts and along propagation direction. Within a wave front in the far field, the decrease starts from the center point to the edges. Along the propagation direction, decrease starts from the boundary of the far field and the near field. The boundary of the far field and the near field is defined as the wave front where the last peak value of the vibration amplitudes shows up along the propagation direction. Figure 3.1 shows the changes in vibration amplitudes along the propagation direction[2, 15].



(a)



(b)

Figure 3.1 Description of ultrasound changes in the near field and the far field[2,15]. (a) the changes of vibration amplitude for a circular disk transducer. (b) the changes of vibration amplitude for a rectangular plate transducer. The changes in both (a) and (b) are along propagation direction.

Within the near field of an ultrasound beam, the frequency of the periodical changes at different wave fronts is decided by the distance of wave fronts to the source active surface. The closer a wave front to the surface, the more frequently changes happen within it.

Within the far field, the beam diverges with a limitation, which is related to the ultrasound interferences and attenuations[2]. The degree of the divergence is described by the angle of divergence[2]. The angle of divergence is defined as the intersection angle between the edge of diverged beam and the central axel of the beam. Divergences with

intersection angles larger than the angle of divergence experience destructive interferences and attenuations, and make the divergences vanish.

3.1.2 Theoretical Distribution of Ultrasound from Circular Disk Transducers

Circular disk transducers are the most popular ultrasound transducers because the symmetric circular active surface can lead to a symmetric output ultrasound beam[3]. As a result of the popularity, ultrasound beams from circular disk transducers have been comprehensively studied[3]. An example of ultrasound beam generated from a circular disk transducer is shown in Figure 3.2[2].

In Figure 3.2(b), changes matching with descriptions in Section 3.1.1 about the frequency of changes are observed within wave fronts at different distance to the source.

Concentric rings are the representation of symmetry in the output. The differences in colors of the rings mean differences in vibration amplitudes. For the two wave fronts selected in the near field, more frequent periodical changes can be observed within the wave front closer to the source. For the wave front selected in the far field, gradually decrease of amplitudes from the center to the edge can be observed.

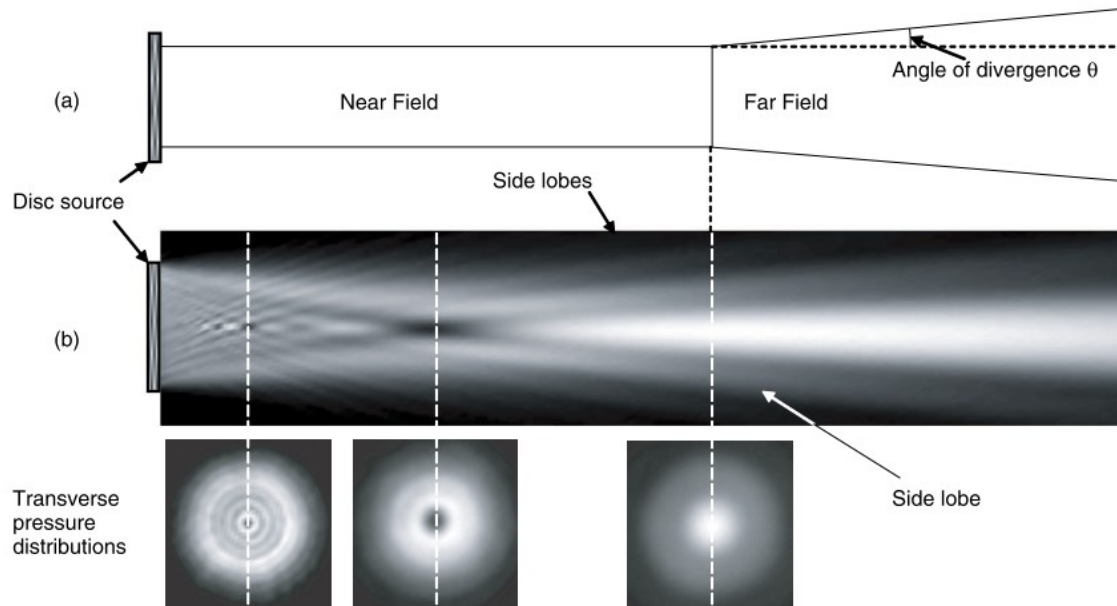


Figure 3.2 The Pressure Distribution of Ultrasound Waves Produced by a Circular Disk Transducer. (a) the divergence angle. (b) the differences in near field and far field[2].

For a circular disk transducer, the near field distance can be calculated by Eq (3.1)[2]

$$F = \frac{D^2}{4\lambda} \quad (3.1)$$

D is the diameter of the transducer. λ is the wavelength of ultrasound wave in the medium.

The angle of divergence for a circular disk transducer can be calculated by [2]

$$\theta = \sin^{-1} 1.22 \frac{\lambda}{D} \quad (3.2)$$

D is the diameter of the transducer, and λ is the wavelength in the medium.

3.1.3 Theoretical Distribution of Ultrasound from Rectangular Transducers

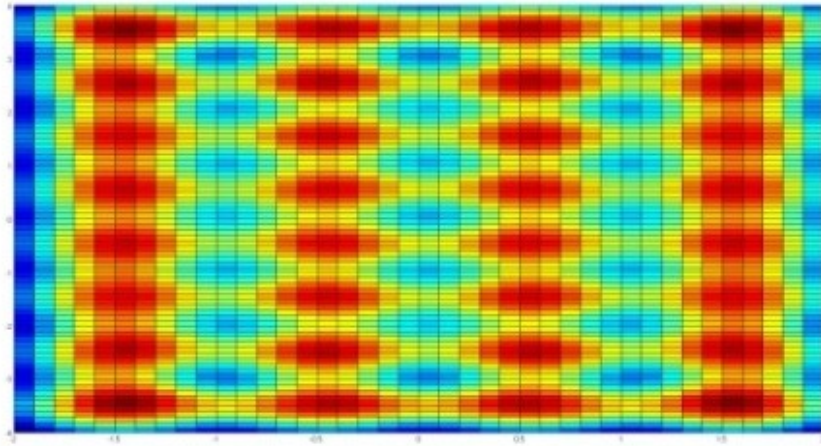
The generic equation describing vibration amplitudes distribution of a rectangular plate transducer was found in literature survey of the project[15]. This equation is shown below, which describes the contribution of a surface differential unit to the pressure at certain point within a wave front of ultrasound beam from a rectangular transducer[15]:

$$P = j \frac{\rho * c * \mu * e^{j(\omega * t - k * r)}}{\lambda * r} ds \quad (3.3)$$

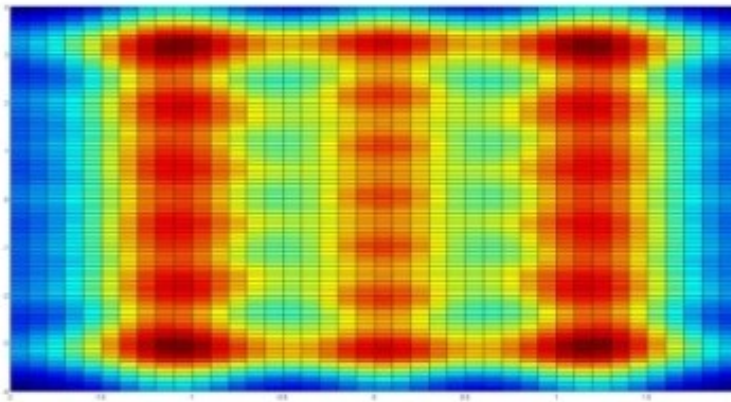
ds is the surface differential unit. r is the distance from a point in the medium to ds. P is the pressure contributed by ds at the r. j is the complex symbol representing phase. ρ is the density of the medium. c is the propagation speed of ultrasound wave in the medium. μ is the vibration velocity of the particle in the medium. ω is the angular frequency of the ultrasound wave. k is the wave number.

Eq (3.3) was calculated using MATLAB. A surface integral was involved in the calculation. The integral was calculated by discrete summation. In a discrete summation, first of all, both the active surface and the wave front to be studied were divided into grids. Then, the vibration amplitudes of every grid on the active surface at a point within the wave front was accumulated. The result of accumulation was considered as the vibration amplitude of the point. The vibration amplitudes distribution was decided by

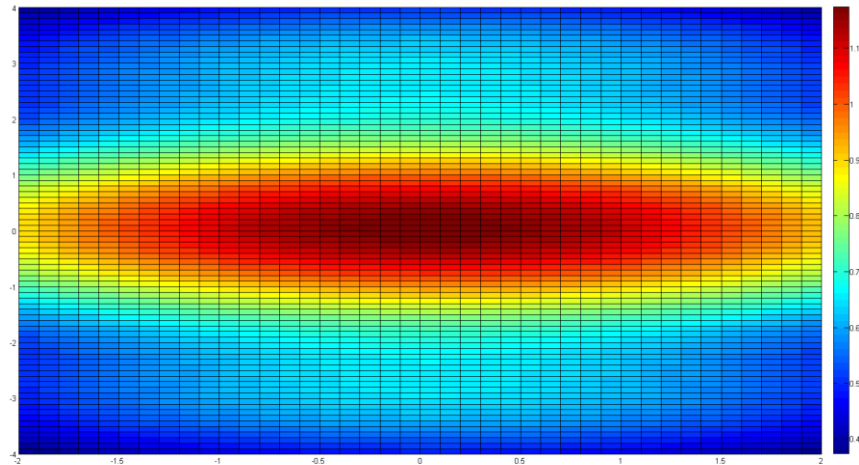
the result of accumulation of every point within the wave front. Figure 3.3 shows the calculation results of Eq(3.3).



(a)



(b)



(c)

Figure 3.3 Calculation Results for Rectangular Transducer using Eq(3.3). (a) the vibration amplitudes distribution calculated within a wave front in the near field. (b) the vibration amplitudes distribution calculated within a wave front in the near field but farther to the active surface. (c) the vibration amplitudes distribution calculated within a wave front in the far field. Whether a wave front is in the near field or far field is decided by the comparison between the distribution in the wave front and description of distribution in Section 3.1.1.

In Figure 3.3 (a) and Figure 3.3(b), it can be observed that in the near field, periodical changes happen in both horizontal direction and vertical direction within the rectangular plane. In Figure 3.3(c), it can be observed that in the far field, decrease happens in both horizontal direction and vertical direction within the rectangular plane as well.

The equation to calculate the near field distance of a rectangular plate transducers is similar to the equation of a circular disk transducers[16].It is described as:

$$F = k \frac{D^2}{4\lambda} \quad (3.4)$$

D is the length of diagonal of the rectangular plate . λ is the wavelength of ultrasound wave in the medium. k is a compensate constant related to the ratio of width and length[16].

Because the divergence of ultrasound beams from rectangular transducers is size-related, there is no accurate equation for calculation of divergence angle of rectangular plate transducers[16].

3.2 Model Building

The cylindrical transducer used in this project is a hollow cylindrical transducer with its sidewall being the active surface. Transducers of this type are usually used in medical research works[17,18].

Cylindrical transducers of this type have cylindrical wave fronts. A beam distribution plot is provided in figure 3.4[17]. It provides the beam distribution along a vertical line within a wave front in the near field. Periodical changes between peaks and troughs can also be observed in vibration amplitudes of points along the line.

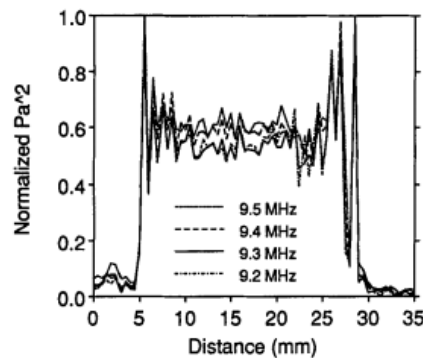


Figure 3.4 Ultrasound field distribution along a vertical line in the side wall[17]. The distribution of ultrasound waves with different frequencies along the same vertical line are illustrated.

It has been pointed out that a cylindrical transducer of this type can be modelled by rectangular transducers in distribution studies[17,18]. The active sidewall is considered as an array of rectangular plate transducers. In this project, a modeling method based on this idea was developed.

3.2.1 Description of The Modeling Method

In the modeling method proposed in this project, the thickness of transducer active surface is considered as an infinitesimal. Rectangular plate transducers are replaced with line sources as modeling elements. A line source is defined as a rectangular plate transducer with its width being infinitesimal.

The ultrasound waves generated by a line source of this type have cylindrical wave fronts, because they have characters of plane waves in direction parallel with the line and circular symmetric characters of sphere waves in the surface perpendicular to the line.

Figure 3.5 illustrates simulation results of vibration amplitudes distributions in a tangent planes of the cylindrical wave fronts of the line sources. Detail of the simulations carried out is provided in Section 3.3

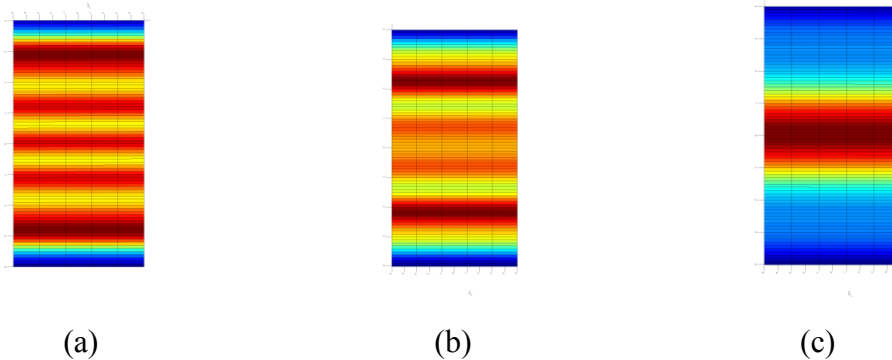


Figure 3.5 Simulation results of vibration amplitudes distribution in tangent planes of wave fronts for the line sources proposed in this project. (a) the vibration amplitudes distribution within a wave front in the near field. (b) the vibration amplitudes distribution within a wave front farther to the active surface in the near field. (c) the vibration amplitudes distribution within a wave front in the far field. Whether a wave front is in the near field or far field is decided by the comparison between the distribution in the wave front and description of distribution in Section 3.1.1. When the color changes from blue to red, the vibration amplitude of a point increases.

It can be inferred from the simulation results in Figure 3.5 that the vibration amplitudes distribution within a wave front of the line source is a stack of concentric rings. Vibration

amplitudes of all points on a single ring are same. Changes of vibration amplitudes follow descriptions in Section 3.1.1. A unique thing for the vibration amplitudes distribution of the line sources is that the vibration amplitudes distribution along the line direction is symmetric to the midpoint of the line.

3.2.2 Modeling of Well-studied Transducers

Line sources of this type can be used to study distributions of circular disk transducers and rectangular plate transducers. Therefore, modeling of these two well-studied structures can be used to validate the effectiveness of the modeling method. It is expected that the modeling results match with descriptions about vibration amplitudes distribution of the two structures[2,15].

The track of spinning a line by 360 degree with its midpoint being the spin center is a circular disk. The spin can be considered as spinning by $d\theta$ at a single step with total steps of $360/d\theta$, in which $d\theta$ is the angular infinitesimal. A circular disk transducer is modeled by placing a line source after every single spin step. Concentric rings with different diameters can be found on the circular disk surface. Due to the circular symmetry, for points on the same ring, the vibration amplitudes are same all the time after interferences. These concentric rings interfere with each other, forming plane wave fronts following patterns introduced in Section 3.1.1. It can be inferred that the periodical changes in the near field is represented by changes between vibration amplitudes of different rings. In addition, the decrease within a wave front in the far field starts from the center point to the edge of the circular.

The track of translating a line with certain distance L is a rectangle. The translation can be considered as translating by dL at a single step with total steps of L/dL , in which dL is the distance infinitesimal. A rectangular plate transducer is modeled by placing a line source after every single translation step. These line sources interfere with each other, forming plane wave fronts following patterns introduced in Section 3.1.1. However, there is no circular symmetry in rectangle. For a point within the rectangular plate, there are at most 3 symmetric counterparts, only which have the same interference effect on the vibration amplitudes with the point all the time. Therefore, it can be inferred that

periodical changes from peaks to troughs within a wave front in the near field happen in both the horizontal direction and vertical direction. In addition, the decrease within a wave front in the far field happens in both the horizontal direction and vertical direction.

The analysis using models built by line sources have similar results to the theoretical descriptions found in literature survey[2,15]. This fact contributes to the validation of the model building method.

3.2.3 Modeling of Cylindrical Transducers

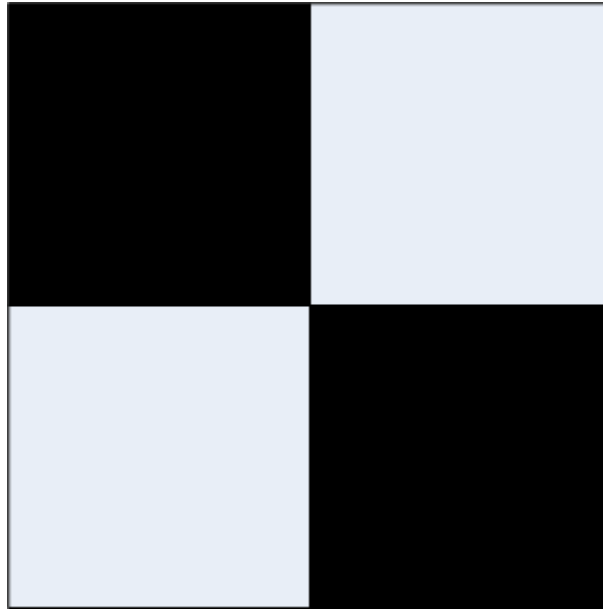
The track of moving a line along a circle with radius being R is a cylinder. The moving can be considered as moving by $Rd\theta$ at a single step with total steps of $2\pi/d\theta$, in which $d\theta$ is the angular infinitesimal. A cylindrical transducer is modeled by placing a line source after every single moving step. It is a 3-D structure. Part of the cylindrical forefront is always blocked by the cylindrical transducer. At certain time, for points within a single line, their interference range is a cylindrical shell. The shell is the result of wave forefront being intercepted by the cylindrical structure. The cut out angle of the cylindrical shell is a function of the radius of the forefront and the radius of the cylindrical structure. Within the shell, the interferences between points are similar to those of a rectangular plate. At certain time, the whole cylindrical transducer side wall is divided into multiple cylindrical shells with same cut out angles. Therefore, it can be inferred that the vibration amplitudes distribution of a cylindrical transducer modeled by the method proposed in this project should have similar patterns to the distribution of a rectangular plate transducer.

3.3 Simulation of The Equivalent Model

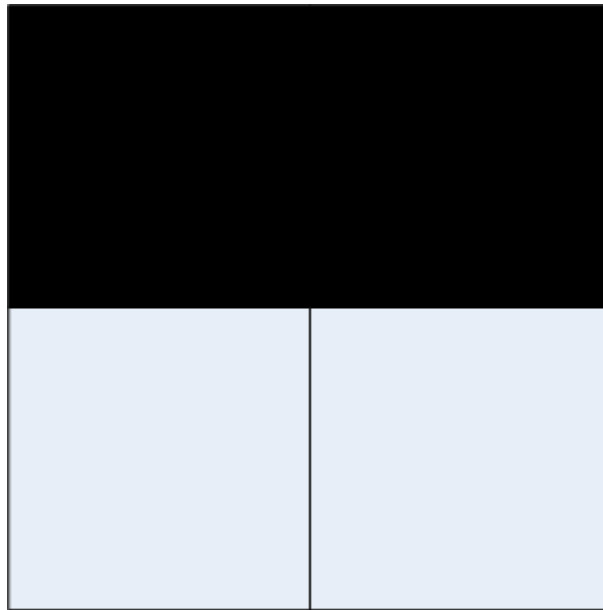
The acoustic simulation tool 'K-wave' has been introduced in Chapter 2. In this project, simulations for a circular disk transducer and simulations for a rectangular plate transducer were carried out first to validate the effectiveness of the simulation tool. The effectiveness of 'K-wave' was validated in this project. Then, the simulations for a elemental line source in the modeling method proposed were carried out to study the vibration amplitudes distribution of the transducer beams from transducers of this type. In

addition, simulations for the cylindrical transducer were carried out to provide reference for validation of the vibration amplitudes distribution inferred from the model built using line sources.

The definition of 'being adjacent ' in 'K-wave' is illustrated in Figure 3.6.



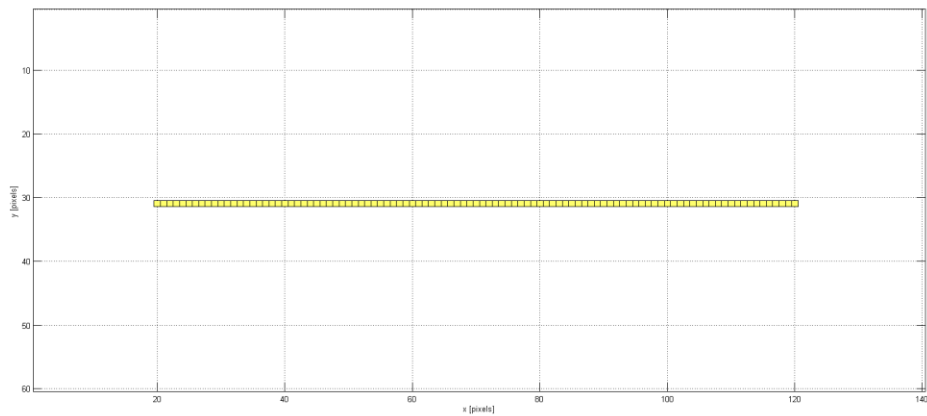
(a)



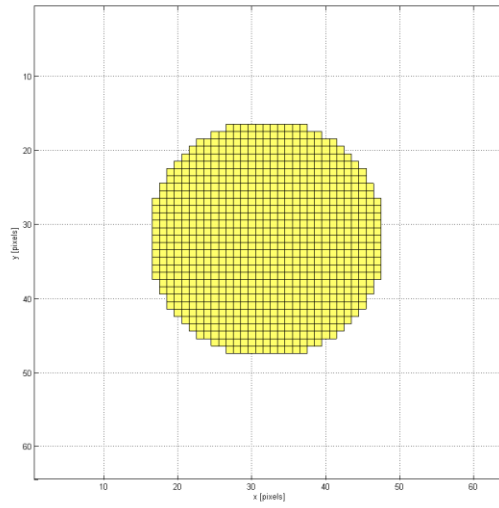
(b)

Figure 3.6 Definition of 'adjacent grids' in 'K-wave'. In both (a) and (b), the black blocks are occupied by geometric structures. They are both considered as 'adjacent' in 'K-wave'.

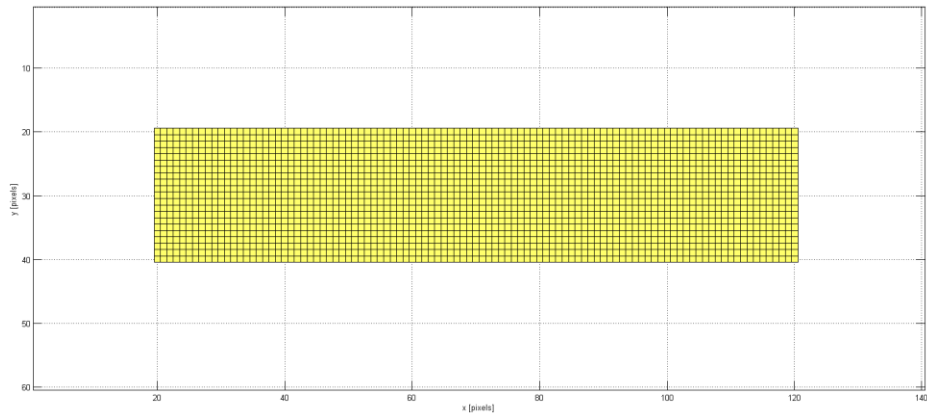
Figure 3.7 illustrates examples of implementation of a line source, a circular structure and a rectangular structure in 'K-wave'. There is a noticeable thing in the examples of implementation. It can be inferred from the definition of 'adjacent grids' that the implementation of circular disk structure and rectangular plate structure in 'K-wave' can be automatically considered as models built in the method proposed in this project. Therefore, it can be inferred that the validation of the effectiveness of 'K-wave' can validate the effectiveness of the model building method proposed in Section 3.2 at the same time by providing simulation results matching the theoretical descriptions for these well-studied structures.



(a)



(b)



(c)

Figure 3.7 Examples of geometric structures in 'K-wave'. (a) the implementation of a line. (b) the implementation of a circular disk. (c) the implementation of a rectangular plate.

3.3.1 Global Environment Settings

Global environment settings are required for every simulation run in 'K-wave'. Global environment settings include computational domain definitions and medium property settings.

Computational domain definitions start from definition of simulation dimensions. 1-dimensional simulations, 2-dimensional simulations and 3-dimensional simulations can all be run in 'K-wave'. Symbols 'x', 'y' and 'z' are used to represent dimensional vectors, which are vertical to each other. After the determination of computational domain dimensions, total amount of grids at each dimension is decided. Symbols 'Nx', 'Ny', and 'Nz' are used to represent the total amount of grids along vectors of 'x', 'y' and 'z'. Total amount of grids within a 1-dimensional domain is Nx. The amount is Nx*Ny within a 2-dimensional domain. The amount is Nx*Ny*Nz within a 3-dimensional domain. Then, size of each grid is defined by assigning values to symbols 'dx', 'dy', 'dz'. Medium property settings include settings of propagation speed, density, attenuation coefficient, attenuation exponent power and non linearity constant. Global environment settings decide the highest frequency of ultrasound waves that can propagate in the domain.

Simulations run in this project were 3-dimensional simulations. Size of the computational domain for simulation of circular disk transducer was 160*160*160. The size of a single grid was 0.25(mm)*0.25(mm)*0.25(mm). Propagation speed of the medium was set to 1540m/s. Medium density was set to 1000kg/m³. Attenuation coefficient was set to 0.002dB/MHz^y*cm⁻¹. Attenuation exponent power was set to 2. Non linearity constant was set to 6. The settings are the same as the properties of degassed water.

Size of computational domain for simulation of rectangular plate was 160*300*160. The size of a single grid was 0.25(mm)*0.25(mm)*0.25(mm). The medium property settings were the same as the settings for circular disk transducers. Global environment settings of simulations for an elemental line source and a cylindrical transducer were the same as the settings for those of simulations for a rectangular plate.

Settings for Table 3.1 shows the global environment settings of simulation carried out in this project.

Table 3.1 Global Environment Settings for Simulation

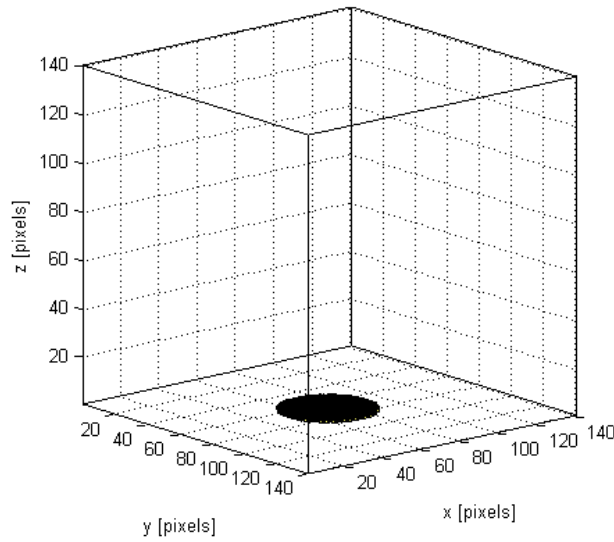
Parameter	Circular Disk	Rectangular plate, elemental line source, cylindrical transducer
Propagation Speed	1540m/s	
Media Density	1000kg/m ³	
Attenuation Coefficient	0.002dB/MHz ^y *cm ⁻¹	
Attenuation Exponent Power	2	
Non linearity Constant	6	
Nx	160	160
Ny	160	300
Nz	160	160
dx	0.25mm	0.25mm
dy	0.25mm	0.25mm
dz	0.25mm	0.25mm

3.3.2 Simulation Steps

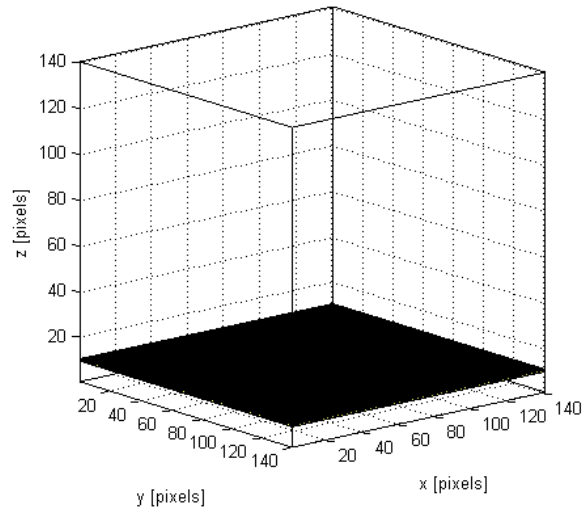
The first step to run a simulation in 'K-wave' is to build a source mask. A source mask defines the shape, position and size of a source. Second, a sensor mask is built. Sensor mask defines the shape, position and size of the data-recording sensors. Then, a source function is defined, which defines the excitation signal. Some optional settings like recording movies for a simulation, displaying the sensor mask and source mask, and the types of data recorded can be done as well by assigning values to corresponding parameters. A simulation is run by calling the K-wave simulation function.

In simulations of the circular disk, the source mask was built as a circular disk with same size as the real transducer used in this project. Sensor mask was built as a rectangle covering the entire wave front selected. Source function was defined as sine function. The frequency of the sine function was set to 1.5MHz. The amplitude of the function was set to 1 MPa. Duration of the excitation signal was set to 1 us. The type of data recorded was set to root mean square of pressure recorded over the duration of excitation signal. Source mask and sensor mask were set to be displayed after the simulation was done. In simulations for rectangular plate, the source mask was built as a rectangle. Its length was the same as the height of the cylindrical transducer. Its width was set to πD , in which D was the diameter of the cylindrical transducer. Other settings were the same as the

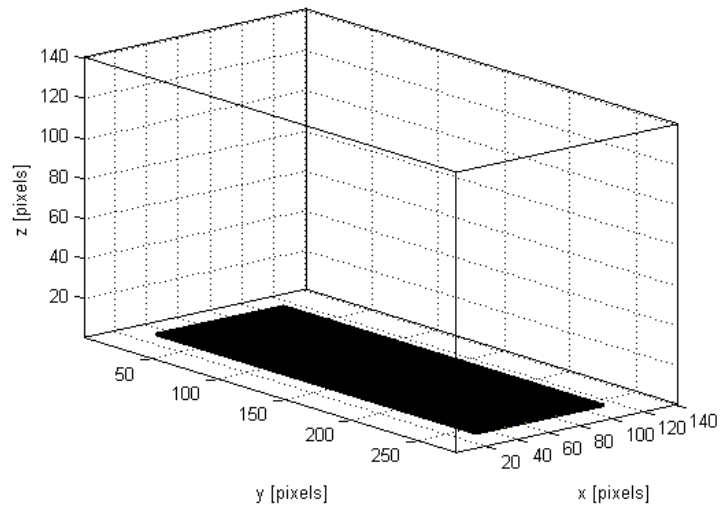
settings in simulations for circular disk. In simulations for a elemental line source, the source mask was a line formed by 100 grids in a row. Other settings of the simulations were the same as those of previous ones. In simulations of a cylindrical transducer, the source mask and the sensor mask were concentric cylinders. The height of the source mask took 64 grids, which was the same as the height of the sensor mask. The radius of the source mask took 16 grids. Amplitude of the vibration signal was set to 2Pa. Other settings were the same as those of previous ones. Source masks and sensor masks for transducers are illustrated in Figure 3.8.



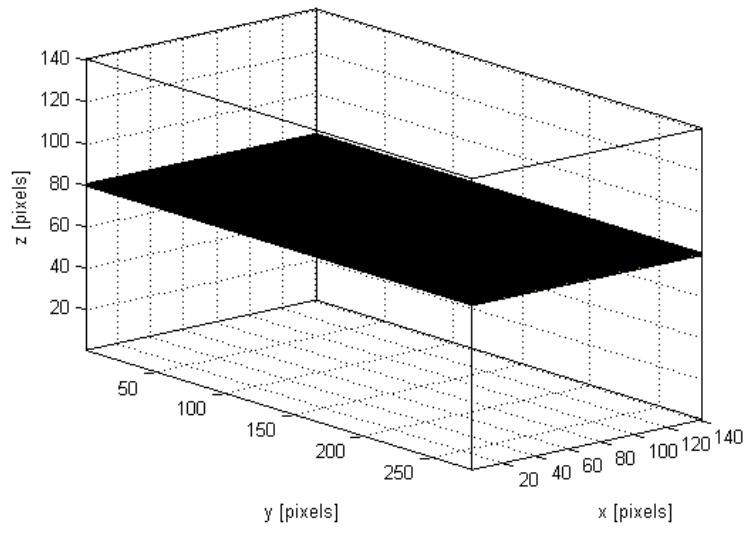
(a)



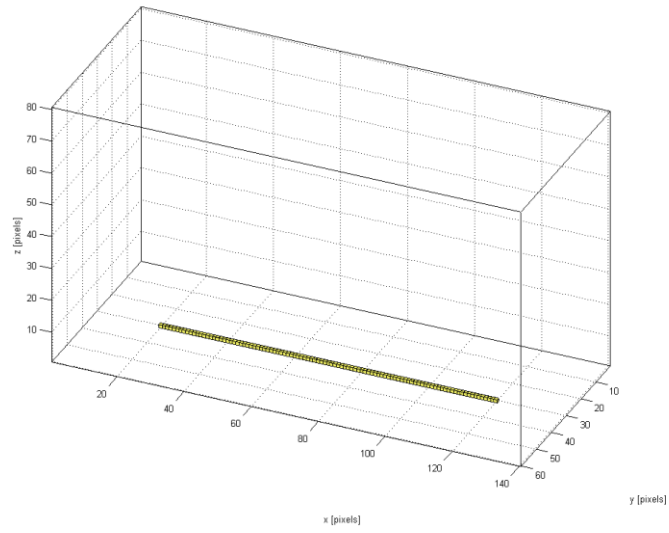
(b)



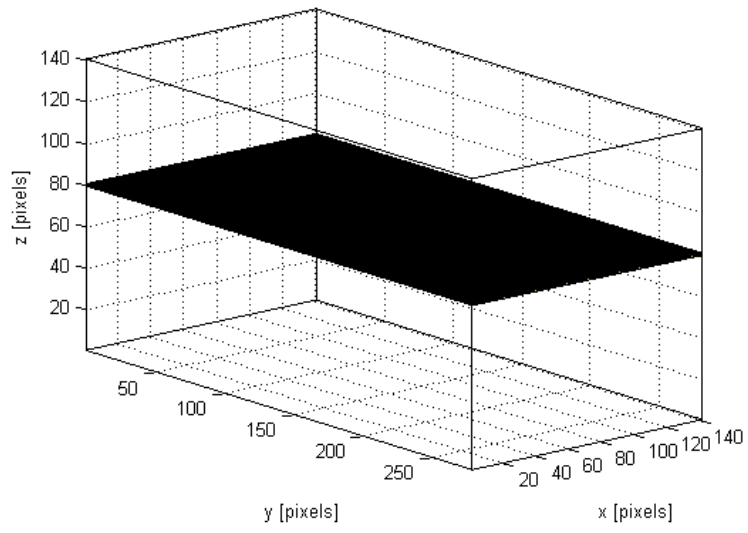
(c)



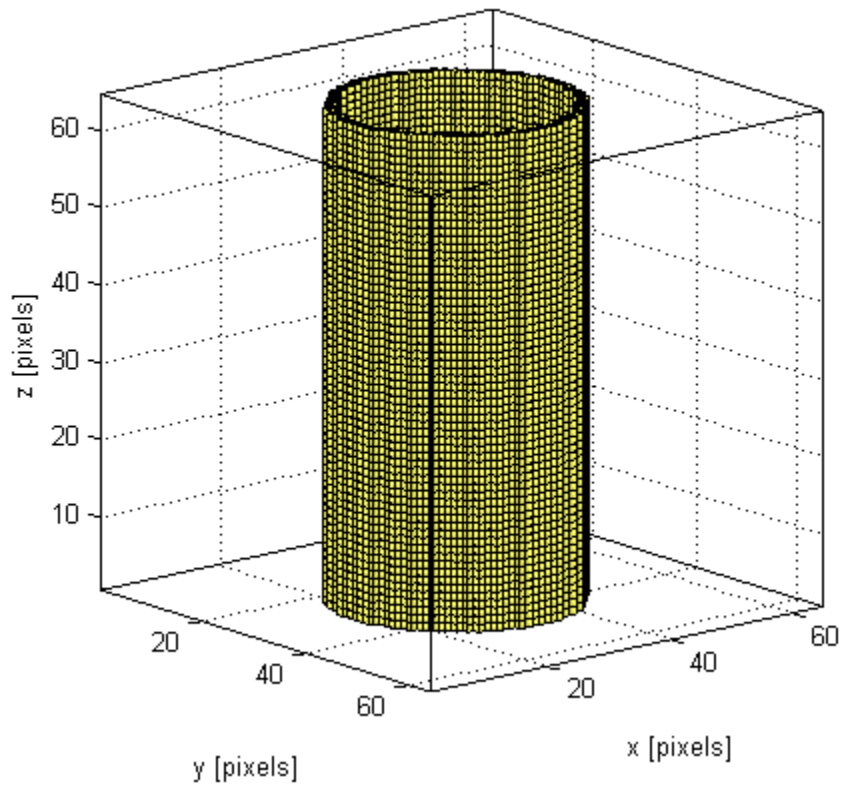
(d)



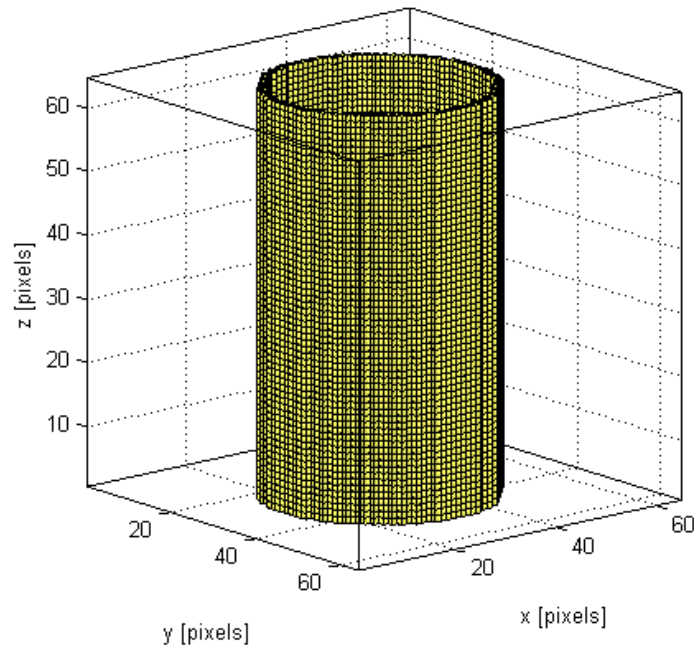
(e)



(f)



(g)



(h)

Figure 3.8 Source array and sensors arrays built for simulations in this project. (a) the source mask built for a circular disk. (b) the sensor mask built for (a) . (c) the source mask built for a rectangular plate transducer. (d) the sensor mask built for (c). (e) the source mask built for an elemental line source. (f) the sensor mask built for (e). (g) the source mask built for a cylinder. (h) the sensor mask built for (g)

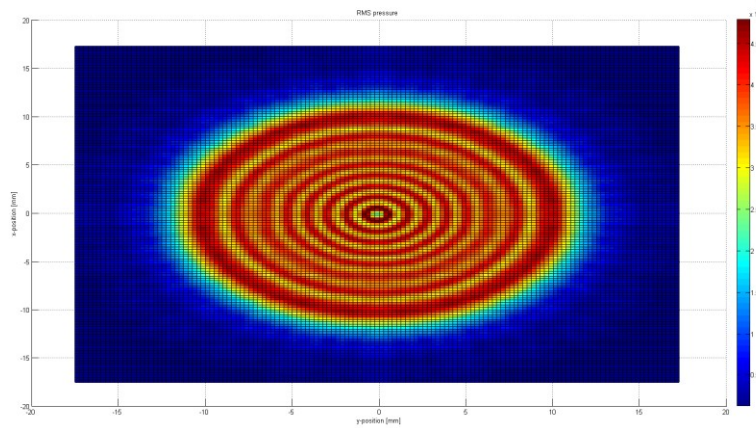
For the circular disk, the rectangular plate and the elemental line source, simulations were run three times. The first time was for vibration amplitudes distribution closer to the active source in the near field. The second time was for the distribution farther in the near field. The third time was for the distribution in the far field. For the cylinder transducer, the computational domain for a simulation of distribution in the far field is so large that it takes over 24 hours to run the simulation. So, no simulations for the distribution of the cylinder in the far field were carried out.

3.3.3 Results and Discussions

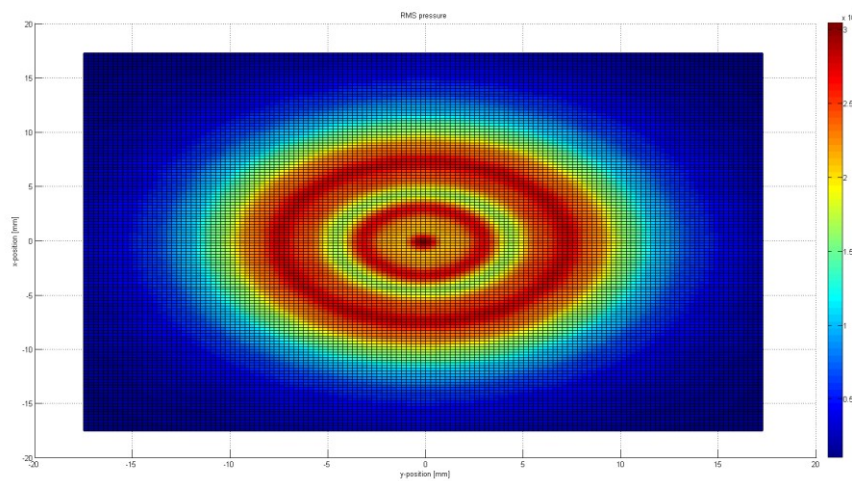
Simulation results in this section are all vibration amplitudes distribution in pressure. The data returned was a $(N \times 1)$ array. N is the total amount of grids in the sensor mask. In

order to display the data in a 2-dimensional figure, the data was reshaped into a $(M \times H)$ array, in which H is the length or the height of the sensor mask, and M is N/H . Reshaping of the data was implemented by function '*reshape()*' in MATLAB 2012b. All figures provided in this section are 2-dimensional figures made by '*Surf()*' function in MATLAB2012b.

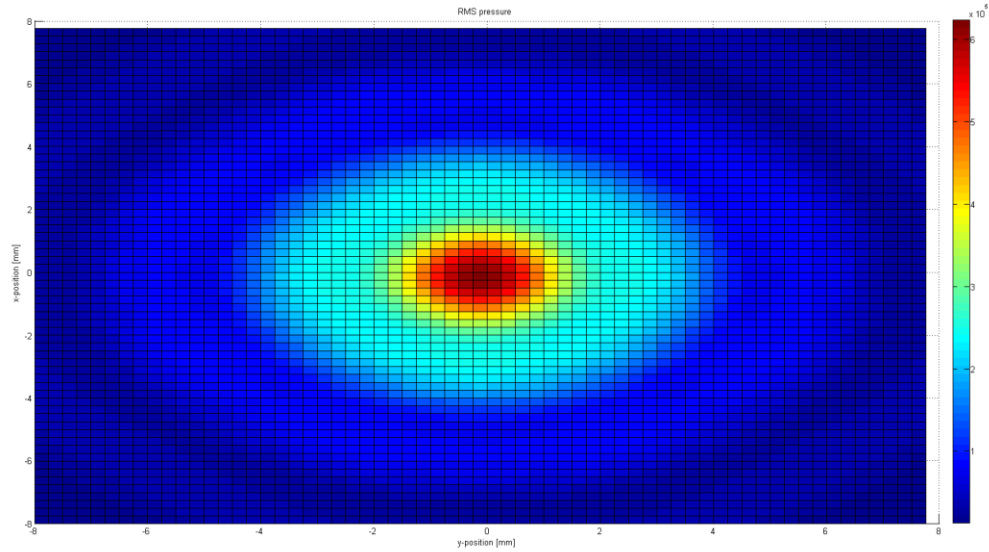
Simulation results for vibration amplitudes distribution of the circular disk are shown in Figure 3.9.



(a)



(b)

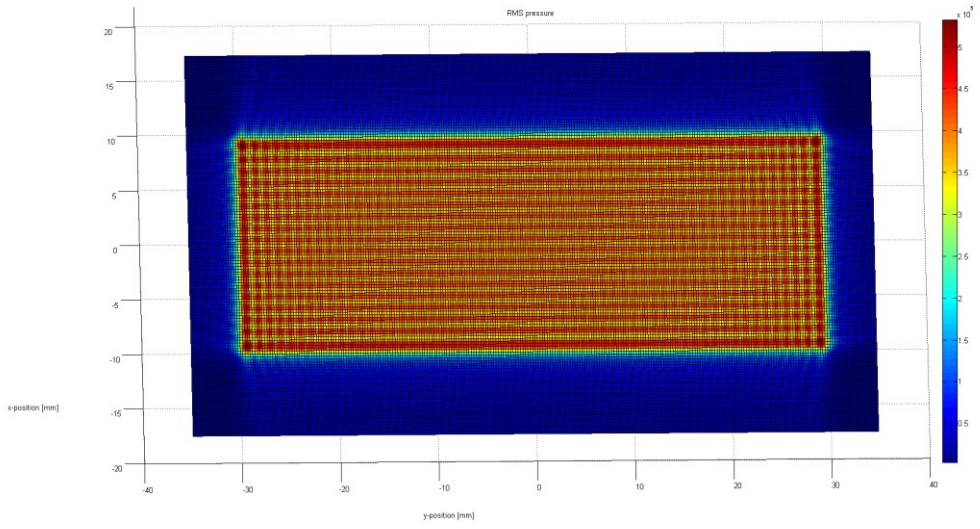


(c)

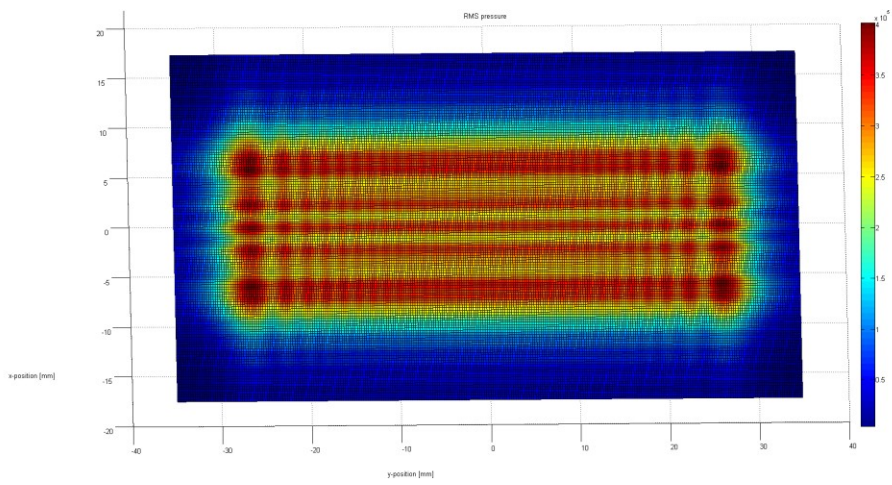
Figure 3.9 Simulation results of vibration amplitudes distribution in tangent planes of wave fronts for the line sources proposed in this project.(a) the vibration amplitudes distribution within a wave front in the near field. (b) the vibration amplitudes distribution within a wave front farther to the active surface in the near field. (c) the vibration amplitudes distribution within a wave front in the far field. Whether a wave front is in the near field or far field is decided by the comparison between the distribution in the wave front and description of distribution in Section 3.1.1. Color bars show the relationship between colors and amplitudes. When the color changes from blue to red, the vibration amplitude of a point increases.

It is observed that the simulation results shown in Figure 3.11 match well with theoretical descriptions[2] and the description provided by the model built in Section 3.2.

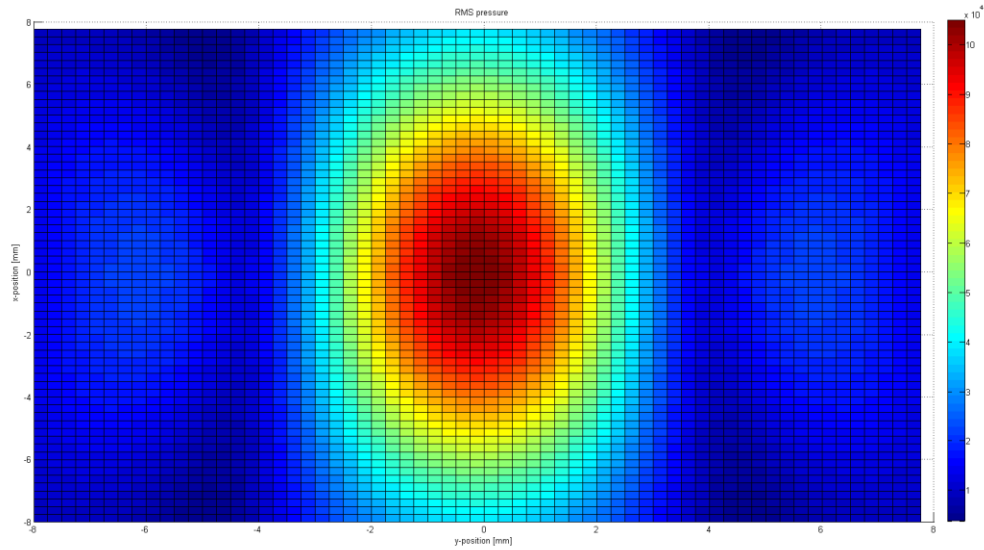
Simulation results for vibration amplitudes distribution of rectangular model for cylindrical transducers are illustrated in Figure 3.10.



(a)



(b)



(c)

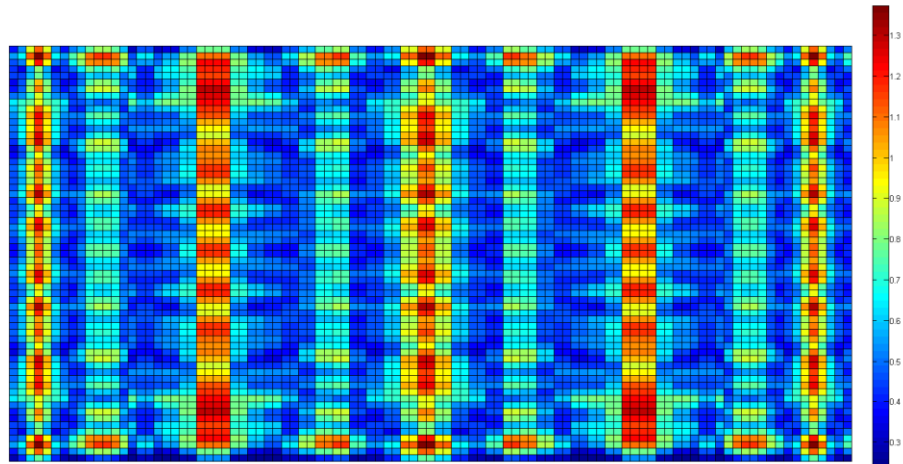
Figure 3.10 Simulation results of vibration amplitudes distribution in tangent planes of wave fronts for the line sources proposed in this project. (a) the vibration amplitudes distribution within a wave front in the near field. (b) the vibration amplitudes distribution within a wave front farther to the active surface in the near field. (c) the vibration amplitudes distribution within a wave front in the far field. Whether a wave front is in the near field or far field is decided by the comparison between the distribution in the wave front and description of distribution in Section 3.1.1. Color bars show the relationship between colors and amplitudes. When the color changes from blue to red, the vibration amplitude of a point increases.

The results shown in Figure 3.10 match well with the calculation of Eq (3.2) and the description by the model built in Section 3.2.

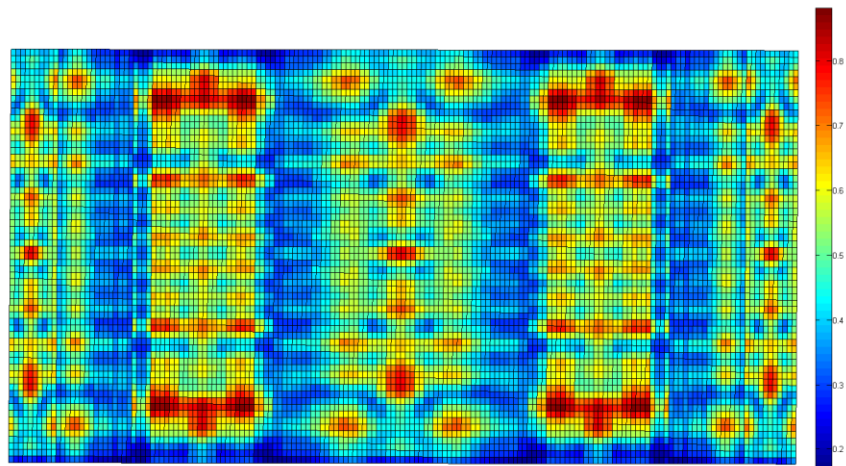
The simulation results of the circular disk and the rectangular plate validate both the effectiveness of the 'K-wave' and the effectiveness of the model building method for distribution study in this project.

Simulation results for the elemental line source have been provided in Figure 3.5.

Simulation results for the cylindrical transducer are illustrated in Figure 3.11.



(a)



(b)

Figure 3.11 Simulation results for the cylinder. (a) the vibration amplitudes distribution in a wave front closer to the cylinder in the near field. (b) the vibration amplitudes distribution in a wave front farther to the cylinder in the near field. Color bars show the relationship between colors and amplitudes. When the color changes from blue to red, the vibration amplitude of a point increases.

It can be observed in Figure 3.13 that the periodical changes from peaks to troughs in vibration amplitudes distribution in the near field of a cylinder happen in both the horizontal direction and vertical direction. The description of the distribution provided by the model built in Section 3.2 matches with the simulation results well.

So far, the effectiveness of the model building method proposed in Section 3.2 has been validated by simulation. In this project, in addition to the simulations, experiments were carried out to validate the method and the distribution of cylindrical transducer described by the method.

3.4 Experiment Materials and Methods

3.4.1 Hydrophone Related Preparation

It has been demonstrated that hydrophones are suitable tools for ultrasound pressure measurement, with the merits including small size, high sensitivity, omnidirectional measurement, high stability, broadband flat frequency response, non-perturbing structure and linearity[1]. In experiments of this project, a hydrophone system provided by Precision Acoustic™ was used to measure and characterize the ultrasound field produced by transducers. To make comparatively accurate measurements, certain preparations were made.

A proper medium is required for the measurement using hydrophones. In this project, water was used as the propagation medium in experiments of circular disk transducers. Water is cheap and convenient to use. In addition, transducers in this project are mainly used for renewable energy production related to metabolic behaviour of algae and yeasts, which is carried out in aquatic environment. Generally, measurements involving hydrophones have requirement on purity and conductivity of medium[1]. A higher purity of the medium can reduce the possibility of deposition on active elements of hydrophones, which reduces the sensitivity or cause damage. Requirement for conductivity has similar reasons[1]. Another problem of medium is the generation of air bubbles. Air bubbles sometimes attach on the active elements of hydrophones. Therefore, degassed water was used. The source of the water was tap water. It was boiled for degassing. In this project, hydrophones were soaked for 40 minutes in the medium before the measurement[1]. For

the cylindrical transducer, ultrasound conductive gel provided by Ultra Phonic™ was used. The properties of the gel is similar to the properties of degassed water.

Hydrophone probes transform mechanical signal into electrical signals. To observe the output, an oscilloscope with certain resolution is required. In this project, a Tektronix TDS 2012B oscilloscope was used.

3.4.2 Transducer Related Preparation

Ultrasound waves are highly directional, therefore, experiments characterizing ultrasound field distribution require alignment and movement of probes[1]. A mount that can clamp hydrophones is recommended to use. The mount should have three degrees of freedom to accurate characterization of ultrasound field. This fact is because that: first of all, the mount should allow the movement of the hydrophone probe in the wave front surface. A free movement in the surface requires at most 2 degrees of freedom. Second, movement along the propagation direction is required for more comprehensive observation of changes introduced in Section 3.1.1. In the experiment carried out in this project, a mount with 3 degrees of freedom was used. Table 3.2 provides details about the movement in each direction. X, Y and Z represent 3 degrees of freedoms that are vertical to each other. Figure 3.12 shows the mount used in this project.

Table 3.2 Information about Degrees of Freedom for the Mount Used

	X	Y	Z
Movement Range (mm)	-5-30	0-30	0-30
Scale Division (mm)	1		

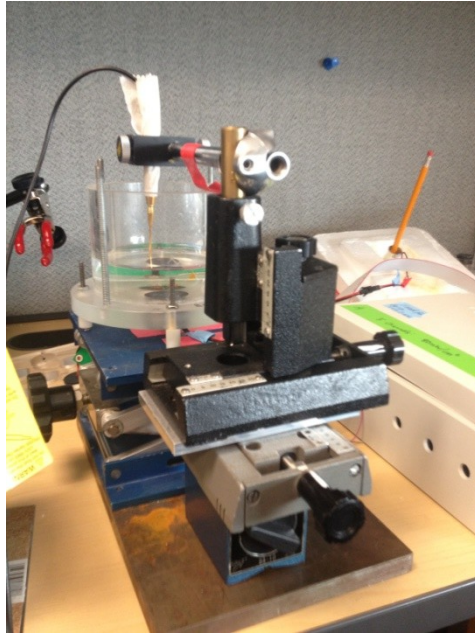


Figure 3.12 The mount with 3 degrees of freedom used in experiments in this project. The movement at each degree of freedom is implemented by adjusting the one of the three screws.

Both circular disk transducers and cylindrical transducers used in the experiment had been used in experiments of ultrasound stimulated renewable energy production before[11]. They were manufactured by American PiezoTM. Pictures for the transducer used are shown in Figure 3.13. Table 3.3 provides the dimensional detail of active working surface of the transducers.

In this project, for circular disk transducers, a plastic holder with holes at the bottom was used. It was manufactured by machine shop of University of Alberta. The dimension of the hole is the same to the dimension of the circular transducers[11]. Since the holder for cylindrical transducer is not commercially available, a simple holder was made using foam plastic box. A ditch was dug at a depth of the transducer's height with a length around 15cm and a width around 10cm. During the measurements, the ditch was filled with ultrasound medium gel mentioned above. A wooden stick was plugged into the ditch, keeping a distance around 1cm to the closed terminal of the ditch. The stick was used to make the cylindrical transducer stable. The active surface of the cylindrical transducer is

its sidewall, so directly putting it on the foam plastic platform didn't affect its output much.



(a)



(b)

Figure 3.13 Transducers used in experiments. (a) one of the circular disk transducers. (b) one of the hollow cylindrical transducers

Table 3.3 Dimension Information of Transducers.

Transducer Type	Dimension of Active Elements		
Circular Disk Transducer	Radius of Active Element(mm)		
	12		
Cylindrical Transducer	Outer Diameter(mm)	Inner Diameter(mm)	Height(mm)
	19	16	20

To drive the transducer, an ultrasound driving circuit was used. The circuit was designed by the BINARY research group[6]. It can provide pulses at 1.5 MHz with a duty ratio of 2:8. The same driving box had been used in renewable energy production experiments[11]. Table 3.4 provides the list of all devices and apparatuses used in the experiments carried out in this project. Figure 3.14 shows how the devices and apparatuses were connected during experiments.

Table 3.4 Devices and Apparatuses Used in Experiments

Name	Amount	Description
Circular disk transducer	1	The active surface is one of its bottom surface
Cylindrical Transducer	1	The active surface of this hollow cylindrical transducer is its sidewall

Transducer Holder	2	One is a plastic holder with a qualified tightness for water, which is used for circular disk transducer. The other one is a hand-made holder for cylindrical transducer made by foam plastic.
Mount	1	The mount has 3 degrees of freedom. The movement range of each degree is -5-30mm, 0-30mm,0-30mm respectively.
Hydrophone System	1	The system includes a hydrophone probe and a DC coupler with power.
Oscilloscope	1	The oscilloscope is a two-channel digital oscilloscope with a maximum frequency of 100MHz



(a)



(b)

Figure 3.14 Apparatuses and devices after connection. (a) the setting up for circular transducer experiment and measurement. (b) the setting up for cylindrical transducer and measurement.

3.4.3 Experiment Method

Figure 3.15 illustrates the spatial relationship between transducers and the degrees of freedom of the mount used.

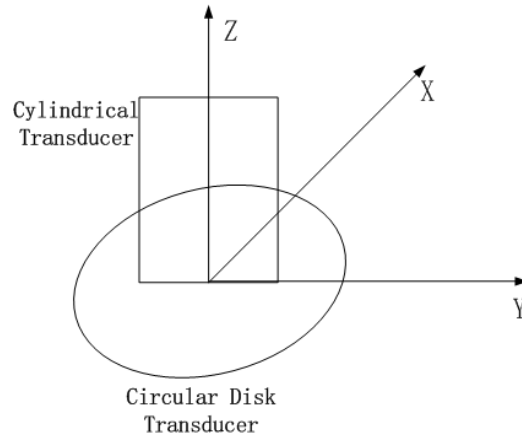


Figure 3.15. The spatial relationship between each degree of freedom and the projection of active surfaces of the transducer on them.

3.4.3.1 Circular Disk Transducer

The measurements using the circular disk transducer were carried out in the following way: The degree of freedom Z on the mount was used to set the distance of the hydrophone probe to the circular active surface. The distance was set to 7mm and 30mm for measurements within near field. The near field distance of the circular disk transducer is 14 cm, which is higher than the height of the holder. Therefore, measurements for far field was not available. Measurements were carried out along diameter lines. For measurements of a single diameter line, first of all, the degrees of freedom X or Y was used for measurements within the selected wave front. The position of minimum value on the degree selected was aligned to one end of a diameter as the start point of measurements. The end point the measurements was the other end of the diameter. Movements were made with a step length of 0.5 mm, followed by recording of readings on the oscilloscope. Measurements along a diameter were carried out 16 times in total. Averaged result of 16 readings was considered as the final reading. In order to learn more about the vibration amplitudes distribution within the whole wave front selected, the holder was spun by 120 degree after measurements along one diameter line was done.

3.4.3.2 Cylindrical Transducer

The measurements using the cylindrical transducer were carried out in the following way: The degree of freedom X on the mount was used to set the distance of the hydrophone probe to the active surface. The distance was set to 1 mm and 10 mm for measurements within the near field. The near field distance of the cylindrical transducer is 99 cm, which is longer than the length of the holder. Therefore, measurements for the far field was not available.

Measurements were taken along height lines of the cylindrical transducer in the vertical direction. The degree of freedom Z was used for measurements within the wave front at selected distance. The ultrasound conductive gel used as medium in cylindrical transducer measurements has a higher viscosity than the degassed water used in circular plate transducer measurements. When the probe is moving inside the gel, the impact on the uniformity of the gel is more significant than the impact on the that of degassed water. The measurements at higher positions are less accurate. Therefore, the measurements for cylindrical transducer started from position of 2.5mm to position of 14.5mm on the degree of freedom Z. For measurements of a single height line, first of all, the position of 0.0 mm on the degree Z was aligned to one end of a height line in order to align the hydrophone probe to the height line selected. Then the hydrophone probe was moved to position of 2.5mm on the degree, which was set as the start point. Movements were made with a step length of 0.5 mm, following by recording of readings on the oscilloscope. Measurements along the diameter line were carried out 16 times in total. Averaged result of 16 readings was considered as the final reading. In order to learn more about the vibration amplitudes distribution within the whole cylindrical wave front selected, the cylindrical transducer was spun by 60 degree after measurements along one height line was done.

3.5 Data Processing

Readings on the oscilloscope was peak-to-peak voltage. The readings were transformed back to vibration amplitudes in unit of MPa using Eq 3.5[1]:

$$P = \frac{V_{pp}}{2 \cdot SC} \quad (3.5)$$

V_{pp} is the peak-to-peak voltage. SC is the sensitivity coefficient. P is the amplitude in unit MPa.

Sensitivity coefficient is related to the frequency of ultrasound waves. It was set to 550 according to Figure 3.16. Figure 3.16 illustrates the relationship between sensitivity coefficients and ultrasound driving frequencies. It is from the user manual of the hydrophone used.

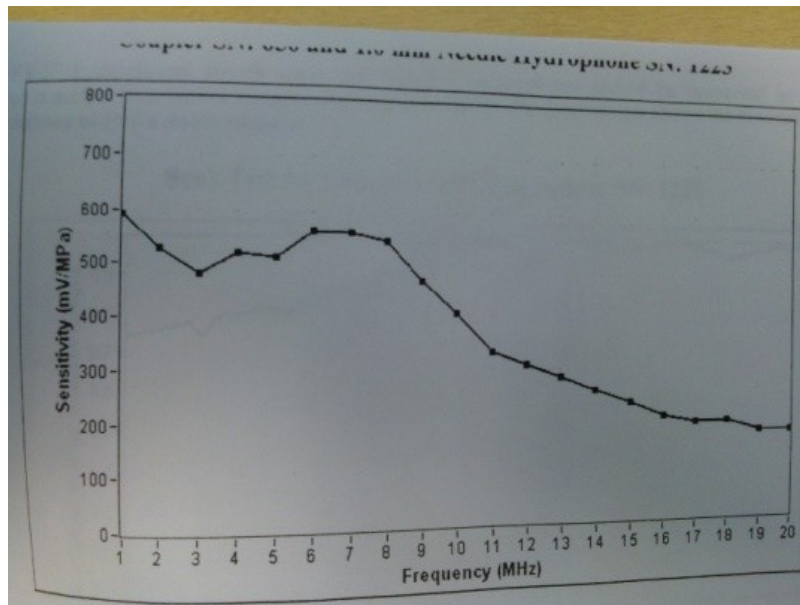
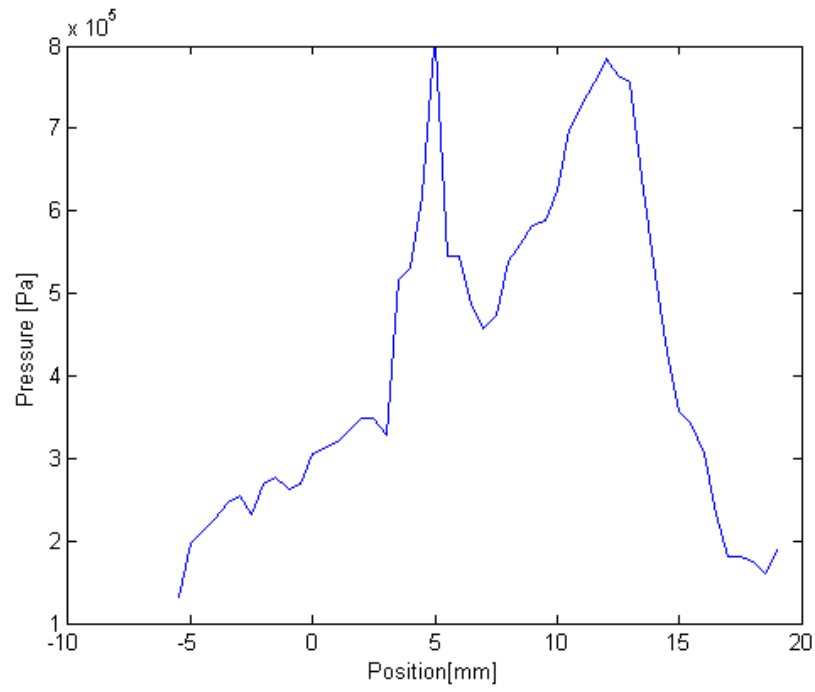


Figure 3.16 Relationship between sensitivity coefficients and ultrasound frequencies of the hydrophone used

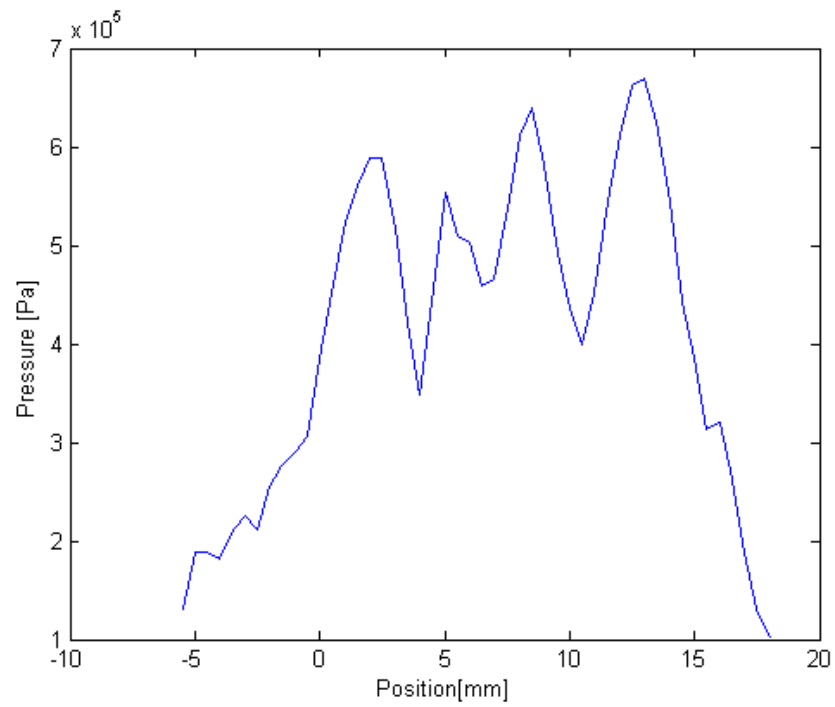
3.6 Discussion

3.6.1 Curves for Circular Disk Transducers

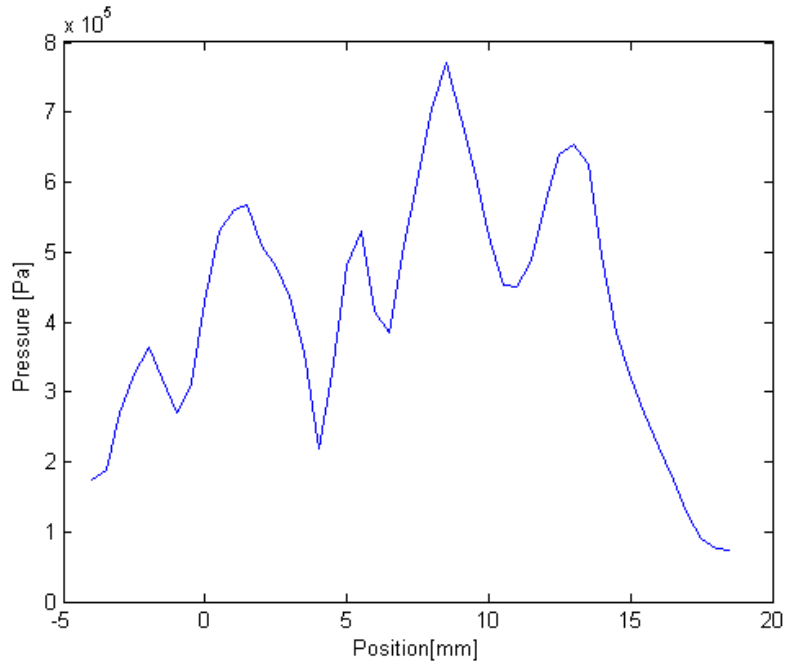
Curves of vibration amplitudes measurement along diameter lines selected are shown in Figure 3.17



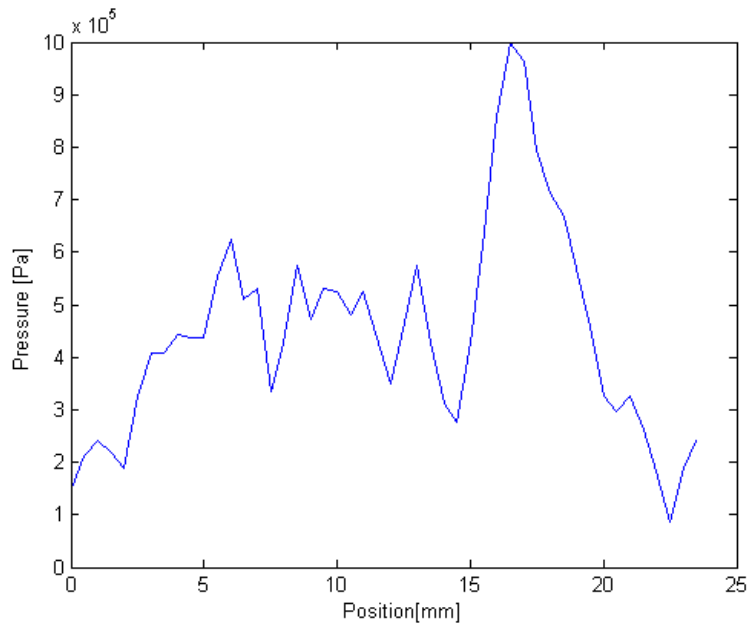
(a)



(b)



(c)



(d)

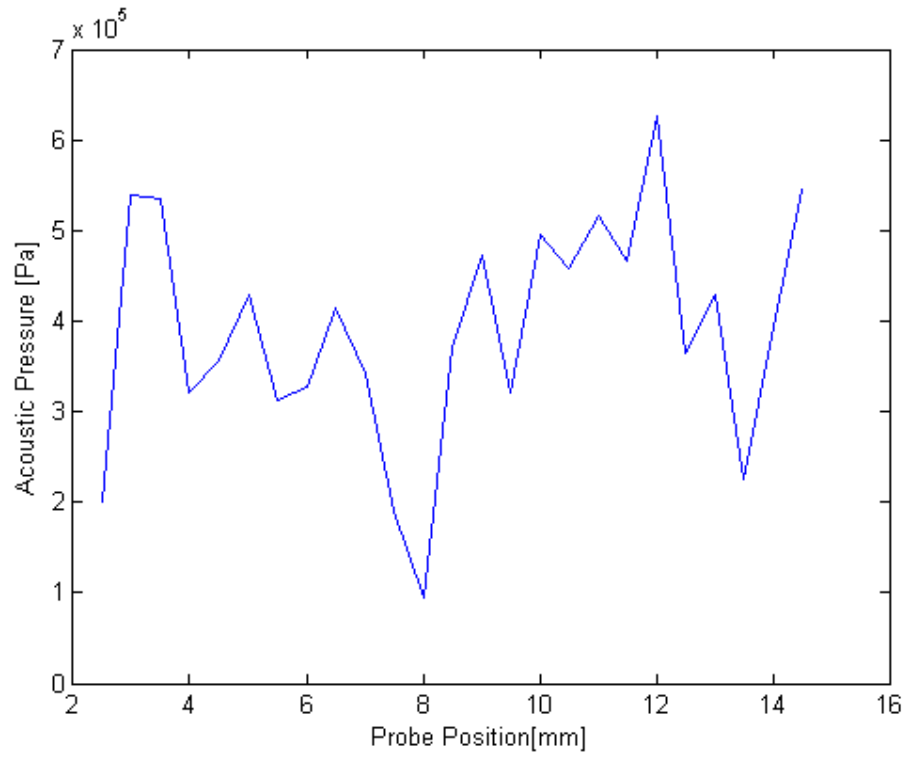
Figure 3.17 Curves of vibration amplitudes distribution measured along diameter lines of the circular disk transducer. (a) the measurement results along a diameter line. (b) the measurement results after the holder was spun by 120 degree. (c) the measurement results

after the holder was spun by 240 degree. (d) the vibration amplitudes distribution along the same diameter line as the one in (a) within a wave front further to the active surface. (a), (b), and (c) are measurements result within the same wave front. For all plots, Y axis is the measured ultrasound amplitude. X axis is the position within a diameter. The distance to the active surface is 30mm. The distance of wave front selected in (d) to the active surface is 7mm.

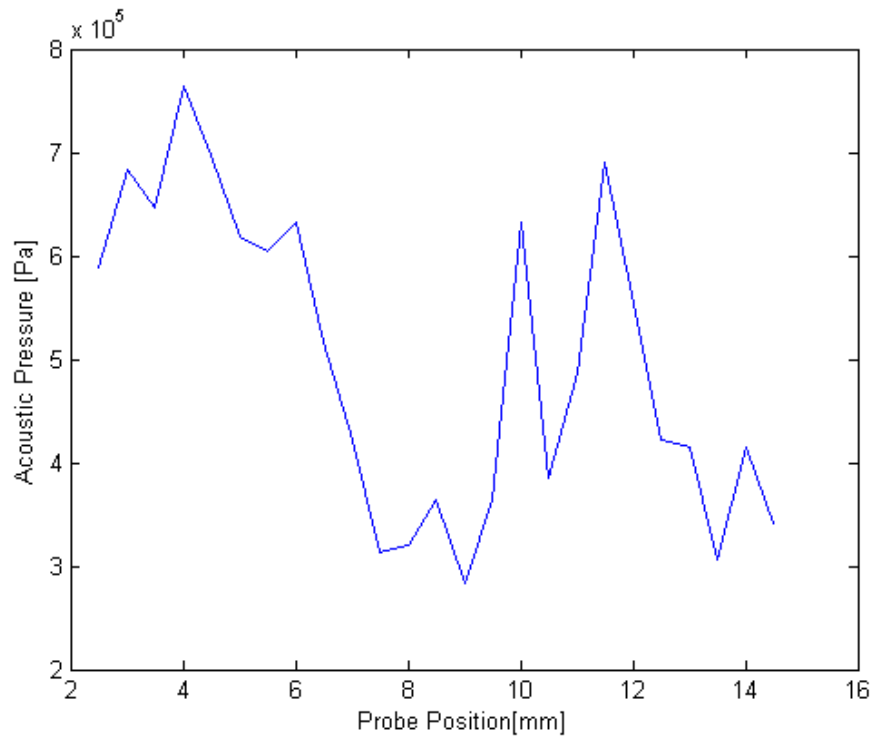
Periodical changes between peaks and troughs can be observed in Figure 3.17. Difference in frequency of the changes can be observed by comparing curves of Figure 3.17(a) and 3.17(d). Changes along the diameter line shown in Figure 3.17(d), which is closer to the active surface, are more frequent than the changes along same diameter line farther to the active surface, which are shown in Figure 3.17(a). These facts match with descriptions in Section 3.1 about vibration amplitudes distributions within the near field of an ultrasound beam from a circular disk transducer.

3.6.2 Curves for Cylindrical Transducers

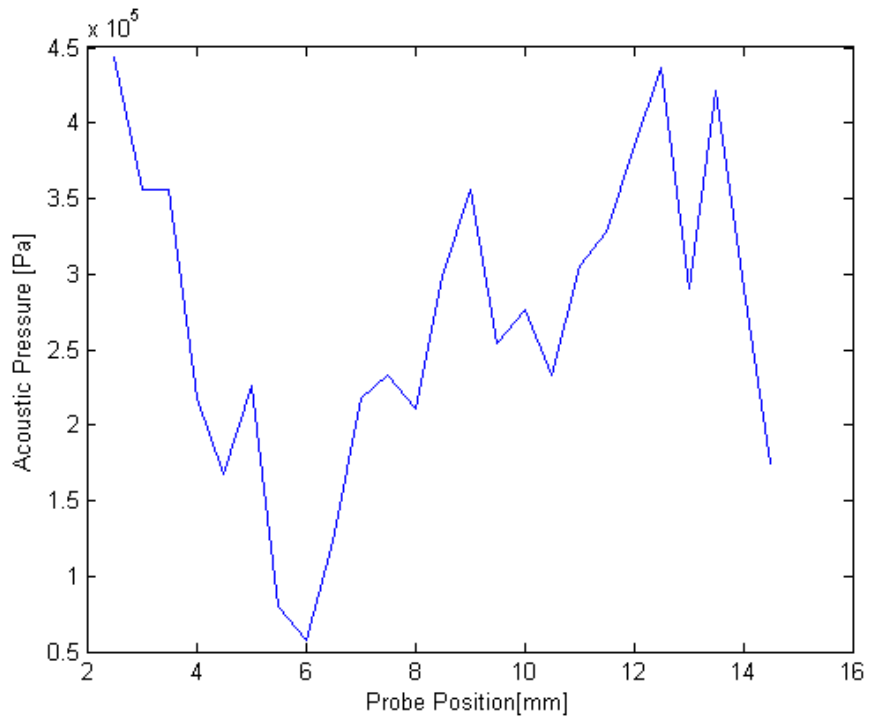
Curves of vibration amplitudes distributions along different height lines are shown in Figure 3.18. The distance of probe to the active surface is 1 mm.



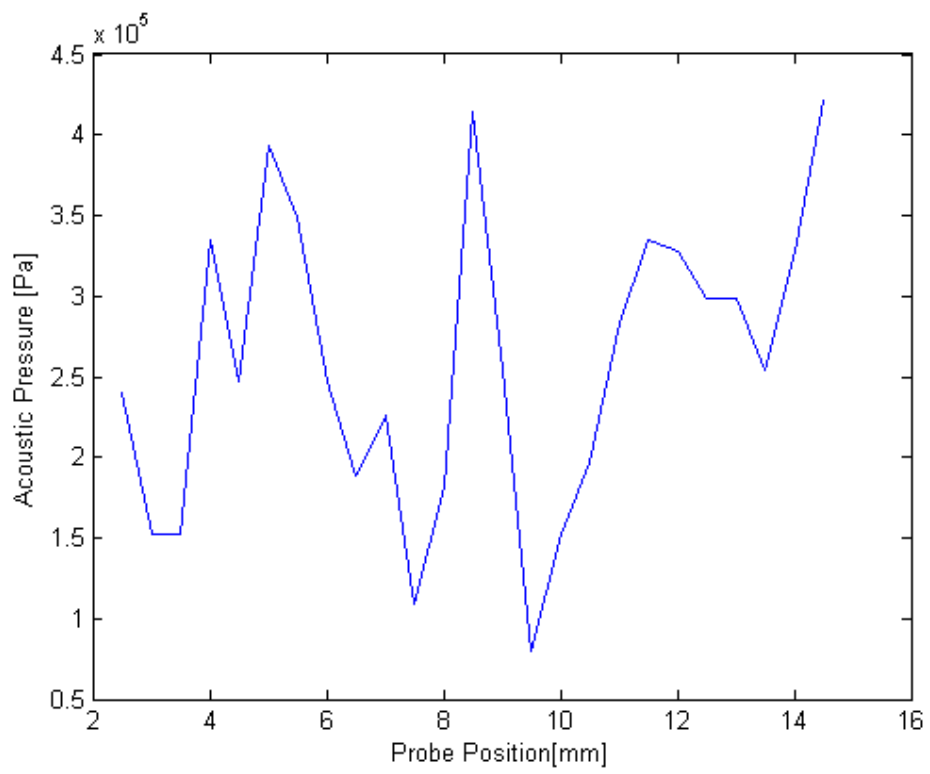
(a)



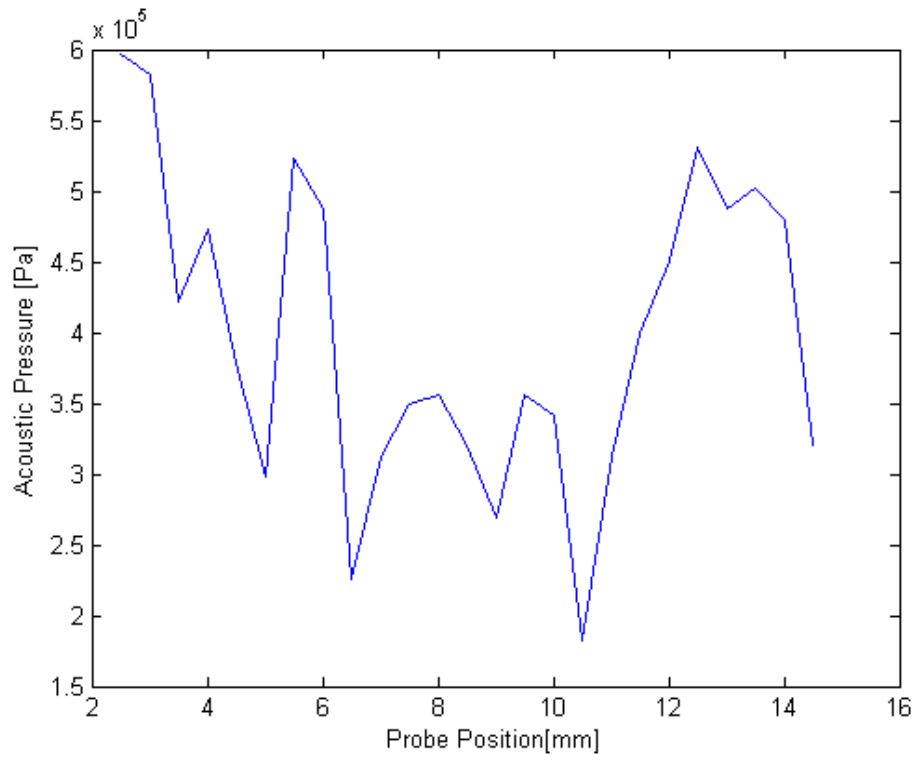
(b)



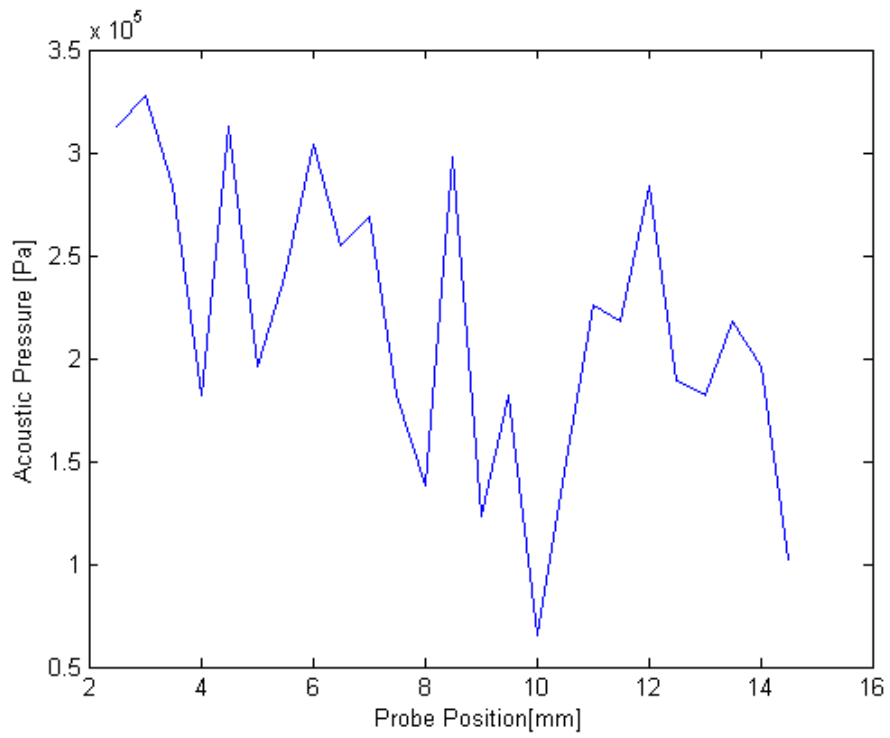
(c)



(d)



(e)

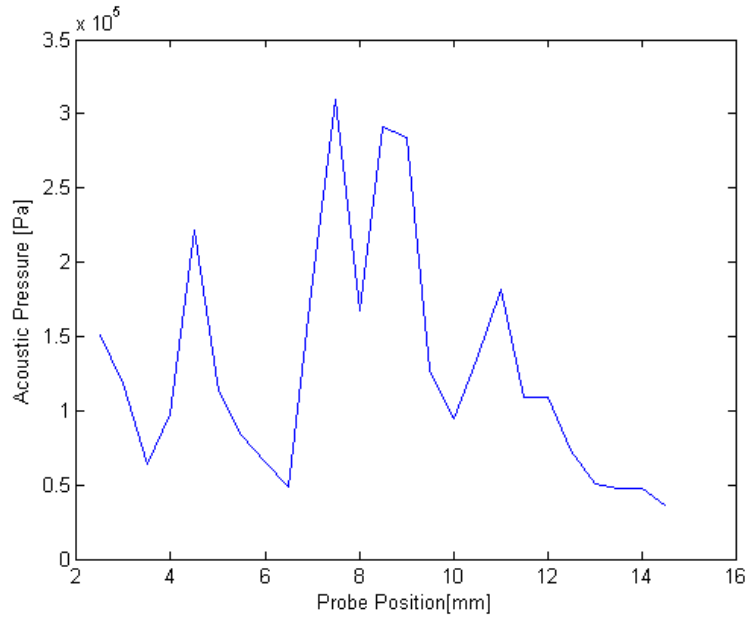


(f)

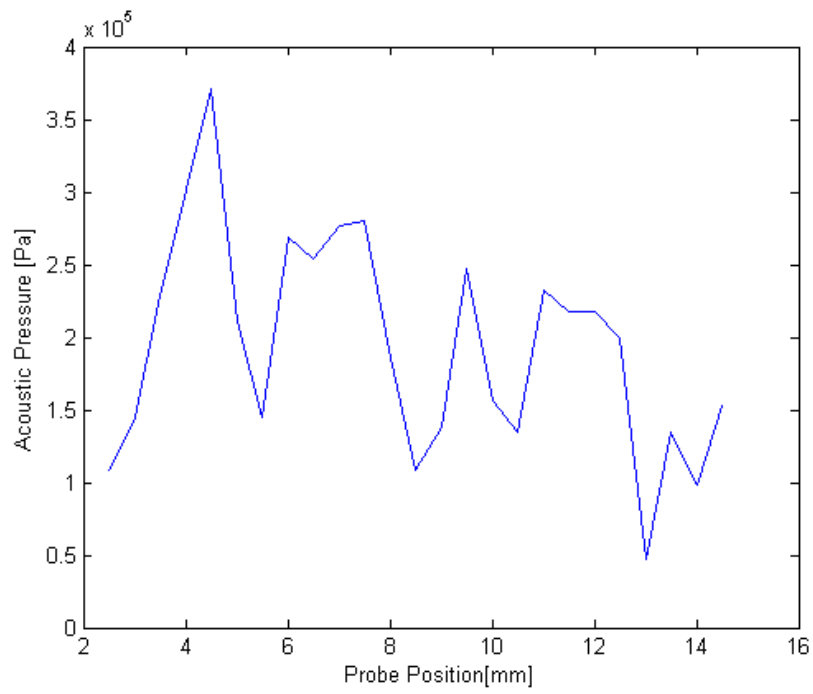
Figure 3.18 Curves of vibration amplitudes distribution measured along height lines of the circular disk transducer with distance to the active surface being 1mm. (a) the measurement results along a height line in vertical direction. (b) the measurement results after the cylindrical transducer was spun by 60 degree. (c) the measurement results after the cylindrical transducer was spun by 120 degree. (d) the measurement results after the cylindrical transducer was spun by 180 degree. (e) the measurement results after the cylindrical transducer was spun by 240 degree. (f) the measurement results after the cylindrical transducer was spun by 300 degree. All height lines are within the same wave front. For all plots, Y axis is the measured ultrasound amplitude. X axis is the position within heightlines.

Due to the small working surface of hydrophone probe, the readings collected were electrical signals of vibration amplitudes distribution at the tangent surfaces of wave fronts. Periodical changes within curves in Figure 3.18 match with simulation results of vibration amplitudes distributions for line sources used in the model shown in Figure 3.5(a). It can also be observed that at same probe position, the vibration amplitudes along different height lines are different, which means periodical changes along direction vertical to the line sources described in Section 3.2 happened. This fact matches with both the distribution described by the method proposed in Section 3.2 and the simulation results of a cylinder provided in Figure 3.11(a).

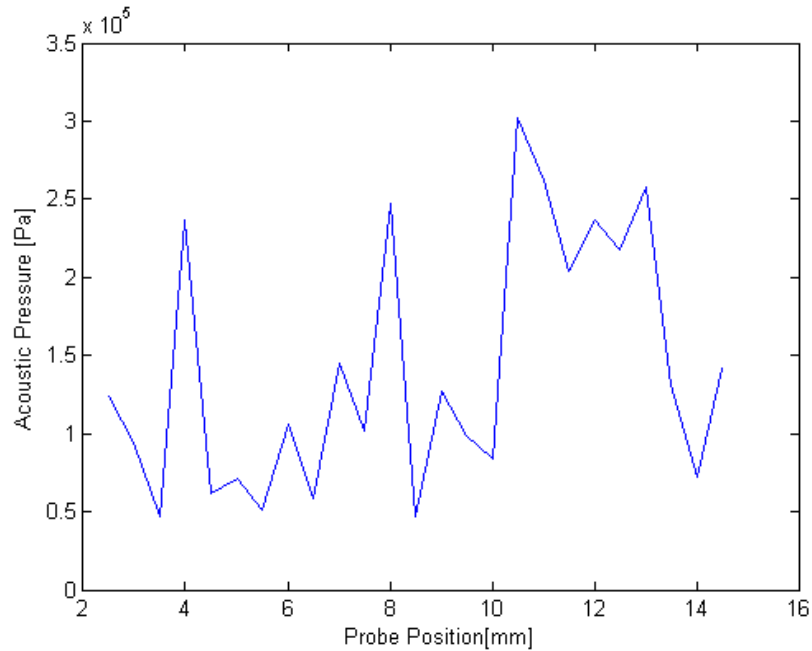
Another group of curves of vibration amplitudes distributions along different height lines are shown in Figure 3.19. The distance of probe to the active surface is 10 mm.



(a)



(b)



(c)

Figure 3.19 Curves of vibration amplitudes distribution measured along height lines of the circular disk transducer with distance to the active surface being 10mm. (a) the measurement results along a height line in vertical direction. (b) the measurement results after the cylindrical transducer was spun by 120 degree. (c) the measurement results after the cylindrical transducer was spun by 240 degree. Height lines in (a), (b) and (c) are the same height lines in Figure 3.21(a),(c) and (e) but the distance to the active surface is farther. For all plots, Y axis is the measured ultrasound amplitude. X axis is the position within height lines.

Fewer changes within curves can be observed in Figure 3.19(a), (b) and (c) compared with the changes within curves in Figure 3.18(a),(c) and (e). This fact matches with simulation results of vibration amplitudes distributions for line sources in Figure 3.5(b). It can also be observed that on different height lines, the readings of same probe position are different. This result matches with both the distribution described by the method proposed in Section 3.2 and the simulation results of a cylinder provided in Figure 3.11(b).

3.6.3 Problems

Symmetry in the simulation results provided in Section 3.3 cannot be observed in the experiment results for both the circular disk transducer and the cylindrical transducer used. This can be attributed to flaws in the manufacture procedures, which can lead to non-uniformity in the thickness of material layers.

3.7 Conclusion

In this chapter, studies about vibration amplitudes distribution within wave fronts of a circular disk transducer and a cylindrical transducer are introduced. A method of model building for studies of vibration amplitudes distribution is proposed. Its effectiveness is validated by both the simulation and the experiment. The vibration amplitudes distribution of the cylindrical transducer described by the method matches with both the simulation results of the distribution and the measurements for a cylinder.

Chapter 4: Optimization of the Efficiency of Transducer Structures

Transducer efficiency is as important as vibration amplitudes distribution within ultrasound beams in ultrasound applications. It can be inferred from studies in Chapter 3 that differences in structures makes differences in vibration amplitudes distribution of ultrasound beams. In this chapter, how the differences in transducer structures influence transducer efficiency is studied. The structures involved are the rectangular plate structure and the cylindrical structure. First of all, mechanics theories about how the differences between these two structures affect the efficiency are introduced. Then, a physical quantity is proposed to describe the efficiency of these transducer structures, followed by a comparison between efficiency of these two structures. The results of comparison are used for optimization of efficiency. Arrays made by rectangular plate transducers were found to be more efficient in this project.

4.1 Mechanics Theories for Transducer Efficiencies

4.1.1 Mechanics Theories of Transducer Ultrasound Generation

Reverse piezoelectric effect has been briefly introduced in Chapter 2. Reverse piezoelectric effect is used to generate ultrasound waves in ultrasound transducers. Internal stress is generated when a piece of piezoelectric material is exposed to certain electric field. The internal stress is described by[21]:

$$S = d * E \quad . \quad (4.1)$$

S is the internal stress. d is the piezoelectric strain coefficient. E is the electric field. Most piezoelectric materials are anisotropic. So, Eq (4.1) is expressed as the equation below in practise[21]:

$$\begin{Bmatrix} S_{11} \\ S_{22} \\ S_{33} \\ 2S_{23} \\ 2S_{31} \\ 2S_{12} \end{Bmatrix} = \begin{Bmatrix} 0 & 0 & d_{31} \\ 0 & 0 & d_{32} \\ 0 & 0 & d_{33} \\ 0 & d_{24} & 0 \\ d_{15} & 0 & 0 \\ 0 & 0 & 0 \end{Bmatrix} * \begin{Bmatrix} E_1 \\ E_2 \\ E_3 \end{Bmatrix} \quad .(4.2)$$

Different directions of the internal stress, strain coefficient and electric field are represented by different indexes in Eq(4.2)[21].

Displacement of the material's particles happens under the internal stress. The displacement is not uniform over the whole piece of material. In mechanics, the displacement distribution is defined as deflection[21]. When the electric field that the piece of piezoelectric material exposed to is an alternating electric field, vibration of the material happens. The deflection determines the vibration amplitude of each point within the material[21]. This vibration is forced. Therefore, the vibration frequency is decided by the frequency of alternating electric field.

If the piezoelectric material is within certain medium during the vibration, ultrasound waves are generated by the propagation of vibration into the medium. The frequency is the same as the frequency of material's vibration. Because ultrasound waves are longitudinal waves, only the stress that is vertical to the surface contributes to the ultrasound generation[21]. In Eq(4.2), the strain coefficient for stress vertical to the surface is d_{31} . In addition, the amplitude of ultrasound waves has a positive relationship with the deflection of the piezoelectric material[21]. According to Eq(2.11), it can be inferred that the ultrasound energy has a positive relationship with the deflection of the piezoelectric material as well.

4.1.2 Ultrasound Generation Efficiency

4.1.2.1 Relationship with Driving Pulses

In practise, ultrasound transducer driving is implemented by electrical pulses generation circuit[5]. The relationship between the voltage and the internal stress generated by reverse piezoelectric effect is described by replacing E in Eq(4.2) with:

$$E = \frac{V}{h} . \quad (4.3)$$

E is the electric field. V is the voltage of the electric pulse. h is the thickness of the piezoelectric material. It can be inferred that the internal stress generated by piezoelectric effect is proportional to the voltage applied for a transducer structure.

4.1.2.2 Deflection Description of A Rectangular Plate Structure

Figure 4.1 illustrates a rectangular plate transducer structure for deflection description[22].

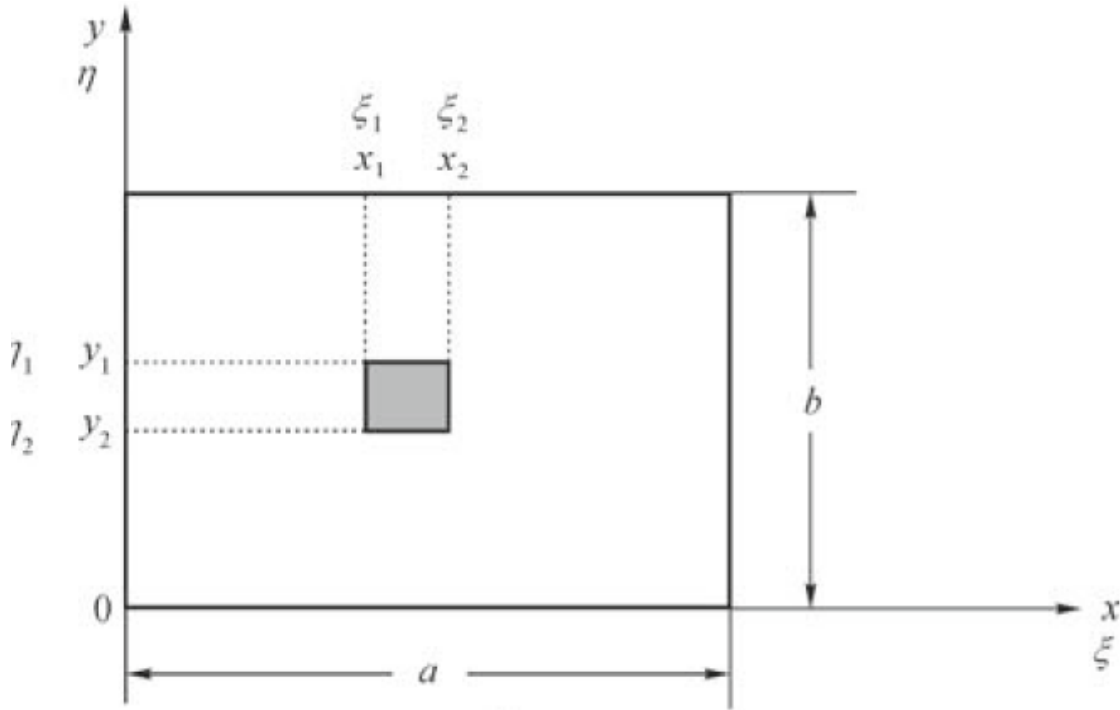


Figure 4.1 Rectangular plate transducer for deflection description[22]. White part is the matching layer of the transducer. It is considered as a load. Grey part is the piezoelectric actuator. The length of the load is a . The width of the load is b . (x_1, y_1) , (x_2, y_1) , (x_1, y_2) , and (x_2, y_2) are coordinates of four corners of the actuator within the load surface. $\xi_1, \xi_2, \eta_1, \eta_2$ are the normalized value of x_1, x_2, y_1 and y_2 . Normalization is implemented as: $\xi = x/a$ and $\eta = y/b$. The thickness of the load is h . The thickness of the actuator is h_p .

The deflection over the load surface is described as[22]:

$$w = \sum_{n=1}^{\infty} \sum_{m=1}^{\infty} \frac{16M_0}{a^2 \rho h} * \frac{\sin \omega t}{\omega_n^2 - \omega^2} * \left(\frac{m}{n} + \frac{n\beta^2}{m} \right) * \sin m\pi\xi_0 * \sin n\pi\eta_0 * \sin m\pi r_\xi * \sin n\pi r_\eta * \sin m\pi\xi * \sin n\pi\eta \quad . \quad (4.4)$$

ρ is the density of the load. a is the length of the load. h is the thickness of the load. (ξ_0, η_0) is the normalized center point of the piezoelectric actuator. r_ξ and r_η are half of the normalized length and width of the actuator. (ξ, η) is the normalized coordinate of an arbitrary point on the load disk. M_0 is a constant related to the internal stress. β is the

ratio of length to width of the load. ω_n is the natural frequency of the rectangular plate. N_x and N_y are the internal constant forces in the load.

M_0 is described as[22]:

$$M_0 = E_p * d_{31} * V(h_p + h)/2 \quad . \quad (4.5)$$

E_p is the Young's Modulus of the piezoelectric material. d_{31} is the piezoelectric strain coefficient. V is the voltage applied. h is the thickness of the load. h_p is the thickness of the actuator.

β is described as[22]:

$$\beta = \frac{a}{b} \quad . \quad (4.6)$$

a is the length of the load. b is the width of the load.

ω_n is described as[22]:

$$\omega_n^2 = \frac{1}{\rho h a^4} * \left[D \left(m^4 \pi^4 + 2\beta^2 m^2 n^2 \pi^4 + \beta^4 n^4 \pi^4 \right) + \left(a^2 N_x^0 m^2 \pi^2 + a^2 \beta^2 N_y^0 n^2 \pi^2 \right) \right] \quad . \quad (4.7)$$

ρ is the density of the material. a is the length of the load. h is the thickness of the load. D is the bending rigidity of the load. β is the ratio of length to width of the load. N_x and N_y are the internal constant forces in the load.

D is described as[22]:

$$D = E h^3 / [12(1 - \nu^2)] \quad . \quad (4.8)$$

E is the Young's Modulus of the load. ν is the Poisson's ratio of the load disk.

When Eq(4.4) was used for studies in this project, the actuator was considered to cover the entire load surface.

4.1.2.3 Deflection Description of A Cylindrical Shell Transducer

Figure 4.2 illustrates the cylindrical shell structure for deflection description[22].

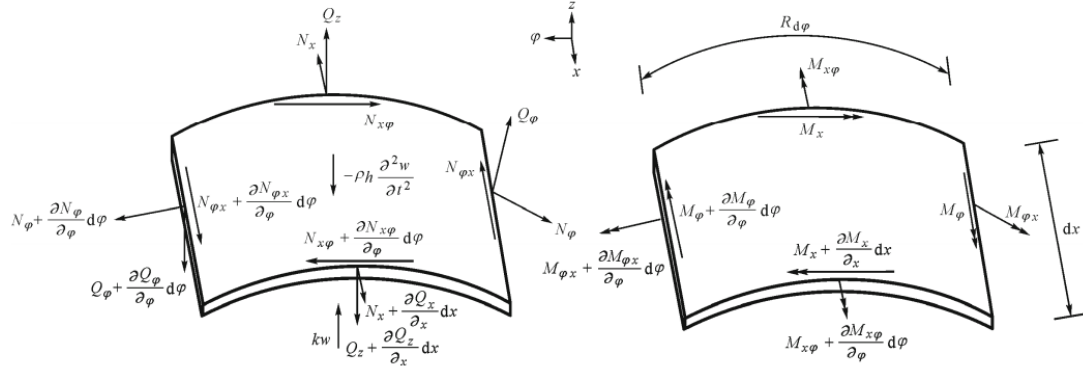


Figure 4.2 Cylindrical Shell for Deflection Description[22]. The Cylindrical shell is driven by two piezoelectric actuators at its top surface and bottom surface. The actuators are driven by two opposite electric fields. The matching layer is considered as a load. The length of the load is L . The radius of the load is R . The cut out angle of the load is Φ . The thickness of the load is h . The length of the actuators are l_p . The radius of the actuators is the same as the radius of the load. The cut out angle of the actuator is θ_p . The thickness of the load is h_p . (l_1, ψ_1) , (l_1, ψ_2) , (l_2, ψ_1) , and (l_2, ψ_2) are the coordinates of four corners of the actuator within the load surface. ξ_1 , ξ_2 , θ_1 and θ_2 are the normalized coordinates of l_1 , l_2 , ψ_1 and ψ_2 . The normalization is implemented as: $\xi=l/L$ and $\theta=\psi/\Phi$.

The deflection is described as[22]:

$$w = \sum_{m=1}^{\infty} \sum_{n=1}^{\infty} \frac{4B_{mn} \sin n\pi \theta_0 \sin m\pi \xi_0}{\omega_n^2 - \omega^2} \sin m\pi \xi \sin n\pi \theta e^{j\omega t} \quad (4.9)$$

B_{mn} is a constant related to the internal stress and the size of the actuators. (θ_0, ξ_0) is the normalized center point of the actuators. ω_n is the natural frequency of the cylindrical shell. (ξ, θ) is the normalized coordinate of an arbitrary point on the load surface.

B_{mn} is described as[22]:

$$B_{mn} = \frac{4M_0}{\rho h} \left(\frac{m}{nL^2} + \frac{n}{mR^2\Phi^2} \right) \sin m\pi l_\xi \sin n\pi \theta_p \quad (4.10)$$

M_0 is the constant related to the internal stress. ρ is the density of the load. h is the thickness of the load. L is the length of the load. R is the diameter of the load. Φ is the cut out angle of the load. l_ξ and θ_p are half of the normalized length and cut out angle of the actuators

The description of M_0 is the same as Eq(4.5).

ω_n is described as[22]:

$$\omega_n^2 = \frac{2}{\rho h} \left[D \left(\frac{m^2 \pi^2}{L^2} + \frac{n^2 \pi^2}{R^2 \Phi^2} \right)^2 + \frac{2\nu m^2 \pi^2}{R^2 L^2} + \frac{6}{R^2 h^2} \right] \quad (4.11)$$

ρ is the density of the load. h is the thickness of the load. D is the bending rigidity of the load L is the length of the load. R is the diameter of the load. Φ is the cut out angle of the load. ν is the Poisson's ratio of the load disk.

The description of D is the same as Eq (4.8).

When Eq(4.9) was used for studies of cylindrical transducer in this project, the actuators were considered to cover the entire loading surface. However, Eq(4.9) can't be directly used for a cylindrical transducer with a cut out angle of 2π , because when the cut out angle of the actuator is 2π , the value of B_{mn} is zero all the time. In addition, when Eq(4.9) is considered as a function of the cut of angle of the actuators, it reaches its maximum when the cut out angle is π . Therefore, a cylindrical transducer was considered as a pair of 2 cylindrical shell with cut out angle of π for studies in this project to represent the maximum efficiency case.

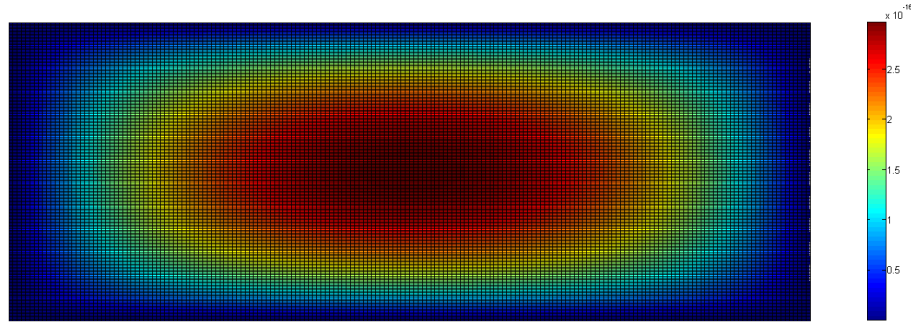
4.1.2.4 Calculation Results of Equations Describing Deflection

Eq(4.4) and Eq(4.9) can be reshaped into:

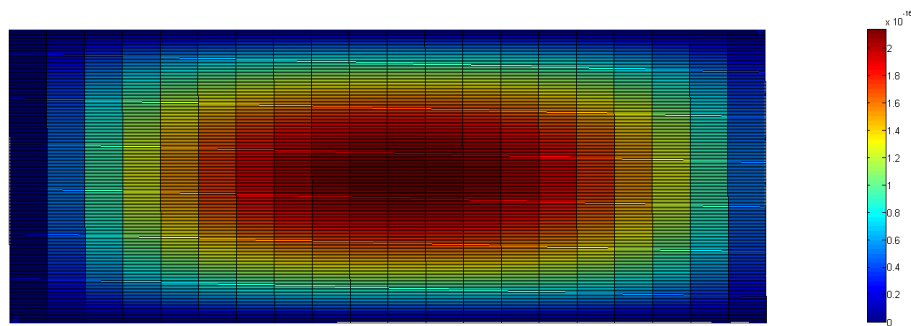
$$W_{rectangular} = \sum_{m=1}^{\infty} \sum_{n=1}^{\infty} \frac{\frac{16M}{\rho h a^2} \left(\frac{m}{n} + \frac{n}{m} \beta^2 \right) (\sin n\pi/2)^2 (\sin m\pi/2)^2 \sin m\pi\xi * \sin n\pi\eta}{\omega_{mn}^2 - \omega^2} \quad (4.12)$$

$$W_{shell} = \sum_{m=1}^{\infty} \sum_{n=1}^{\infty} \frac{\frac{16M}{\rho h a^2} \left(\frac{m}{n} + \frac{n}{m\pi^2} \beta^2 \right) (\sin n\pi/2)^2 (\sin m\pi/2)^2 \sin m\pi\xi \sin n\pi\theta e^{j\omega t}}{\omega_{mn}^2 - \omega^2} \quad (4.13)$$

It can be inferred from Eq(4.12) and Eq(4.13) that the deflection of different structures is series of m and n . Calculations of Eq(4.12) and Eq(4.13) were carried out in this project, in which $\frac{16M}{\rho h a^2}$ was simplified to be 1 for a more general conclusion. This simplification is reasonable because transducers involved in this project were made by same materials, and the thickness of actuators and loads is same. Figure 4.3 illustrates the calculation results of Eq(4.12) and Eq(4.13).



(a)



(b)

Figure 4.3 Calculation results of equations describing deflection of different transducer structures. (a) Calculation result of the equation describing deflection of a rectangular plate. (b) Calculation result of the equation describing deflection of a cylindrical shell. The cut out angle of the cylindrical shell is π . The height of the rectangular plate and the cylindrical shell is same. The width of the rectangular plate is equal to the diameter of the cylindrical shell. Color bars show the relationship between colors and amplitudes. When the color changes from blue to red, the vibration amplitude of a point increases.

It can be observed in Figure 4.3 that the displacement over the entire structure is not uniform in both the rectangular plate and the cylindrical shell. Therefore, Eq(4.4) and Eq(4.9) cannot be directly used for efficiency comparison. In addition, in Figure 4.3, the maximum displacement of the rectangular plate is larger than the maximum displacement of the cylindrical shell. This fact suggests the possibility of higher efficiency of the rectangular plate transducer.

4.1.2.5 Deflection Volume and Efficiency

The amplitude of ultrasound waves generated is decided by the overall effect of deflection within the entire active surface of a transducer. Integrals of Eq(4.4) and Eq(4.9) were made for studies of overall deflection effect in this project in order to compare the overall effect of deflection between different transducer structures. The integrals were carried out in the normalized coordinates.

The results of integral of Eq(4.4) and Eq(4.9) are:

$$W_{plate} = \sum_{m=1}^{\infty} \sum_{n=1}^{\infty} \frac{\frac{16M}{\rho h a^2} (\frac{m}{n} + \frac{n}{m} \beta^2) (\sin n\pi/2)^2 (\sin m\pi/2)^2 \frac{(1-(-1)^m)(1-(-1)^n)}{m n}}{\omega_{mn}^2 - \omega^2} . \quad (4.14)$$

$$W_{shell} = \sum_{m=1}^{\infty} \sum_{n=1}^{\infty} \frac{\frac{16M}{\rho h a^2} (\frac{m}{n} + \frac{n^4}{m\pi^2} \beta^2) (\sin n\pi/2)^2 (\sin m\pi/2)^2 \frac{(1-(-1)^m)(1-(-1)^n)}{m n}}{\omega_{mn}^2 - \omega^2} . \quad (4.15)$$

Eq(4.14) and Eq(4.15) are convergent. It is suggested that their values become stable when m and n are larger than 50[22].

The overall deflection effects were defined as deflection volumes in this project. When the deflection volume is multiplied by the internal stress, the result represents the energy consumed by a transducer structure to reach the deflection volume, in other words, to generate ultrasound waves with same amplitudes and same energy. For a rectangular plate structure and a cylindrical shell, comparisons of ultrasound generation efficiency can be made by the ratio of deflection volumes under the same driving conditions.

W_{shell}/W_{plate} is the comparison between the voltage or internal stress required for the rectangular plate and the cylindrical shell to get same deflection volume, in other words, to generate ultrasound waves with same energy under same conditions. When it is larger than 1, it means more energy is consumed by the rectangular plate, therefore, the cylindrical shell is more efficient. When it is smaller than 1, it means more energy is consumed by the cylindrical shell, therefore, the rectangular plate is more efficient.

Transducer structures have been introduced in Chapter 2. Generally, only one layer of piezoelectric actuator is used. In addition, in forced vibration, when the driving frequency is away from the natural frequency, the deflection can be considered to be proportional to

the driving force[21]. Table 4.1 shows the square value of angular natural frequency and angular driving frequency in this project. The driving frequency was 1.5 MHz.

Table 4.1 Calculation Result for Frequency Involved

Square Value of Frequency	ω_{mndisk}^2	ω_{mshell}^2	1.5MHz
Minimum	$6.47 \cdot 10^{15}$	$6.11 \cdot 10^{15}$	$8.88 \cdot 10^{13}$
Maximum	$6.47 \cdot 10^{23}$	$6.11 \cdot 10^{23}$	$8.88 \cdot 10^{13}$

It can be inferred from Table 4.1 that the driving frequency is away from the natural frequency.

Therefore, for Eq(4.15), W_{shell} was divided by 2 before efficiency comparison.

W_{shell}/W_{plate} was used for comparison of efficiency in this project.

4.2 Theoretical Efficiency Comparison

Eq(4.14) and Eq(4.15) were calculated by MATLAB with m and n set to 50 and the thickness of matching layer ranging from 0 to 1mm. The matching layer in a transducer structure was represented by the load in Eq(4.4), Eq(4.9), Eq(4.14) and Eq(4.15). The length of the rectangular plate was set to 20mm. The height was set to 19mm. The thickness of the actuator was set to 0.6mm. The length of cylindrical shell with cut out angle of π was set to 20mm. The diameter was set to 19mm. The thickness of the actuator was set to 0.6mm. Driving frequency in both cases was 1.5MHz. These settings were the same as the real dimensional parameters of the circular transducer and the cylindrical transducer used in this project. Figure 4.4 illustrates the results of W_{shell}/W_{plate} .

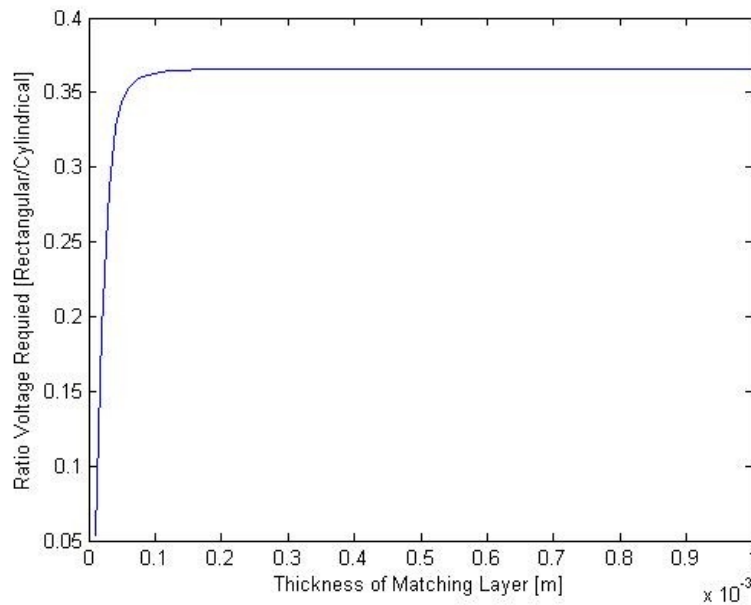


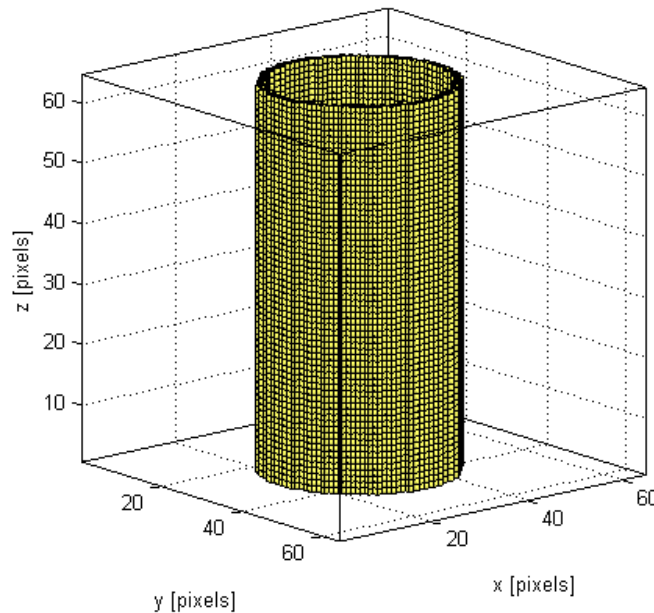
Figure 4.4 The Ratio of voltage required for a rectangular plate transducer and a cylindrical shell with cut out angle being π . The thickness of matching layer refers to the thickness of loads.

Because the thickness of matching layers is always set to a quarter of the ultrasound wavelength, it can be inferred from Figure 4.3 that the rectangular plate structure is more efficient than the cylindrical shell with a cut out angle of π , because the voltage required for the rectangular plate structure to get to certain deflection volume is only 0.35 times of the voltage required for the cylindrical shell structure to get to the same deflection volume. In addition, the efficiency increases when the frequency of ultrasound waves increase.

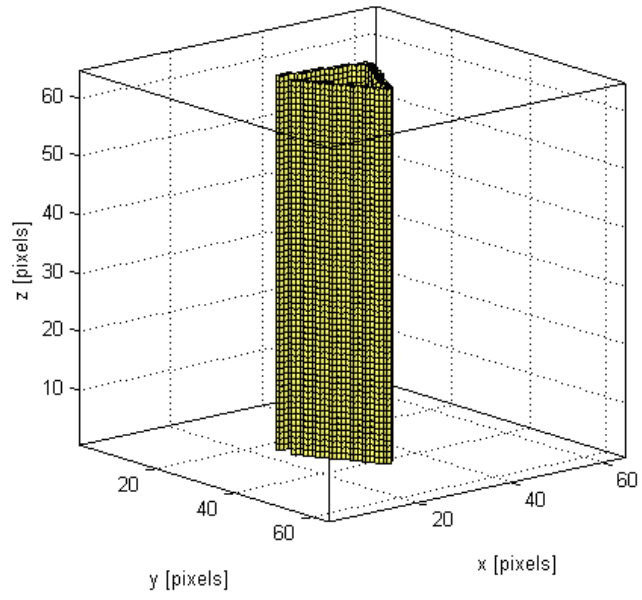
4.3 Optimization of Efficient Structure

Though the rectangular plate is more efficient, the cylindrical shell structure has a omnidirectional ultrasound distribution. Simply replacing the cylindrical structure with a pair of rectangular plate transducers can lead to negative impact on the uniformity of ultrasound distribution in the medium. Arrays made by rectangular plate transducers can be used as trade-offs for both efficiency and the uniformity of distribution.

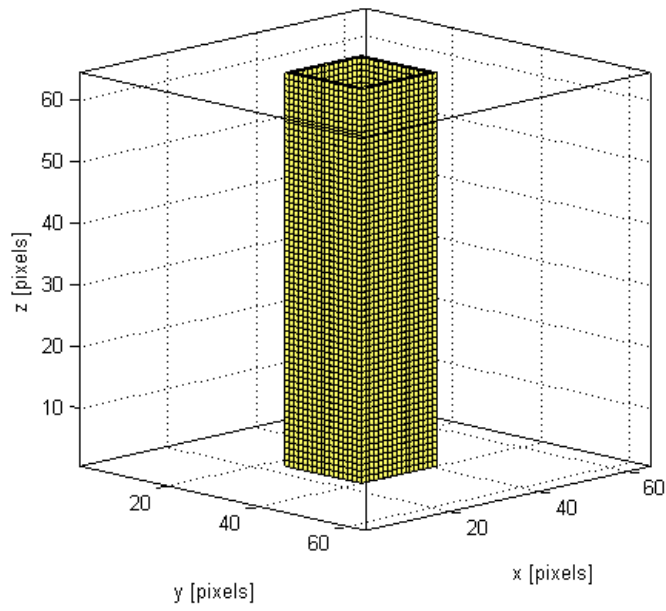
In this project, the amount of rectangular transducers used in arrays was decided by the voltage efficiency. The voltage required for the whole cylindrical transducer used in this project to get to certain deflection volume was considered as $2U$, in which U was the voltage required for the cylindrical shell with a cut out angle of π to get the same deflection volume. If the amount of rectangular plate transducers used was N , $0.35 N$ is not expected to exceed 2. Therefore, for the cylindrical transducer studied, the rectangular plate transducers could be placed in the shapes of a triangular prism, a quadrangular, and a pentagonal prism. The uniformity of ultrasound waves generated by arrays in these shapes was compared with the uniformity of ultrasound waves generated by the cylindrical transducer. The comparison was carried out between simulation results of different structures in 'K-wave'. For all simulations, the size of computational domain was $64*64*64$ with dx , dy and dz being 0.25mm . The excitation signal was a sine function with an amplitude of 2Pa and frequency of 1.5MHz . The simulation medium was degassed water. Figure 4.5 illustrates the source masks implemented for different structures in 'K-wave'.



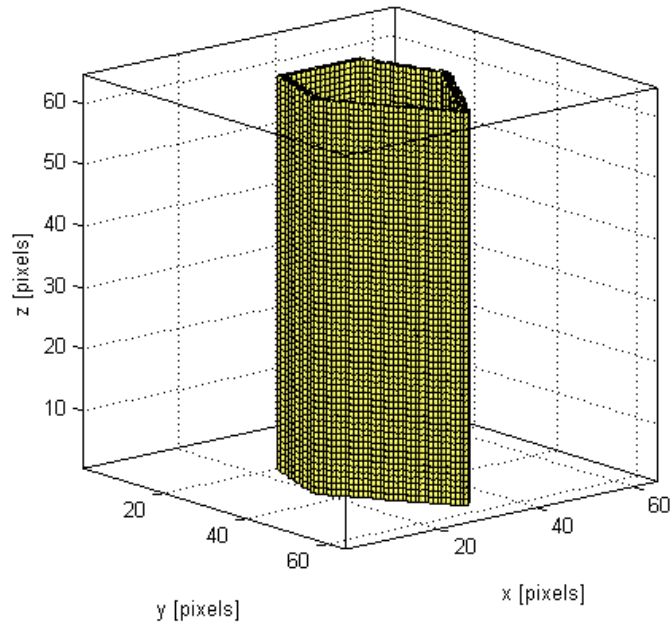
(a)



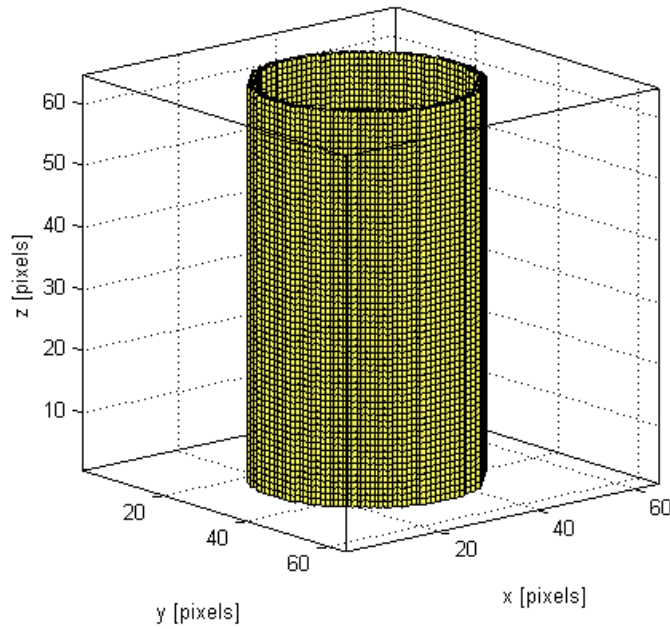
(b)



(c)



(d)

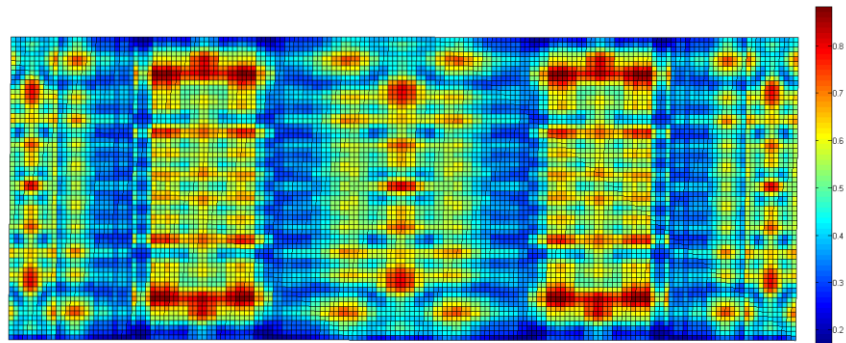


(e)

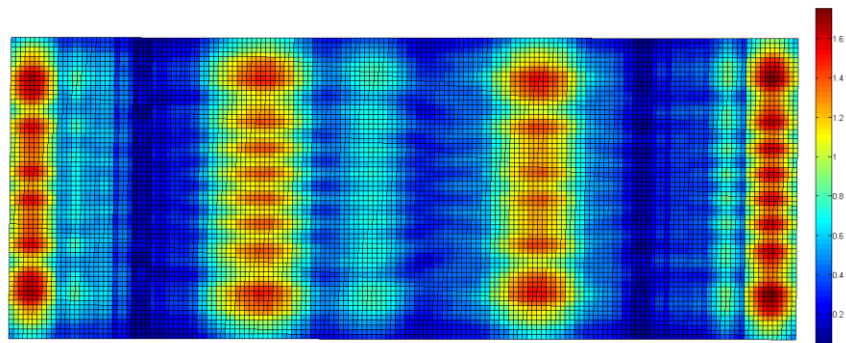
Figure 4.5 Implementations of different transducer structures in 'K-wave'. (a) Implementation of a cylindrical transducer. (b) Implementation of a triangular prism array. (c) Implementation of a quadrangular array. (d) Implementation of a pentagonal

prism array. (e) Implementation of the sensor mask collecting data. The height and thickness of the four structures are same. The width of the elemental rectangular plate for the triangular array, the quadrangular array and the pentagonal array is equal to the diameter of the cylindrical transducer.

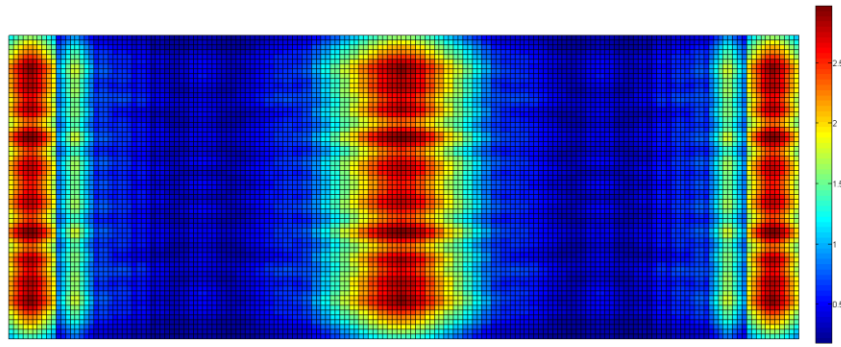
Figure 4.6 illustrates the simulation results of different structures. The simulation results were planarized before illustration.



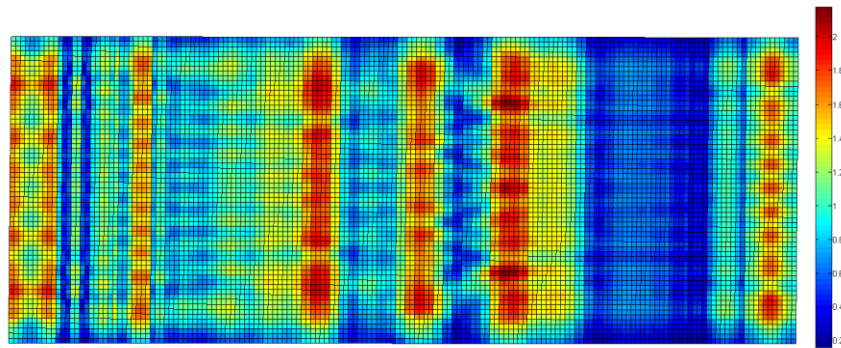
(a)



(b)



(c)



(d)

Figure 4.6 Simulation results of different transducer structure. (a) the result of the cylindrical transducer. (b) the result of an array in triangular prism arrangement. (c) the result of an array in quadrangular arrangement. (d) the result of an array in pentagonal prism arrangement. Color bars show the relationship between colors and amplitudes. When the color changes from blue to red, the vibration amplitude of a point increases.

In Figure 4.6, it can be observed that the maximum amplitude of the cylindrical transducer is only around 0.8 Pa, while the maximum amplitudes of the triangular array, the quadrangular array and the pentagonal array are over 1.6 Pa, which are over 2 times higher. The effectiveness of the simulation tool has been validated in Chapter 3. Therefore, the higher efficiency of transducer arrays, which was proposed in this project, is validated by the simulation result. Compared with the ultrasound amplitude distribution of the cylindrical transducer, the triangular prism array and the pentagonal prism array

have the distribution more similar to the one of the cylindrical transducer. The symmetry of the distribution of the triangular array is better compared with the one of the pentagonal array.

As a conclusion, a cylindrical transducer can be replaced by a triangular prism array in applications. The elements of the triangular prism array are rectangular plate transducers. Their height and thickness are same as those of the cylindrical transducer. Their width is equal to the diameter of the cylindrical transducer.

4.4 Conclusion

In this chapter, the transducer structure was optimized based on the results of theoretical analysis and simulation. Optimized transducer structures were arrays with rectangular plate transducers as elements. They could be used to replace the cylindrical transducer in applications. Before this project, the ultrasound transducer arrays was mainly used in imaging applications and detections[23,26], where the arrays were used to improve imaging quality or detection resolution. Using transducer arrays in renewable energy production for higher efficiency is a relatively novel idea.

Chapter 5 Conclusion and Scope on Future Work

5.1 Conclusion

In this project, theoretical analysis, experiment and simulation for ultrasound field distribution of circular disk transducer and cylindrical transducer were conducted. A model building method for distribution study of cylindrical transducers was built up. Its effectiveness was validated by experiment and simulation results. An idea of transducer structure optimization for higher efficiency was proposed. Based on the related mechanical theories about deflection, a physical quantity called deflection volume was defined, calculated and compared. The comparison result shows that a higher efficiency can be acquired using transducer arrays with rectangular disk elements. Triangular arrays are validated to have higher efficiency compared with cylindrical transducers.

5.2 Scope on Future Work

On the transducer side, the future work can be focused on the related work on driving circuit and the implementation of the array structures proposed in this project. Both the circuit and the structure of the transducer affect efficiency. For the circuit, the matching output impedance should be close to the equivalent impedance of the transducer or transducer arrays used so that the output driving power can reach the maximum value. Transducers or transducer arrays using different materials can also be made for selection of arrays used in production.

References

- [1] Preston, Roy C. *Output measurements for medical ultrasound*. Springer, 1991.
- [2] Rumack, Carol M., Stephanie R. Wilson, and J. William Charboneau, eds. *Diagnostic ultrasound*. Vol. 1. Mosby-Year Book, 1991.
- [3] Cheeke, J. David N. *Fundamentals and applications of ultrasonic waves*. CRC press, 2012.
- [4] Wells, Peter NT. "Ultrasonic imaging of the human body." *Reports on progress in physics* 62.5 (1999): 671.
- [5] Vives, Antonio Arnau, ed. *Piezoelectric transducers and applications*. Vol. 200. New York: Springer, 2008.
- [6] Ang W T. Design of a Portable Low-power Intensity Pulsed Ultrasound (LIPUS) Generator[M]. ProQuest, 2008.
- [7] Szabo, Thomas L. *Diagnostic ultrasound imaging: inside out*. Academic Press, 2004.
- [8] Watson, Tim. "Ultrasound in contemporary physiotherapy practice." *Ultrasonics* 48.4 (2008): 321-329.
- [9] Sadick, Neil S. "Overview of ultrasound-assisted liposuction, and body contouring with cellulite reduction." *Seminars in cutaneous medicine and surgery*. Vol. 28. No. 4. WB Saunders, 2009.
- [10] Crum, Lawrence, et al. "Therapeutic ultrasound: Recent trends and future perspectives." *Physics Procedia* 3.1 (2010): 25-34.
- [11] Shaheen M, Choi M, Ang W, et al. Application of low-intensity pulsed ultrasound to increase bio-ethanol production[J]. *Renewable Energy*, 2013, 57: 462-468.
- [12] Chen J, El-Bialy T H A, Tsui Y Y. Ultrasound stimulation devices and techniques: U.S. Patent Application 13/292,628[P]. 2011-11-9.
- [13] <http://www.ieee-uffc.org/ultrasonics/software.asp>

- [14] Treeby, Bradley E., and Benjamin T. Cox. "k-Wave: MATLAB toolbox for the simulation and reconstruction of photoacoustic wave fields." *Journal of biomedical optics* 15.2 (2010): 021314-021314.
- [15] Marini J, Rivenez J. Acoustical fields from rectangular ultrasonic transducers for non-destructive testing and medical diagnosis[J]. *Ultrasonics*, 1974, 12(6): 251-256.
- [16] Krautkrämer J, Krautkrämer H. *Ultrasonic testing of materials*[M]. Springer, 1983
- [17] Hynynen K, Davis K L. Small cylindrical ultrasound sources for induction of hyperthermia via body cavities or interstitial implants[J]. *International journal of hyperthermia*, 1993, 9(2): 263-274.
- [18] Ebbini E S, Umemura S, Ibbini M, et al. A cylindrical-section ultrasound phased-array applicator for hyperthermia cancer therapy[J]. *Ultrasonics, Ferroelectrics and Frequency Control, IEEE Transactions on*, 1988, 35(5): 561-572.
- [19] Mažeika L, Greševičius M. The fast technique for calculation of ultrasonic field of rectangular transducer[J]. *Ultragarsas= Ultrasound/Kauno technologijos universitetas. Kaunas: Technologija. ISSN*, 2008: 1392-2114.
- [20] Shung K K, Zippuro M. Ultrasonic transducers and arrays[J]. *Engineering in Medicine and Biology Magazine, IEEE*, 1996, 15(6): 20-30.
- [21] Preumont A. *Piezoelectric Beam, Plate and Truss*[M]//*Vibration Control of Active Structures*. Springer Netherlands, 2011: 61-101.
- [22] Yang Y W, Zhang L, Jin Z L, et al. *Smart Plates and Shells*[M]//*Smart Materials in Structural Health Monitoring, Control and Biomechanics*. Springer Berlin Heidelberg, 2012: 333-393.
- [23] Brown J A, Démoré C E M, Lockwood G R. Design and fabrication of annular arrays for high-frequency ultrasound[J]. *Ultrasonics, Ferroelectrics and Frequency Control, IEEE Transactions on*, 2004, 51(8): 1010-1017.

[24] Manthey W, Kroemer N, Magori V. Ultrasonic transducers and transducer arrays for applications in air[J]. Measurement Science and Technology, 1992, 3(3): 249.

[25] Butler S C, Tito F A. A broadband hybrid magnetostrictive/piezoelectric transducer array[C]//Oceans 2000 MTS/IEEE Conference and Exhibition. IEEE, 2000, 3: 1469-1475.

[26] Smith S W, Pavy Jr H G, von Ramm O T. High-speed ultrasound volumetric imaging system. I. Transducer design and beam steering[J]. Ultrasonics, Ferroelectrics and Frequency Control, IEEE Transactions on, 1991, 38(2): 100-108.

Appendix

MATLAB simulation code for circular disk transducers

`%Circular Disk Transducer Simulation`

```
clear all;
PML_X_SIZE=10;
PML_Y_SIZE=10; %PML high absorbtion and reflection attenuation
PML_Z_SIZE=10;
PML_alpha=10;
% The size in 3 dimension in grid
Nx=180-2*PML_X_SIZE;
Ny=180-2*PML_Y_SIZE;
Nz=180-2*PML_Z_SIZE;

%Unit in each dimension
dx=0.25e-3; %[m],dy dz follow the same
dy=0.25e-3;
dz=0.25e-3;

%Build up the computational domain
kgrid=makeGrid(Nx,dx,Ny,dy,Nz,dz); %Function in K-wave that generates simulation
domain

disk=makeDisc(Nx,Ny,80,80,50); %Function in K-wave defining transducer structures

mask=zeros(Nx,Ny,Nz);
mask_2=zeros(Nx, Ny, Nz);
mask_3=zeros(Nx,Ny,Nz);
mask(:,:,1)=disk;

for l2=1:Nx
    for m2=1:Ny
        mask_2(l2,m2,64)=1; %This make a binary mask for the sensor array
        mask_3(l2,m2,10)=1;
        mask_3(l2,m2,11)=1;
    end
end
%Visualization of the source(transducer)'s profile
voxelPlot(mask);
view([50,15]); % Matlab Function to adjust view angle for 3D plot
voxelPlot(mask_2);
view([50,15]);
%Define the media properties
```

```

medium.sound_speed =1540;
medium.alpha_power = 2;           % [dB/(MHz^y cm)]
medium.alpha_coeff = 0.00222;% [dB/(MHz^y cm)]
medium.BonA=5;
medium.sound_speed_ref=1540;
medium.density=1000;             % [Kg/m^3]

%Define the simulation time length
t_end = 30e-6;                   % [s]
[kgrid.t_array,dt] = makeTime(kgrid, medium.sound_speed, [], t_end);

%Define the source
source.p_mask=mask;
source_freq = 1.5e6;             % [Hz]
source_mag = 0.6*10^6;          % [Pa]
source.p = source_mag*sin(2*pi*source_freq*kgrid.t_array); %The square wave for the
source
source.p = filterTimeSeries(kgrid, medium, source.p); %Filter the frequency not
supported by the grid

%Define the sensor array to record the data

sensor.mask=mask_2;
sensor.record={'p_rms','p_final','I_avg'}; % Here two types of data are recorded: root
mean square of the pressure and average intensity over the simulation time
display_mask = source.p_mask;
input_args = {'DisplayMask', display_mask, 'PMLInside', false, 'PlotPML',
false,'RecordMovie', true, 'MovieName','Planar'}; %Set the arguments of the display
sensor_data = kspaceFirstOrder3D(kgrid, medium, source, sensor, input_args{:}); %Run
the simulation function of 3D simulation

%Visualization of the Simulation Result

%Reorder the average acoustic intensity recorded here. The data returns as the
%Matlab column wise order
intensity_1=sensor_data.Iy_avg;
intensity_2=sensor_data.Ix_avg;
intensity_3=sensor_data.Iz_avg;
pressure_rms=sensor_data.p_rms;
Map_intensity_1=zeros(Nx,Ny);
Map_intensity_2=zeros(Nx,Ny);
Map_intensity_3=zeros(Nx,Ny);
Map_intensity_4=zeros(Nx,Ny);

```

```

Map_pressure_rms=zeros(Nx,Ny);
for p=1:Nx
    for q=1:Ny
        Map_intensity_1(q,p)=abs(intensity_1((p-1)*Nx+q,1));
        Map_intensity_2(q,p)=abs(intensity_2((p-1)*Nx+q,1));
        Map_intensity_3(q,p)=abs(intensity_3((p-1)*Nx+q,1));
        Map_intensity_4(q,p)=( Map_intensity_1(q,p)^2+
Map_intensity_2(q,p)^2+Map_intensity_3(q,p)^2)^0.5;
        Map_pressure_rms(q,p)=pressure_rms((p-1)*Nx+q,1);
    end
end

figure;
surf(kgrid.x_vec*1000,kgrid.y_vec*1000, Map_pressure_rms);
ylabel('x-position [mm]');
xlabel('y-position [mm]');
%axis image;
title('RMS pressure ');

```

MATLAB simulation code for rectangular plate transducers:

```
%Rectangular Plate Transducer Simulation
```

```

clear all;
PML_X_SIZE=10;
PML_Y_SIZE=10; %PML high absorbtion and reflection attenuation
PML_Z_SIZE=10;
PML_alpha=10;
% The size in 3 dimension in grid
Nx=180-2*PML_X_SIZE;
Ny=320-2*PML_Y_SIZE;
Nz=160-2*PML_Z_SIZE;

%Unit in each dimension
dx=0.25e-3; %[m],dy dz follow the same
dy=0.25e-3;
dz=0.25e-3;

%Build up the computational domain
kgrid=makeGrid(Nx,dx,Ny,dy,Nz,dz);

mask=zeros(Nx,Ny,Nz);
mask_2=zeros(Nx, Ny, Nz);

```

```

mask(20:140,20:300,1)=1; % define the rectangular transducer structure

for l2=1:Nx
    for m2=1:Ny

        mask_2(l2,m2,10)=1; %This make a binary mask for the sensor array

    end
end
%Visualization of the source(transducer)'s profile
voxelPlot(mask);
view([50,15]); % Matlab Function to adjust view angle for 3D plot
voxelPlot(mask_2);
view([50,15]);
%Define the media properties

medium.sound_speed =1540;
medium.alpha_power = 2; % [dB/(MHz^y cm)]
medium.alpha_coeff = 0.00222;% [dB/(MHz^y cm)]
medium.BonA=5;
medium.sound_speed_ref=1540;
medium.density=1000; % [Kg/m^3]

%Define the simulation time length
t_end = 30e-6; % [s]
[kgrid.t_array,dt] = makeTime(kgrid, medium.sound_speed, [], t_end);

%Define the source
source.p_mask=mask;
source_freq = 1.5e6; % [Hz]
source_mag = 2; % [Pa]
source.p = source_mag*sin(2*pi*source_freq*kgrid.t_array); %The square wave for the
source
source.p = filterTimeSeries(kgrid, medium, source.p); %Filter the frequency not
supported by the grid

%Define the sensor array to record the data

sensor.mask=mask_2;
sensor.record={'p_rms','p_final','I_avg'}; % Here two types of data are recorded: root
mean square of the pressure and average intensity over the simulation time
display_mask = source.p_mask;
input_args = {'PMLInside', false, 'PlotPML', false, 'RecordMovie', true,
'MovieName','Planar'}; %Set the arguments of the display
sensor_data = kspaceFirstOrder3D(kgrid, medium, source, sensor, input_args{:}); %Run
the simulation function of 3D simulation

```

```

%Visualization of the Simulation Result
%sensor_data.p_rms = reshape(sensor_data.p_rms, Nx, Ny, Nz);
%sensor_data.p_rms(source.p_mask ~= 0) = 1;

%Reorder the average acoustic intensity recorded here. The data returns as the
%Matlab column wise order
intensity_1=sensor_data.Iy_avg;
intensity_2=sensor_data.Ix_avg;
intensity_3=sensor_data.Iz_avg;
pressure_rms=sensor_data.p_rms;

Map_pressure_rms=zeros(Nx,Ny);

Map_pressure_rms=reshape(pressure_rms,Nx,Ny);

figure;
surf(kgrid.y_vec*1000,kgrid.x_vec*1000, Map_pressure_rms);
% ylabel('x-position [mm]');
% xlabel('y-position [mm]');
%axis image;
title('Output Distribution');

```

MATLAB simulation code for transducer arrays

```

% Simulation of the Transducer arrays
%=====
clear all;
PML_X_SIZE=10;
PML_Y_SIZE=10; %PML high absorbtion and reflection attenuation
PML_Z_SIZE=10;
PML_alpha=10;
% The size in 3 dimension in grid
Nx=84-2*PML_X_SIZE;
Ny=84-2*PML_Y_SIZE; %
Nz=84-2*PML_Z_SIZE;

%Unit in each dimension
dx=0.25e-3; %[m],dy dz follow the same
dy=0.25e-3;
dz=0.25e-3;

%Build up the computational domain

```

```

kgrid=makeGrid(Nx,dx,Ny,dy,Nz,dz);

%Make the sensor and source mask for transducer arrays
line1=makeLine(Nx,Ny,[24,24],[40,27]);
line2=makeLine(Nx,Ny,[24,28],[32,42]); %Triangular array
line3=makeLine(Nx,Ny,[40,28],[32,42]);
shape1=line1 | line2 | line3;
% % line1=makeLine(Nx,Ny,[24,24],[40,24]);
% % line2=makeLine(Nx,Ny,[24,24],[24,40]);
% % line3=makeLine(Nx,Ny,[24,40],[40,40]);
% % line4=makeLine(Nx,Ny,[40,24],[40,40]); %Quadrangular array
% % shape1=line1 | line2 | line3 | line4;
% line1=makeLine(Nx,Ny,[24,21],[40,21]);
% line2=makeLine(Nx,Ny,[24,21],[19,36]);
% line3=makeLine(Nx,Ny,[40,21],[45,36]);
% line4=makeLine(Nx,Ny,[19,36],[32,56]);
% line5=makeLine(Nx,Ny,[45,36],[32,56]); %Pentagonal Array
% shape1=line1|line2|line3|line4|line5;

circle2=makeCircle(Nx,Ny,32,32,30);
disk=makeDisc(Nx,Ny,32,32,16);
mask=zeros(Nx,Ny,Nz);
mask_2=zeros(Nx, Ny, Nz);
for l=1:Nz
    mask(:,l)=shape1;
end

for l2=1:Nz
    mask_2(:,l2)=circle2; %This make a binary mask for the sensor array
end

%Visualization of the source(transducer)'s profile
voxelPlot(mask);
view([50,15]); % Matlab Function to adjust view angle for 3D plot
voxelPlot(mask_2);
view([50,15]);
%Define the media properties
medium.sound_speed = 1540; % [m/s]
medium.sound_speed_ref=1540;
medium.alpha_power = 2; % [dB/(MHz^y cm)]
medium.alpha_coeff = 0.02; % [dB/(MHz^y cm)]
medium.density=1000; % [Kg/m^3]
medium.BonA=5;

%Define the simulation time length
t_end = 40e-6; % [s]

```

```

[kgrid.t_array,dt] = makeTime(kgrid, medium.sound_speed, [], t_end);

%Define the source
source.p_mask=mask;
source_freq = 1.5e6;    % [Hz]
source_mag = 2;        % [Pa]
source.p = source_mag*sin(2*pi*source_freq*kgrid.t_array); %The square wave for the
source
source.p = filterTimeSeries(kgrid, medium, source.p); %Filter the frequency not
supported by the grid

%Define the sensor array to record the data

sensor.mask=mask_2;
sensor.record={'p_rms','p_final','I_avg'}; % Here two types of data are recorded: root
mean square of the pressure and average intensity over the simulation time
display_mask = source.p_mask;
input_args = {'DisplayMask', display_mask, 'PMLInside', false, 'PlotPML',
false,'RecordMovie', true, 'MovieName','Cylindrical'}; %Set the arguments of the display
sensor_data = kspaceFirstOrder3D(kgrid, medium, source, sensor, input_args{:}); %Run
the simulation function of 3D simulation

%Visualization of the Simulation Result
%sensor_data.p_rms = reshape(sensor_data.p_rms, Nx, Ny, Nz);
%sensor_data.p_rms(source.p_mask ~= 0) = 1;

%Reorder the average acoustic intensity recorded here. The data returns as the
%Matlab column wise order
intensity_1=sensor_data.Iy_avg;
intensity_2=sensor_data.Ix_avg;
intensity_3=sensor_data.Iz_avg;
Pressure=sensor_data.p_rms;
Size2=size(Pressure);
Size1=64;
Size3=Size2(1)/Size1;
Data=reshape(Pressure,Size3,Size1);
vec1=1:1:Size1;
vec2=1:1:Size3;

figure;

surf(vec1,vec2,Data);

```

MATLAB simulation code for cylindrical transducers

```

% Build up of The Cylindrical Transducer Simulation
%=====
clear all;
PML_X_SIZE=10;
PML_Y_SIZE=10; %PML high absorbtion and reflection attenuation
PML_Z_SIZE=10;
PML_alpha=10;
% The size in 3 dimension in grid
Nx=180-2*PML_X_SIZE;
Ny=320-2*PML_Y_SIZE; %
Nz=180-2*PML_Z_SIZE;

%Unit in each dimension
dx=0.25e-3; %[m],dy dz follow the same
dy=0.25e-3;
dz=0.25e-3;

%Build up the computational domain
grid=makeGrid(Nx,dx,Ny,dy,Nz,dz);

%Make the circle profile of the cylindrical transducer
circle=makeCircle(Nx,Ny,80,80,50); %center 1.6 cm
circle2=makeCircle(Nx,Ny,80,80,60);
%Make the mask for the source and the sensor
mask=zeros(Nx,Ny,Nz);
mask_2=zeros(Nx, Ny, Nz);
for l=1:Nz
    mask(:,l)=circle;
end

for l2=1:Nz
    mask_2(:,l2)=circle2; %This make a binary mask for the sensor array
end

%Visualization of the source(transducer)'s profile
voxelPlot(mask);
view([50,15]); % Matlab Function to adjust view angle for 3D plot
voxelPlot(mask_2);
view([50,15]);
%Define the media properties
medium.sound_speed = 1540; % [m/s]
medium.sound_speed_ref=1540;
medium.alpha_power = 2; % [dB/(MHz^y cm)]
medium.alpha_coeff = 0.02; % [dB/(MHz^y cm)]
medium.density=1000; % [Kg/m^3]
medium.BonA=5;

```

```

%Define the simulation time length
t_end = 40e-6;          % [s]
[kgrid.t_array,dt] = makeTime(kgrid, medium.sound_speed, [], t_end);

%Define the source
source.p_mask=mask;
source_freq = 1.5e6;    % [Hz]
source_mag = 2;        % [Pa]
source.p = source_mag*sin(2*pi*source_freq*kgrid.t_array); %The square wave for the
source
source.p = filterTimeSeries(kgrid, medium, source.p); %Filter the frequency not
supported by the grid

%Define the sensor array to record the data

sensor.mask=mask_2;
sensor.record={'p_rms','p_final','I_avg'}; % Here two types of data are recorded: root
mean square of the pressure and average intensity over the simulation time
display_mask = source.p_mask;
input_args = {'DisplayMask', display_mask, 'PMLInside', false, 'PlotPML',
false,'RecordMovie', true, 'MovieName','Cylindrical'}; %Set the arguments of the display
sensor_data = kspaceFirstOrder3D(kgrid, medium, source, sensor, input_args{:}); %Run
the simulation function of 3D simulation

%Visualization of the Simulation Result
%sensor_data.p_rms = reshape(sensor_data.p_rms, Nx, Ny, Nz);
%sensor_data.p_rms(source.p_mask ~= 0) = 1;

%Reorder the average acoustic intensity recorded here. The data returns as the
%Matlab column wise order
intensity_1=sensor_data.Iy_avg;
intensity_2=sensor_data.Ix_avg;
intensity_3=sensor_data.Iz_avg;
Pressure=sensor_data.p_rms; %here rms pressure is used for ultrasound amplitude
distribution research
Size2=size(Pressure);
Size1=160;
Size3=Size2(1)/Size1;
Data=reshape(Pressure,Size3,Size1);
vec1=1:1:Size1;
vec2=1:1:Size3;

figure;

```

```
surf(vec1,vec2,Data);
```

Matlab simulation code for the calculation of ratio of deflection volumes

```
%Theoretical Calculation of Ratio of Deflection
```

```
clear all;
```

```
density=2700;
```

```
samplenum=100;
```

```
thicknessunit=0.01*10^-3;
```

```
for i=1:samplenum
```

```
    h(i)=i*thicknessunit;
```

```
end
```

```
length=size(h);
```

```
E=7*10^10;    %Material propeties setting
```

```
u=0.31;
```

```
a=20*10^-3;
```

```
b=19*10^-3;
```

```
R=b/2;
```

```
c=b*1/1;
```

```
k=7*10^9;
```

```
w=(2*pi*1.4*10^6);
```

```
w1=(2*pi*1.5*10^6);
```

```
W=w^2;
```

```
W3=w1^2;    % Excitation signal setting
```

```
beta=a/c;
```

```
beta1=beta^2;
```

```
beta2=(a/b)^2;
```

```
num1=50;
```

```
num2=50;
```

```
for i=1:length(2)
```

```
    sum(i)=0;
```

```
    D=E*h(i)/(12*(1-u^2));
```

```
    displacement1=0;
```

```
    displacement2=0;
```

```
    for m=1:num1
```

```
        for n=1:num2
```

```
            W1(m,n)=(D*(m^2*pi^2/(a^2)+n^2*pi^2/(b^2))^2+0*m^2*pi^2/a^2+0*n^2*pi^2/b^2+k  
            )/(density*h(i));    %Calculation of natural frequencies
```

```
W2(m,n)=2/(density*h(i))*(D*(m^2*pi^2/(a^2)+4*n^2/(b^2))^2+8*u*m^2*pi^2/(a^2*b^2)+24/(b^2*h(i)^2)+k);
```

```
x1=m/n;
x2=n/m;
result1=(x1+x2*beta1);
result2=(x1+x2*beta2*4/(pi)^2);
```

```
displacement1=displacement1+result1*(1-(-1)^m)*(1-(-1)^n)*sin(m*pi/2)^2*sin(n*pi/2)^2/(m*n*(W1(m,n)-W)); %Calculation of the deflection volume
```

```
displacement2=displacement2+result2*(1-(-1)^m)*(1-(-1)^n)*sin(m*pi/2)^2*sin(n*pi/2)^2/(m*n*(W2(m,n)-W));
```

```
end
end
ratio(i)=displacement2/(displacement1*2);
%Calculation of the ratio
end
```

```
figure;
plot(h,ratio);
xlabel('Thickness of Matching Layer [m]');
ylabel('Ratio of Voltage Required');
```